Development of New MPP Estimation Schemes and Maximizing the Power Generation of a PV Array Under Partial Shading Conditions

Himanshu Sekhar Sahu

Development of New MPP Estimation Schemes and Maximizing the Power Generation of a PV Array Under Partial Shading Conditions

A

Thesis submitted

for the award of the degree of

Doctor of Philosophy

By

Himanshu Sekhar Sahu

Department of Electronics and Electrical Engineering

Indian Institute of Technology Guwahati

Guwahati -781039, Assam, India

June 2017

Dedicated to

To

My Supervisor

Dr. Sisir Kumar Nayak

and

To

My dear **parents,**

My wife **Bobby,** my brother **Manoj** for their love and support

Certificate

This is to certify that the thesis entitled "**Development of New MPP Estimation Schemes and Maximizing the Power Generation of a PV Array Under Partial Shading Conditions**", submitted by **Himanshu Sekhar Sahu** (11610232), a research scholar in the *Department of Electronics and Electrical Engineering, Indian Institute of Technology Guwahati*, for the award of the degree of **Doctor of Philosophy**, is a record of an original research work carried out by him under my supervision and guidance. The thesis has fulfilled all the requirements as per the regulations of the institute and in my opinion has reached the standard needed for submission. The results embodied in this thesis have not been submitted to any other University or Institute for the award of any degree or diploma.

Date:

Place: Guwahati.

Dr. Sisir Kumar Nayak
Associate Professor
Dept. of Electronics and Electrical Engg
Indian Institute of Technology Guwahati
Guwahati - 781 039, Assam, India.

Acknowledgements

First and foremost, I feel it as a great privilege in expressing my deepest and most sincere gratitude to my supervisor Dr. Sisir Kumar Nayak, for his excellent guidance throughout my study. His kindness, dedication, hard work and attention to detail have been a great inspiration to me. I would particularly like to thank you sir for all your help in patiently and carefully correcting all my manuscripts. I have no doubts that finishing my degree in a proper and timely manner was impossible without his help, suggestions and advice.

I am also very thankful to my doctoral committee members Prof. Somnath Majhi, Dr. Praveen Kumar and Dr. Praveen Tripathy for sparing their precious time to evaluate the progress of my work. Their suggestions have been valuable. I would like to express my heartfelt thanks to Prof. Sukumar Mishra, IIT Delhi for providing valuable suggestions for my work.

I would also like to thank the Head of the Department and the other faculty members for their kind help in carrying out this work. I am also grateful to all the members of the research and technical staff of the department without whose help I could not have completed this thesis. My special thanks to Mr. Sanjib Das for maintaining the excellent computing facility and various resources useful for this work. I am also thankful to Mr. Ridib Bharali, Mr. Sidananda Sonowal and Mr. Dimpul Gogoi for supporting in my experimental work.

I would like to thank Umesh, Shekha, Ankit, Venkat, Gautam and all the research scholars of the power control laboratory, IIT Guwahati, for their coperation.

My deepest gratitude goes to my parents and my brother for their continuous love and support throughout my studies. My wife also played a significant role during my Ph.D and without her support and unlimited sacrifices, I would not have accomplished so far.

Finally, I would like to thank the Almighty God for bestowing me this opportunity and showering his blessings on me to come out successful against all odds.

Himanshu Sekhar Sahu

Abstract

This thesis presents the new maximum power point (MPP) estimation schemes for a single diode model (SDM) and double diode model (DDM) photovoltaic (PV) module under different environmental conditions (DEC). It also addresses maximizing the power generation of a PV array under partial shading conditions (PSC).

In the present study, a novel approach is proposed to estimate the MPP of an SDM PV module on an hourly basis using meteorological data. The MPP of a PV array is estimated based on its characteristic equation by using Levenberg Marquardt (LM) method. The actual and estimated maximum powers of a PV array of monthly averaged daily and hourly basis is calculated using MATLAB. It is observed from the results that each of the estimated maximum power of a PV array on an hourly basis is nearly equal to each of the actual maximum power. The MPP of a PV module estimated by the LM method is validated with the actual and experimental results. A comparative study of MPP of a PV module estimated from the proposed method with different existing method is performed. The performance of the proposed algorithm for estimation of MPP of a PV array ensures the accuracy and faster convergence.

An explicit function of current with the voltage derived from an implicit current-voltage (I-V) relationship to estimate the MPP of a PV module is presented. The MPP of a PV module is estimated from the proposed explicit function of an I-V relationship using bisection technique. Therefore, it ensures that the estimation of MPP of a PV module is simple and accurate. The estimation of MPP of a PV array under DEC is presented using MATLAB program. Also, a comparison of the proposed method with different existing methods for tracking of MPP of a PV module under steady and rapid variation

of solar irradiation conditions is presented. The results show that the estimated MPP of a module is more or less same as the actual MPP values. The percentage of deviation of estimated maximum power obtained by using the proposed technique as compared to experimentally obtained maximum power is minimal. Therefore, the performance of the proposed method is more accurate and computationally efficient.

A robust technique to estimate the MPP of a double diode model (DDM) PV module is presented. The MPP of the DDM PV module under DEC are estimated by using the simple and computationally efficient LM method. The variation of double diode PV module parameters with the change of temperature and irradiation is analyzed. The MPP of the DDM PV array at non-standard test condition (non-STC) obtained from the proposed method is verified with the MPP obtained experimentally and by MATLAB simulation. A comparative study of MPP of a DDM PV module estimated from the proposed method with different existing methods is performed for different operating conditions. The maximum measurement error in power generation of a DDM PV module for different methods under DEC is presented which indicates the better performance of the proposed method for the estimation of MPP of a DDM PV module.

As per energy efficiency of a PV system is concerned, partial shading is an important issue. Under PSC, the modules of a PV array receive different levels of solar irradiation, so the power generation of a PV system decreases. The power-voltage characteristic of a partially shaded PV array contains multiple local maxima, and the global maximum power point is one of them. The losses in a PV array depend on the shading pattern and the physical location of shaded modules. The proposed Futoshiki puzzle pattern for the arrangement of the modules of an $m \times n$ ($m = n$, where m and n are the number of rows and columns) PV array under PSC ensures the enhancement of the power generation with respect to totally crossed tired (TCT) structure. In this method, the physical locations of modules in a TCT structure PV array are rearranged without changing the electrical connection of the modules. A comparison between the power generation in TCT, electrical array reconfiguration (EAR) and Futoshiki puzzle pattern configuration is presented. It is

observed that the power generated by a PV array in the Futoshiki configuration method is enhanced, and mismatch loss is minimized under different shading patterns by theoretical, simulation, and experimental results.

Finally a generalized algorithm for the physical relocation of the modules with a fixed electrical connection (PRM-FEC) in TCT configuration of an $m \times n$ ($m = n$ and $m \neq n$) PV array is proposed. This rearrangement of the TCT configuration distributes the shadows over the array, and hence, it increases the power output of an array under PSC. The PRM-FEC scheme is simple and cost effective. The comparison of power generated by an array with the TCT, EAR, and the PRM-FEC configuration is performed with MATLAB simulation and also the simulation results are validated with experimental results. The performance of the PRM-FEC configuration is superior to the TCT configuration.

Contents

List of Figures

List of Tables

List of Acronyms

AI	Artificial intelligence
ANN	Artificial neural network
ASEB	Assam State Electricity Board
AT	Ambient temperature
BL	Bridge link
BM	Bisection method
DDM	Double diode model
DEC	Different environmental conditions
DG	Distribution generation
EAR	Electrical array reconfiguration
GA	Genetic algorithm
GMPP	Global maximum power point
GN	Gauss-Newton
GS	Gauss-Seidel
GSI	Global solar irradiation
HC	Hony comb
HCB	Hill climbing
IC	Incremental conductance
IDM	Ideal diode model
I-V	Current-voltage
LM	Levenberg Marquardt
LMPP	Local maximum power point

LN	Long narrow
LW	Long wide
ML	Mismatch loss
MPP	Maximum power point
MPPT	Maximum power point tracking
MVT	Mean value theorem
NLS	Non-linear least square
NR	Newton-Raphson
OCV	Open circuit voltage
PEE	Power electronics equalizer
PI	Proportional integral
PO	Perturb and observe
PRM-FEC	Physical relocation of modules with fixed electrical connections
PS	Pattern search
PSC	Partial shading conditions
PV	Photovoltaic
P-V	Power-voltage
RH	Relative humidity
SCC	Short circuit current
SD	Steepest descent
SDM	Single diode model
SF	Shading factor
SN	Short narrow
SP	Series parallel
SSI	Shaded solar irradiation
STC	Standard test conditions
SW	Short wide
TCT	Total cross tied

USI	Unshaded solar irradiation

List of Symbols

A	Diode quality factor
I_{ph}	Photogenerated current
I_o	Dark saturated current
V_{mp}	Voltage at MPP
I_{mp}	Current at MPP
I_{sc}	Short circuit current
V_{oc}	Open circuit voltage
R_s	Series resistance
R_{sh}	Shunt resistance
k	Boltzman's constant
T	Junction operating temperature
V_t	Junction thermal voltage
n_s	Number of cells are connected in series
k_i	Temperature coefficient of current of the PV module
$I_{ph(STC)}$	Photogenerated current at STC
k_v	Temperature coefficient of voltage of the PV module
N_{ss}	Number of series PV modules to form a string
N_{pp}	Number of parallel string to form a PV array
E_g	Band gap energy
$I_{o(STC)}$	Dark saturation current at STC
G_{TH}	GSI
G_{BH}	Direct beam radiation

G_{DH}	Diffuse solar radiation
θ_z	Zenith angle
ω	Hour angle
δ	Declination angle
δ_n	Calender day the year
G_{PH}	Beam received on perpendicular surface to incoming radiation
G_{oh}	Solar constant
τ	Atmospheric transmittance
m	Air mass number
P_a	Atmospheric pressure
G_{max}	Maximum GSI
$J(x_i)$	Jacobian matrix
$H(x_i)$	Hessian matrix
λ	Combination coefficient
P_{act}	Actual power
P_{est}	Estimated power
$P_{max,(act)}$	Actual maximum power
$P_{max,(est)}$	Estimated maximum power
t_{MPP}	Time taken to obtain MPP
η_{track}	Tracking efficiency
V_{frac}	Fractional open circuit voltage
V_{oc-i}	Initial voltage
V_{oc-f}	Final voltage
V_{BM}	Bisection voltage

1

Introduction

Contents

1.1 Renewable energy

Nowadays the hydrocarbon based fossil fuels are the primary sources of energy. The energy produced from the combustion of these fuels increase the pollutants like carbon dioxide which in turn increases the atmospheric temperature due to the greenhouse effect. However, the amount of fossil fuels available for future consumption is limited. Therefore, the renewable energy sources such as wind, solar, tidal, and fuel cells are the alternative options for the future energy demand. Since these renewable energy sources are environmentally friendly, these are called as green energy. Usually, the hydrocarbons or nuclear fuels are used in the power plants to generate a large scale of energy in thousand megawatts and to transmit this energy to the consumer requires a complex transmission and distribution systems. This leads to an increase of transmission and distribution losses and cost. Therefore, in the future, the small scale energy generation in the site of the consumer is being proposed, and the alternative sources of energy are the best choice for the generation of electrical power in small scale in kilowatts to meet the requirement of localized demand. The renewable energy sources can be installed in commercial or residential complexes to fulfill the energy demand of that particular area, and this mode of energy generation is called as distributed generation (DG). Photovoltaic (PV) energy is more popular among the other renewable sources and fastest growing [3] due to the facts stated as follows:

- Sufficient amount of solar irradiation is available with no fuel cost,
- PV power generation is free from an environmental pollution,
- Maintenance free as compared with other alternatives, and
- Long transmission systems are not required due to localization of the PV power generation.

The solar energy incident on the surface of the Earth is estimated from the reflection and absorption of sunlight by the atmosphere, and this incident energy is ten thousand times more than the world energy consumption [4]. Solar power is more friendly and will make the biggest contribution to the generation of energy by 2040 [5]. Nowadays many countries are giving importance for installation of PV power to fulfill their energy requirement because it is easy for development, testing, faster

implementation, and more accurate models of PV modules are available to suite different purposes. There is an increasing demand for solar power in countries like India, China, Britain, Italy and the United States. India has a solar grid cumulative capacity of 8.626 GW till 30 September 2016. In January 2015, the government of India set an ambitious plan to increase the solar power generation capacity up to 100 GW by 2022. The main disadvantages of the PV power generation are high installation cost, low efficiency in energy conversion and variation in power generation due to variation in weather condition (i.e., irradiation) [6, 7]. With the development of technology, it is expected that cost of installation will decrease in future.

1.2 PV power generation

PV cells are used for the direct conversion of light energy into DC power using semiconductors that exhibit the photovoltaic effect. The photovoltaic effect was first observed by Alexandre-Edmond Becquerel in 1839.

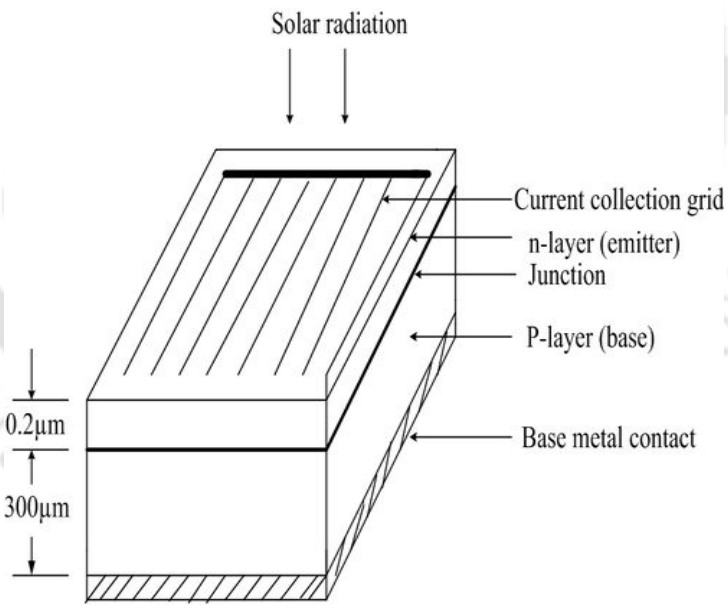

Figure 1.1: Typical p-n junction PV cell.

Figure 1.1 shows a typical p-n junction PV cell [8]. Due to absorption of solar light by PV cell, the p-n junction provides an inherent field separating the charges created and also the created electrons and holes move towards the front and back of the cell respectively. The carriers from the cell are collected by a base metal contact that generally covers the p-type material and attaching a metallic

fine grid on the front side of cell. Then a potential difference will be developed between the front and back of the PV cell and hence, the current will flow when a load is connected across the PV cell. The PV cells based on the material are of three types such as mono-crystalline, poly-crystalline and thin-film. Mono-crystalline PV cell is made up of single material known as silicon material, and it is more efficient but more expansive than other types of PV cell. Poly-crystalline PV cell is made up of poly-crystalline silicon which is composed of a number of small silicon crystal. The poly-crystalline PV cells are less expansive. However, they are less efficient as compared to mono-crystalline PV cell. A thin-film PV cell is formed by depositing one or more thin layer of materials like CdTe, CIGS, CIS and amorphous silicon (a-Si). These PV cells have low energy efficiency but perform better in insufficient light condition. The PV cells are connected in series to form a module and then number of modules are connected in series to form a string to deliver a power according to the voltage level of the load. The PV array formed by connecting the strings in parallel has the same characteristic as that of module with increase voltage and current [9].

1.2.1 Modeling of a PV module

Accurate modeling of a PV module is required for the estimation of maximum power point (MPP) under different environmental conditions (DEC). Since the current-voltage (I-V) characteristic of the PV module is highly non-linear, a proper mathematical modeling is needed. In the literature, a number of mathematical models for an ideal PV module such as single diode model (SDM) and double diode model (DDM) are available. An ideal model of a PV module for single diode and double diode model are shown in Figure 1.2(a) and (b) respectively.

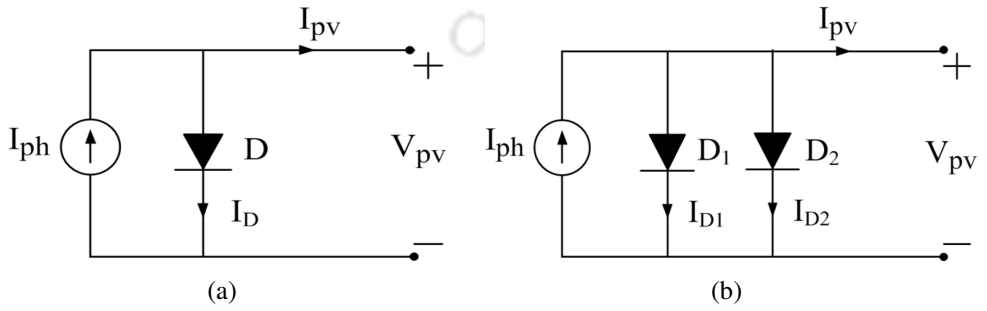

Figure 1.2: Ideal PV module of (a) SDM and (b) DDM.

Since the ideal model of the PV module is assumed to be loss less, the model is simple and the

accuracy of this model is less. For the improvement of accuracy of this model, a series resistance, R_S and a shunt resistance, R_{sh} are considered in the circuit which are shown in Figure 1.3(a) and (b).

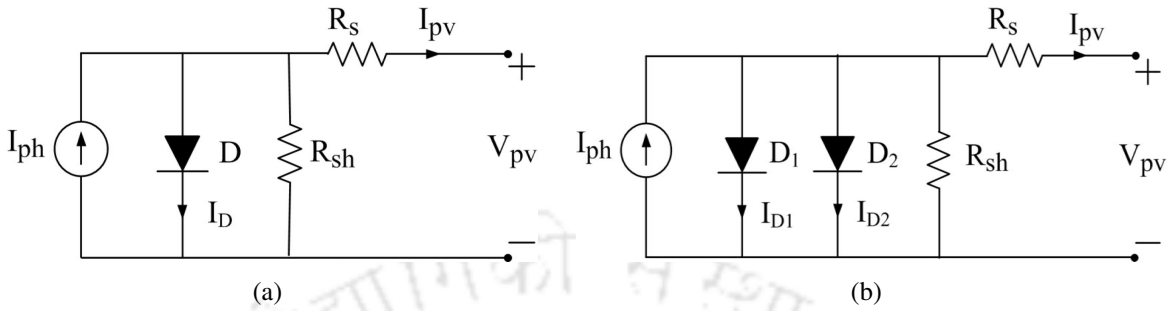

Figure 1.3: Practical PV module of (a) SDM and (b) DDM.

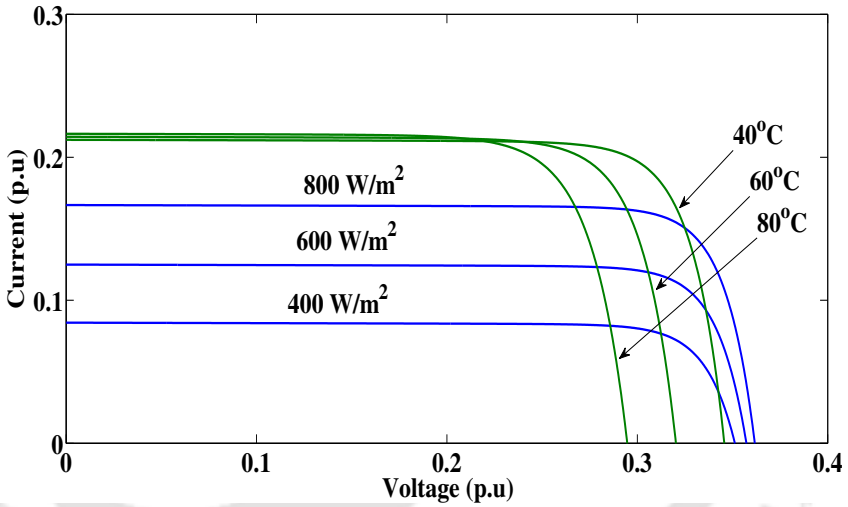

Figure 1.4: I-V characteristics of a PV module at standard temperature (25 °C) with varying irradiation and at an irradiation of 1000 W/m^2 with varying temperature.

For the further improvement in the accuracy of the SDM as shown in Figure 1.3(a), another diode is considered in parallel with the first diode and this is called DDM as shown in Figure 1.3(b). In this model, the current flowing through the diode 1 is the diffusion current due to the major charges and the current flowing through the diode 2 is the recombination current due to the minor charges. The DDM is non-linear and the mathematical analysis is very complex. The mathematical analysis of SDM is simple as compared to DDM. Hence, an SDM of five-parameter such as photo generated current (I_{ph}), dark saturated current (I_o), diode quality factor (A), series resistance (R_s) and shunt resistance (R_{sh}) are considered [10]. Three operating points in the I-V characteristics such as, short

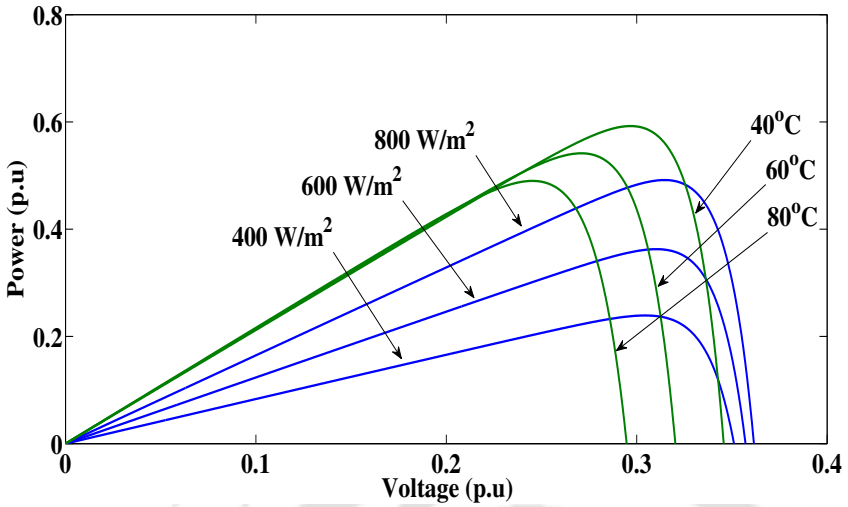

Figure 1.5: P-V characterstics of a PV module at standard temperature (25 °C) with varying irradiations and at an irradiation of 1000 W/m^2 with varying temperatures.

circuit current (0, I_{sc}), open circuit voltage (V_{oc}, 0) and MPP i.e., voltage at MPP (V_{mp}) and current at MPP (I_{mp}) are given by the manufacturer. Hence, the accurate estimation of PV parameters by using the data sheet value given by the manufacturer is very much essential. The accurate value of the PV parameters estimate the accurate value of MPP under DEC. The point on the I-V characteristic of a PV module at which the maximum power is delivered by the PV module is called as MPP [11]. The I-V and power-voltage (P-V) characteristics of the module under change of solar irradiation with fixed temperature and change of temperature with fixed irradiation are presented in Figure 1.4 and 1.5 respectively [12].

1.2.2 Estimation of maximum power from a PV array

The amount of power generation from a PV array depends on the solar irradiation and ambient temperature conditions [13]. There are many research work have been carried out in the past for the improvement of efficiency and power quality of the PV system [14]. Since the PV array has low power conversion efficiency due to its nonlinear characteristics of I-V, the PV array is required to operate at MPP. To improve the power conversion efficiency of the PV system, an efficient maximum power point tracking (MPPT) controller is required and therefore, it is the essential part of the PV system. The maximum power of a PV array is extracted from the power region of the I-V characteristic as shown in Figure 1.6. The power region of the I-V curve is found out by taking the effect of series

and shunt resistance of a PV array at open circuit and short circuit condition respectively [15]. The slopes of the I-V curve at open circuit and short circuit condition meet at an intersection point (V_{int}, I_{int}). Dropping a perpendicular from this intersection point to the voltage axis and to the current axis of the I-V curve will give a point (V_{int}, 0) and (0, I_{int}) respectively. The point (V_{int1}, 0) is obtained by dropping a perpendicular from the point corresponds to I_{int} on the I-V curve to the voltage axis.

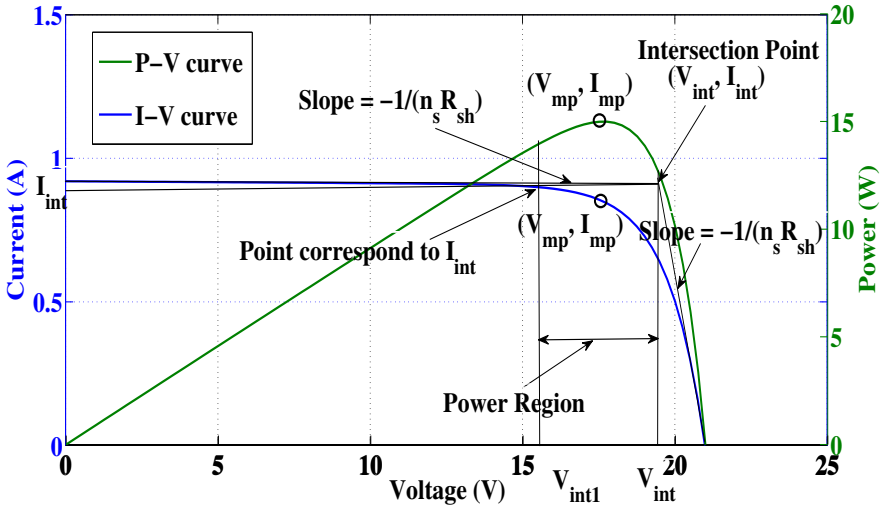

Figure 1.6: MPP extraction from the power region of I-V characteristic of a PV array.

The region between the points corresponds from V_{int1} to V_{int} of the I-V and P-V curves of a PV array is called power region. The MPP of a PV array is estimated from this power region of the I-V characteristic by using different MPPT methods. Since the MPP of an array changes with the environmental conditions in the power region of I-V characteristic, the converter is controlled in such a way that the array operates at MPP and this is called as MPPT.

1.2.3 Partial shading conditions (PSC) of a PV array

Partial shading conditions (PSC) of a PV array occur due to the moving clouds, deposition of sand or dust and shadows of nearby trees or house. During PSC of a PV array, the modules of the array receive non-uniform solar irradiation and under such condition the non-linear I-V and P-V characteristics of the array get more complicated and both the characteristics contain multiple peaks. So, there is a mismatch between the modules current, and hence, the power generated by the PV array is reduced [16].

The bypass and blocking diodes used in the PV array under PSC are presented in Figure 1.7.

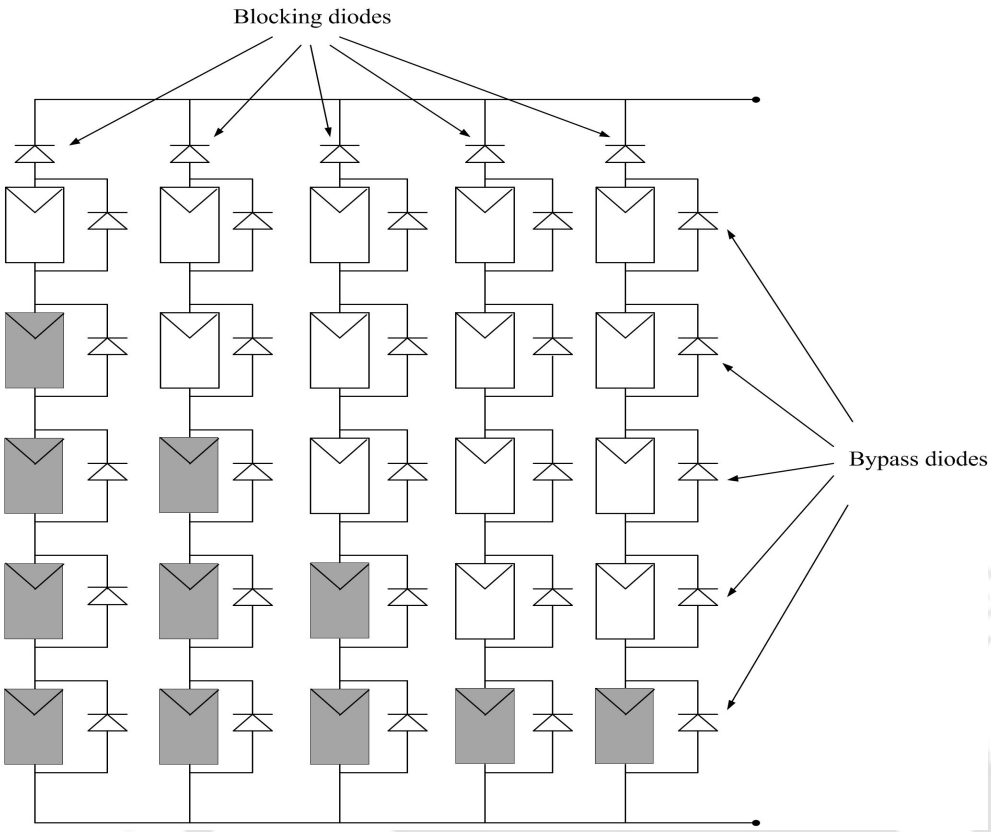

Figure 1.7: PV array with bypass and blocking diodes.

In this figure, the dark modules represent the shaded and the white color modules represent the un-shaded. The bypass diodes connected in parallel across the PV modules in the series string of an array, allow the un-shaded modules of all the series strings to flow their maximum current at a given solar irradiation and temperature condition [17]. On the contrary, if the bypass diodes are not used, the shaded modules will limit the reduced current of the un-shaded module in the series connected string. Therefore, the power generated by the PV array decreases and the thermal destruction of the PV module may occurs. The blocking diodes will oppose the reverse current via the string, that generates lower output voltage with comparison to the other parallel connected strings. On the other hand, if the blocking diodes are not used, the reverse current may cause more heat generation and thermal breakdown of PV modules.

The I-V characteristic of a PV array under PSC contains multiple steps with the presence of bypass and blocking diodes as shown in Figure 1.8, whereas the P-V characteristic of an array under PSC contains multiple peaks as shown in Figure 1.9. The presence of multiple peaks reduces the

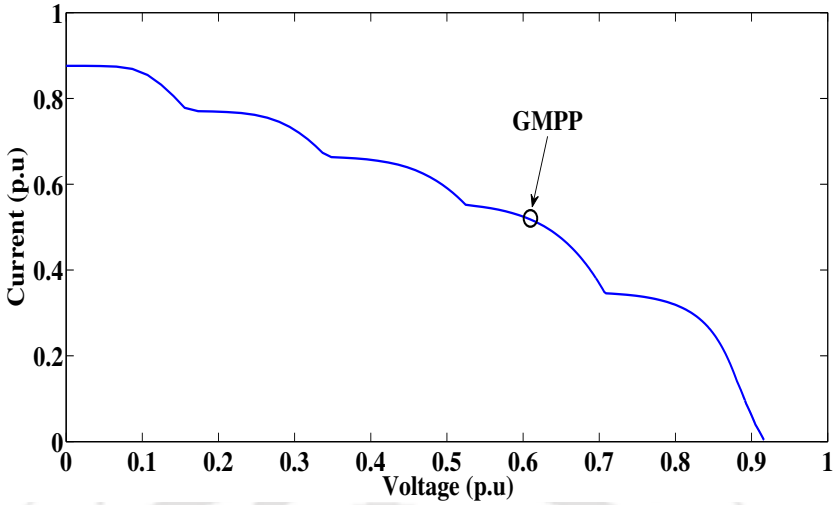

Figure 1.8: I-V characteristic of a PV array under PSC.

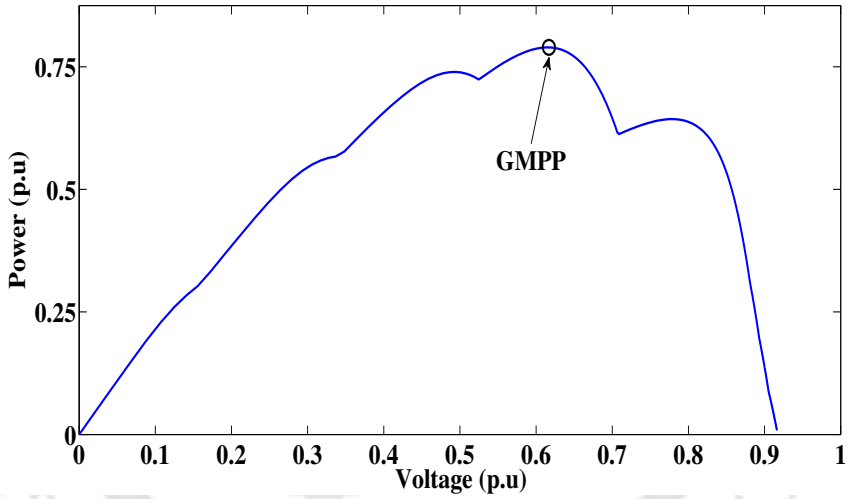

Figure 1.9: P-V characteristic of a PV array under PSC.

effectiveness of the existing MPPT methods [18–20] because these existing methods are unable to differentiate between the local and global maximum power point (GMPP).

1.3 Literature review

The renewable energy sources such as PV, wind and fuel cells are injected into the distributed generation network to meet the energy demand. PV in a power system is getting more importance in research prospective in the last few years because of its low operational and maintenance cost, free from pollution and noise during power generation, long life cycles and also suitable even in isolated and remote areas [19, 21]. The PV devices use p-n junction and are called as PV cells [22]. The

literature review classified into broad groups such as estimation of parameters of an SDM and DDM PV module, estimation of global solar irradiation (GSI), MPP of a PV array, and partial shading of a PV array are presented bellow.

1.3.1 Estimation of parameters of an SDM and DDM PV module

In the literature, many researchers have designed the PV cells and modules by considering the SDM and DDM. The single-diode PV model is commonly used because of it has the simple circuit and low computational cost [23–27]. However, in this model, the recombination losses are not taken into account, so the accuracy at open circuit voltage (OCV) highly diminishes at low solar irradiation level [28, 29]. DDM PV module is used to improve the modeling accuracy by connecting another diode in parallel with SDM. DDM takes into account the recombination losses, and hence it is more accurate than the SDM at low solar irradiation for representing the cell behaviors [11, 29–33]. The PV parameters of an SDM [12] and DDM [11, 34], of a module are estimated analytically under standard test conditions (STC) by using data sheet values provided by the manufacturer. To demonstrate the I-V characteristics and MPP of a PV array for certain parameter variation, a simple PV module electrical model is designed [9, 35]. The PV parameters of an SDM are calculated by arranging the I-V characteristic at three points such as, OCV (V_{oc}, 0), short-circuit current (SCC) (0, I_{sc}) and MPP (V_{mp}, I_{mp}) [23]. In the recent contribution, the parameters of an SDM PV module are estimated from the datasheet values using Gauss Seidel (GS) method [10], and it is reported that this method may converge at the wrong point in some cases.

1.3.2 Estimation of GSI and MPP of a PV array

The output power of the PV plant depends on the GSI, which is measured by using pyranometer installed at meteorological centre. Since pyranometer is not installed at every meteorological centre, nowadays many researchers have developed the empirical relation to estimate the GSI using the meteorological data [36, 37]. The accurate estimation of GSI is needed for integration of PV with the power system network. The GSI on an hourly basis is estimated considering the meteorological data (temperature and relative humidity (RH)) using an empirical expression.

Tracking of MPP of a PV array is essential for the integration of solar power to the microgrid. Since the output I-V characteristic of an array is non-linear, and this characteristic varies with solar

irradiation and temperature, the tracking of MPP of a PV array is not simple. Many researchers have used broadly classified three different methods such as direct methods, artificial intelligence methods and indirect methods to track the MPP of an array [38–40]. Most widely used direct methods for MPP tracking are perturb-and-observe (PO) [13], incremental conductance (IC) [41, 42], and hill climbing (HCB) [19]. The PO and HCB are efficient techniques, reliable, and track the MPP accurately. But, the accuracy and time required to reach MPP depend on the size of the perturbation and not suitable for the rapid change of environmental conditions. In these methods, the output voltage and current signal of the PV array oscillate even at steady state. Therefore, the searching nature of these methods is slow to some extent, and hence these methods are not suitable for the rapid change of environmental conditions (i.e. solar car, moving broken clouds) [38,43]. The efficiency of IC method is same as PO, and it gives good results under rapid change of environmental conditions. But sensors, complex and costly control circuits are required to implement this method [41]. However, with the application of various advanced search based algorithms [18, 44–48], the performance of the above direct methods improves. The artificial intelligence (AI) techniques are neural fuzzy logic, neural network and genetic algorithm (GA) [49–52]. However, the AI techniques are computationally demanding, and their practical implementation is difficult. Hence, the implementation of AI techniques may not be the first choice for many applications.

The indirect methods are based on mathematical functions derived from an empirical data to estimate the MPP of a PV array [40], and these methods are fractional OCV and fractional SCC [53]. The above mentioned indirect methods are very simple, but the power loss reduces the accuracy of these methods. The measurement of the OCV is simpler even if the accuracy of fractional OCV is less than that of fractional SCC method. Therefore, a novel approach has been proposed for the estimation of the SCC from the measured OCV [53]. A new technique based on analytical solution has been proposed for the estimation of MPP using mean value theorem (MVT) [54]. The accuracy of this technique is good enough, but it requires the periodic measurement of the OCV by power interruption. A real-time MPP of a PV array, estimated by fourth-order polynomial curve fitting is presented in [55], but it requires a lot of calculations because of real-time identification of the parameters. The MPPT of a PV module is estimated by considering the linear MPP locus [56]. However, the linear

approximation is not valid in the low irradiation level as well as the assumptions made on irradiation independence on the OCV may not be valid. A non-linear least square (NLS) method based on trust region reflective algorithm has been proposed to estimate the PV module parameters [57], but it may fail to converge at an optimum point.

1.3.3 PSC of a PV array

The power generation of a PV array convey many challenges. The SCC of the PV cell varies due to the partial shading of an array. Partial shading is one of the causes of decrease of the power generation of an array. It occurs due to the moving clouds, deposition of sand or dust and shadows of nearby trees or house. The modules of an array receive nonuniform solar irradiation under PSC, and hence there is a mismatch between the modules current [16].

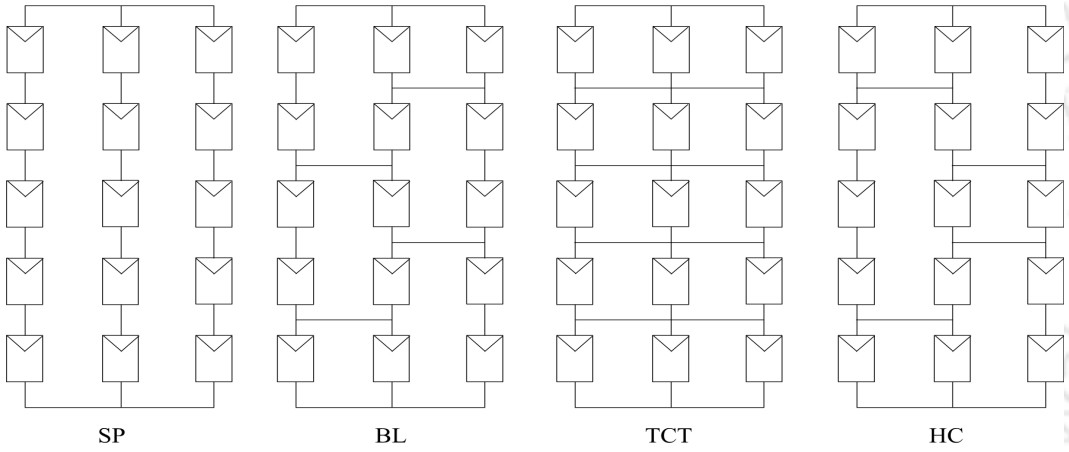

Figure 1.10: Different type of configuration of a PV array.

Since the shaded modules generate less current than the unshaded modules, and the current of shaded modules limits the output current of an array, the power generation of an array under partial shading reduces. In the shaded cells hot spot regions are formed which causes the localized heating, lower power output, material degradation, and increase in the affected area with time. To overcome this phenomenon and improve the power generation of the shaded solar cell of an array, each row of parallel cell strings is shunted by the bypass diode [58]. The modules of an array receive different levels of solar irradiation under PSC, which may give multiple peaks in P-V characteristics [59]. Under PSC, different MPPT algorithms are used to track the local maximum power point (LMPP) of

a PV array [60], and also different methods are proposed to track the GMPP of a PV array [48,61–65]. The four different types of topology of an array such as series-parallel (SP), bridge link (BL), total cross tied (TCT) and honey comb (HC) as shown in Figure 1.10 [66] are used in the PV plants. The power generated in the TCT configuration is higher than the other three configurations for four different standard shading conditions such as short wide (SW), short narrow (SN), long wide (LW) and long narrow (LN) as shown in Figure 1.11 [1, 67] as well as any random shading condition.

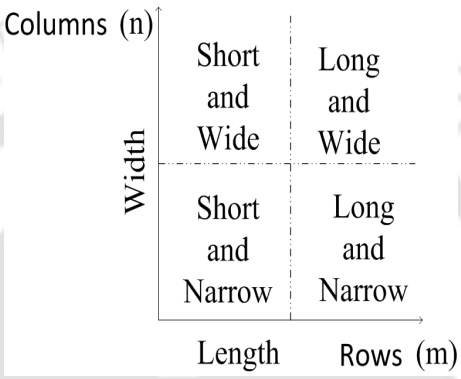

Figure 1.11: Different types of shading conditions [1].

Table 1.1: Four different standard shading conditions of a 7 × 5 PV Array

(a) SW

11	12	13	14	15
21	22	23	24	25
31	32	33	34	35
41	42	43	44	45
51	52	53	54	55
61	62	63	64	65
71	72	73	74	75

(b) LW

11	42	73	34	65
21	52	13	44	75
31	62	23	54	15
41	72	33	64	25
51	12	43	74	35
61	22	53	14	45
71	32	63	24	55

(c) SN

11	12	13	14	15
21	22	23	24	25
31	32	33	34	35
41	42	43	44	45
51	52	53	54	55
61	62	63	64	65
71	72	73	74	75

(d) LN

11	12	13	14	15
21	22	23	24	25
31	32	33	34	35
41	42	43	44	45
51	52	53	54	55
61	62	63	64	65
71	72	73	74	75

The example for four standard shading conditions such as SW, LW, SN, and LN, and different types of random shading conditions occurred in a 7 × 5 PV array are shown in Table 1.1 and 1.2, respectively. The PV mismatch losses (MLs) for three different configurations such as SP, BL, and TCT have been presented in different shading conditions [68]. The mismatch losses of an array in the TCT configuration are less than the other configurations under different shading conditions. The performance of a PV powered water pump is improved under different irradiation levels by using an electrical array reconfiguration (EAR) controller [69]. The irradiation levels for optimum switching

Table 1.2: Different random shading conditions of a 7×5 PV Array

(a) Shading condition 1

11	12	13	14	15
21	22	23	24	25
31	32	33	34	35
41	42	43	44	45
51	52	53	54	55
61	62	63	64	65
71	72	73	74	75

(b) Shading condition 2

11	12	13	14	15
21	22	23	24	25
31	32	33	34	35
41	42	43	44	45
51	52	53	54	55
61	62	63	64	65
71	72	73	74	75

(c) Shading condition 3

11	12	13	14	15
21	22	23	24	25
31	32	33	34	35
41	42	43	44	45
51	52	53	54	55
61	62	63	64	65
71	72	73	74	75

of a multistage EAR controller for a PV powered water pump is determined [70]. However, the above mentioned two techniques are complex, costly and applicable only for small scale system. The reconfiguration technique has been proposed for minimum deviation from the PV operating voltage, and this technique is based on removing the shaded modules from an array by identifying the current through the bypass diode [71]. However, in this reconfiguration strategy, number of switches are needed for the connection and disconnection of modules and number of current sensors are needed for the measurement of the currents through each bypass diodes. An array reconfiguration technique was proposed to increase the power generation by operating each element of an array at MPP by using minimum switches. But, implementation of this technique in a PV array requires many sensors [72]. An ANN based method is used for the reconfiguration of a PV array to maximize the power generation [73]. In this method the module current is compared with the reference value, and an appropriate switching signals are derived according to the specific rule. However, many measurements increase the complexity of this method. A mathematical formula is proposed for the optimal reconfiguration of an array [74]. An optimization technique is used for the array reconfiguration where the voltage is measured at each line and current is measured at each module. Thus this method requires many sensors for its implementation. To reduce the mismatch losses of a PV array, an optimal TCT interconnection scheme was proposed, and this interconnection scheme is mathematically formulated in accordance with the shading condition, irradiation levels and the duration of each shading conditions [75]. But the development of such interconnection scheme is difficult for an irregular shading conditions in a large scale PV array because the computations must be performed in accordance with the shading data. The power electronics equalizer (PEE) has been used to increase the power genera-

tion of a PV array under PSC [3]. In the PEE method, the shading effect is distributed over the entire PV array, and hence minimize the number of multiple peaks. However, a large number of switches and a complex control algorithm are needed for the application of PEE in a large scale PV plant. The power generated from an array is enhanced using the EAR technique under different shading conditions [76–78]. In EAR method, the electrical connection of the PV modules is changed dynamically in accordance with the shading condition. Therefore, a large number of switches and sensors are needed for changing the electrical connections of the PV modules during the practical implementation of a large scale PV system.

1.4 Motivation

Considering the aforementioned limitations, the motivation of this research work are as follows:

- The proper modeling of a PV array using simulation study is required for grid integration or stand alone or hybrid system.
- The accurate mathematical models such as an SDM and DDM of a PV module are required for the accurate analysis of a PV system. Since the I-V characteristic of the PV module is highly non-linear, the proper mathematical modeling of the PV module is not straight forward. Therefore, an accurate estimation of the parameters is required for an accurate modeling of the module.
- Since the energy efficiency of the PV module is low, the enhancement of the energy efficiency is very much essential. PV modules exhibit nonlinear output I-V characteristic, and this characteristic has a unique MPP which depends on environmental conditions (solar irradiation and temperature). Therefore, for the grid integration of the PV system, the estimation of MPP of an SDM array based on its characteristic equation using a simple and robust algorithm under DEC is desired.
- Since the non-linear I-V relationship of a module is an implicit function, it is difficult to estimate the MPP of a PV module accurately. For the simple and an accurate estimation of MPP of an SDM PV module, the conversion of the I-V implicit function of the module into an ex-

plicit function, i.e., current is a function of voltage only is required. The performance of the proposed method for the estimation of MPP of a PV module ensures more accuracy, simple and computationally efficient.

- A new approach for the estimation of MPP of a DDM PV module based on its characteristic equation under DEC is required. The MPP of the DDM PV module under different irradiation and temperature conditions should be estimated by using a robust algorithm.

- The PV systems are susceptible to large amounts of power losses due to partial shading on the array. So it is necessary to enhance the power generation of a PV array under PSC using a new approach for reconfiguration of an array to distribute the shading effect over the entire array, and hence minimize the mismatch losses between the modules of a PV array.

1.5 Objective of the thesis

The objectives of the thesis are described as follows:

- To estimate the GSI during sunshine hours of Guwahati city by taking RH and ambient temperature (AT) data using empirical expressions.

- To propose an efficient algorithm for the estimation of parameters of an SDM and DDM PV module at STC using the data sheet values provided by the manufacturer.

- To propose an efficient algorithm for the estimation of MPP of a PV array based on its characteristic equation under uniform and nonuniform irradiation conditions considering SDM and DDM PV module.

- To propose a new technique for the conversion of an implicit I-V relationship of an SDM PV module into a simple explicit function of current in terms of voltage to estimate the MPP of a PV module accurately and computationally efficient under DEC.

- To propose a novel configuration for the enhancement of the power generation and the minimization of ML of a partially shaded PV array.

- To propose a generalized algorithm for the physical relocation of the modules at the time of installation without changing the electrical connection of the modules in the TCT configuration of a PV array to improve the power generation under different shading patterns.

1.6 Main contribution

The main contribution of the thesis are given as follows:

- A robust estimation of MPP of an SDM and DDM PV module under different solar irradiation and temperature conditions has been proposed, and the estimation of MPP of a PV array is carried out by using Levenberg-Marquardt (LM) algorithm based on its characteristic equation.
- A novel approach for the conversion of I-V relationship of a PV module from an implicit function into an explicit function, i.e., current is a function of voltage only for the simple and accurate estimation of the MPP of a PV module under DEC has been proposed.
- A Futoshiki puzzle pattern for the arrangement of the modules of a PV array under PSC has been proposed for the power enhancement with respect to the TCT configuration. Also minimized the ML of the PV array in the Futoshiki configuration with respect to the TCT configuration under different shading conditions.
- A generalized algorithm for the physical relocation of the modules with a fixed electrical connection (PRM-FEC) in the TCT configuration of a PV array under different shading pattern has been proposed for the power improvement with respect to the TCT configuration.

1.7 Organization of the thesis

This thesis has been organized in seven chapters as follows:

In Chapter 2, the parameter estimation of an SDM PV module at STC and the estimation of GSI at a given location by using empirical expressions are presented. The estimation of MPP of a PV array based on its characteristic equation by using LM method has been proposed. The proposed method is also used for an estimation of MPP of a PV array for rapid change of solar irradiation conditions and in PSC. A comparative analysis of the performance in terms of the accuracy and computational

efficiency of the proposed method with other direct and indirect MPPT methods for the steady and rapid change of solar irradiation conditions have been performed.

A novel approach to estimate the MPP of a PV array under DEC is proposed in Chapter 3. The I-V relationship of a PV module which is an implicit function is converted into an explicit function, i.e., current is a function of voltage only. Therefore, it ensures that the estimation of MPP of a PV module is simple and accurate. A comparison of the proposed method with different existing methods is presented for tracking of MPP of a PV array under steady and rapid change of solar irradiation conditions. The proposed method is validated by comparing the simulation results with experimental results of a 250 W PV module under DEC.

Chapter 4 presents the estimation of MPP of a DDM PV module based on its characteristic equation using LM method. The MPP of the DDM PV array at non-STC obtained from the proposed method is verified with the MPP obtained experimentally and by MATLAB simulation. A comparative study between LM method with different existing methods, such as GA, PS, MVT, Saloux, NLS, and GS is presented under DEC. From the simulation results, it is observed that the accuracy of the proposed method is as high as compared to other methods and the execution time to obtain the MPP of a DDM PV module in the LM method is comparatively low. Therefore, the proposed method is more accurate and computationally efficient for the estimation of MPP of a DDM PV module under DEC.

In Chapter 5, the Futoshiki puzzle pattern for the arrangement of the modules of an $m \times n$ ($m = n$) PV array under PSC has been proposed for the power enhancement with respect to the TCT configuration. In this proposed method, the physical locations of modules in a TCT configuration of an array are rearranged without changing the electrical connection of the modules. The power enhancement in the Futoshiki configuration with respect to the TCT configuration of an array under different shading conditions by using MATLAB simulink are varified with the experimental results. A comparison between the power generation in the TCT, EAR, and Futoshiki puzzle pattern configuration is presented. Maximum measurement and parameter errors in power generation of an array in the Futoshiki configuration under different shading conditions are presented.

In Chapter 6, a generalized algorithm for the physical relocation of the modules with a fixed

electrical connection (PRM-FEC) in the TCT configuration of an $m \times n$ ($m = n$ & $m \neq n$) PV array is proposed for the power improvement under PSC. The comparison of power generated by an array with the TCT, EAR, and the PRM-FEC configuration is performed with MATLAB simulation and the simulation results are validated with the experimental results. The performance of the PRM-FEC configuration is superior to the TCT configuration.

Chapter 7 presents the conclusion of the thesis and the suggestions for the extension of this work in future research problems.

2

Numerical Approach to Estimate the MPP of a PV Array

Contents

2.1 Introduction

Solar power generation is achieving more importance due to reducing the cost of the PV modules with the development of technology in the area of power electronics. The PV array converts light energy into an electrical energy without any environmental pollution. Proper estimation of GSI is needed for integration of PV with the power system network. In this work, empirical relations are used to estimate the GSI on an hourly basis by using meteorological data. The SDM PV module parameters are estimated using different numerical methods as discussed in Chapter-1. In the recent contribution, the parameters of an SDM module are estimated from the datasheet values using the GS method [10] and it is reported that this method may converge at the wrong point in some cases. The number of iterations in the GS method is more as compared to the Newton Raphson (NR) method. Therefore, in the present work, the NR method is used to estimate the PV parameters for SDM. The estimation of MPP of a PV array is very much essential for integration of solar power to grid. The MPP estimation techniques of a PV array are classified into three different categories, such as direct methods, AI methods and indirect methods. As discussed in Chapter 1, the direct methods are most commonly used for online tracking of MPP of a PV module. However, these methods are sluggish in nature for rapid change of environmental conditions [38, 43]. The AI methods are computationally demanding, and the real time implementation of AI methods may not be the first choice for many applications. The indirect methods are based on mathematical functions derived from empirical data to estimate MPP of a PV array [40]. The fractional OCV and SCC methods are simple but the power loss reduces the accuracy of these methods. As discussed in the literature reviews of MPP estimation methods provided in Chapter-1, an efficient algorithm is required for estimation of MPP of a PV array based on its characteristics equation. In the present work, the LM algorithm for the estimation of MPP of an SDM PV module is categorized into the indirect methods.

The combination of steepest descent (SD) algorithm and Gauss-Newton (GN) algorithm is called as LM algorithm. As the SD algorithm gives the stable solution, and GN algorithm has fast response, so the LM algorithm is stable and computationally efficient. Since the LM algorithm is a robust algorithm [79, 80], it converges to an actual solution even if the initial Gauss is far away from the actual solution. Considering the aforementioned limitations of previous work and the advantages of

LM algorithm, in the present work, the estimation of MPP of a PV array on an hourly basis under DEC based on its characteristic equation using this method has been proposed. It is investigated that each of the estimated maximum power of a PV array on an hourly basis is nearly equal to each of the actual maximum power on an hourly basis. Also the estimated MPP results of a 15 W PV module are validated with the actual and experimental results. Finally, the MPP of a PV array under PSC is estimated by using the LM method and the results of estimated MPP closely match with the actual MPP. Thus, the performance of the proposed method for estimation of MPP of a PV array is more accurate.

In this chapter, Section 2.2 describes the parameter estimation of the PV module. The detail description of a 100 kW PV array is presented in this section. In Section 2.3, the GSI is estimated by using meteorological data and also the estimation of GSI results is presented in this section. In Section 2.4, the estimation of MPP of a PV array is described and also, a comparison of LM method with the different existing MPPT methods is presented. Experimental validation is presented in Section 2.5. Finally, the estimation of MPP of a PV array under PSC is presented in Section 2.6.

2.2 Estimation of PV parameters

An electrical equivalent circuit of an SDM PV module consisting of a current source parallel with a diode is shown in Figure 1.3(a) of Chapter 1. The I-V characteristic of an SDM PV module is [10] given in (2.1).

$$I_{pv} = I_{ph} - I_o \left\{ \exp\left(\frac{V_{pv} + I_{pv} R_s}{N_s V_t} \right) - 1 \right\} - \frac{V_{pv} + I_{pv} R_s}{R_{sh}} \tag{2.1}$$

where V_{pv} and I_{pv} are module output voltage and current, respectively, I_{ph} is the photo-generated current, I_o is the dark saturation current, N_s is the total number of cells connected in series in the module, R_s and R_{sh} are the series and parallel resistances, respectively, and V_t is the junction thermal voltage.

$$V_t = \frac{kTA}{q} \tag{2.2}$$

where k is the Boltzman's constant, T is the junction operating temperature, and *'A'* is the diode quality factor. The photo-generated current depends upon solar irradiation and temperature is given

as follows [81]:

$$I_{ph} = \frac{G}{G_{STC}} I_{ph(STC)} \left(1 + k_i (T - T_{STC})\right) \tag{2.3}$$

where $I_{ph(STC)}$ is the photo generated current at STC (i.e., 1000 W/m^2 and 25 °C), k_i is the temperature coefficient of the PV module.

The datasheet of a solar panel provides the values of I_{sc}, V_{oc}, V_{mp}, I_{mp} and N_s. The five model parameters I_{ph}, I_o, R_s, R_{sh} and *'A'* are estimated by using these datasheet values. As the value of exponential term is high as compared to 1 in (2.1), so the term *'-1'* is neglected. The three important points of the I-V characteristic of a PV module are the points at which the circuit is short circuited, open circuited, and MPP [23]. Using these three points, (2.1) is written as follows:

$$I_{sc} = I_{ph} - I_o \exp\left(\frac{I_{sc} R_s}{N_s V_t}\right) - \frac{I_{sc} R_s}{R_{sh}} \tag{2.4}$$

$$I_{mp} = I_{ph} - I_o \exp\left(\frac{V_{mp} + I_{mp} R_s}{N_s V_t}\right) - \frac{V_{mp} + I_{mp} R_s}{R_{sh}} \tag{2.5}$$

$$I_{oc} = 0 = I_{ph} - I_o \exp\left(\frac{V_{oc}}{N_s V_t}\right) - \frac{V_{oc}}{R_{sh}} \tag{2.6}$$

MPP is estimated from the condition [10] given in (2.7).

$$\left.\frac{dP}{dV_{pv}}\right|_{V_{pv}=V_{mp}, I_{pv}=I_{mp}} = 0 \tag{2.7}$$

To estimate the fifth model parameters, the slope of the I-V curve at short-circuit has been utilized [11].

$$\left.\frac{dI_{pv}}{dV_{pv}}\right|_{V_{pv}=0, I_{pv}=I_{sc}} = \frac{-1}{R_{sh}} \tag{2.8}$$

Using the specified conditions in (2.7) and (2.8) into (2.4)-(2.6), the equations obtained are [10]

$$V_t = \frac{I_{mp} R_s + V_{mp} - V_{oc}}{N_s \log B} \tag{2.9}$$

where

$$B = \left(\frac{-I_{mp} R_s + I_{sc} R_s - I_{mp} R_{sh} + I_{sc} R_{sh} - V_{mp}}{I_{sc} R_s + I_{sc} R_{sh} - V_{oc}}\right)$$

$$I_{mp} = V_{mp} \times \frac{C + \frac{1}{R_{sh}}}{1 + R_s \times C + \frac{R_s}{R_{sh}}} \tag{2.10}$$

$$C = \frac{(I_{sc}R_s - V_{oc} + I_{sc}R_{sh})\left\{\exp\left(\frac{V_{mp}+I_{mp}R_s-V_{oc}}{N_sV_t}\right)\right\}}{N_sV_tR_{sh}}$$

$$\frac{1}{R_{sh}} = \frac{D + \frac{1}{R_{sh}}}{1 + R_s \times D + \frac{R_s}{R_{sh}}} \tag{2.11}$$

where

$$D = \frac{(I_{sc}R_s - V_{oc} + I_{sc}R_{sh})\left\{\exp\left(\frac{I_{sc}R_{sc}-V_{oc}}{N_sV_t}\right)\right\}}{N_sV_tR_{sh}}$$

The values of the unknown parameters, such as V_t, R_s and R_{sh} are obtained by solving (2.9)-(2.11) using NR method. The value of 'A' is found out from (2.2), and the values of the other two unknown parameters I_0 and I_{ph} are deduced from (2.4) and (2.6) as given bellow.

$$I_o = \left(I_{sc} - \frac{V_{oc} - I_{sc}R_s}{R_{sh}}\right)\exp\left(-\frac{V_{oc}}{N_sV_t}\right) \tag{2.12}$$

$$I_{ph} = I_o \exp\left(\frac{V_{oc}}{N_sV_t}\right) + \frac{V_{oc}}{R_{sh}} \tag{2.13}$$

The 100 kW solar panels installed at Bijulee Bhawan, Assam State Electricity Board in Guwahati (ASEB) in Guwahati, India are taken as a reference for the present study. The power output of each module is rated at 250 W. The datasheet values of the parameters of the module are given in Table 2.1(a). The estimated values of the module parameters are given in Table 2.1(b).

Table 2.1: PV parameters

(a) Datasheet values

Module Parameters	Actual Values
I_{sc}	8.760 A
V_{oc}	37.30 V
V_{mp}	30.30 V
I_{mp}	8.25 A
N_s	60
k_i	0.05 %
k_v	- 0.36 %

(b) Estimated values

Module Parameters	Estimated Values
I_{ph}	8.760 A
I_o	0.0037 μA
A	1.121
R_s	0.250 Ω
R_{sh}	5728.7 Ω

2.2.1 Description of a PV array

The 100 kW installed solar panels supply power to the sixth floor of Bijulee Bhawan where the load varies from 60 to 80 kW. As a single module generates 250 W, the total number of modules required is 400. Out of these 400 modules, 10 modules are connected in series to form a string and 40 strings connected in parallel to form a 10×40 PV array [38].

The parameters of the array are estimated from the datasheet values of the PV module. Let the number of modules in series be N_{ss} to form a string and N_{pp} be the such number of strings are connected in parallel to form an array. Thus, the module parameters converted to an array parameters are given in Table 2.2.

Table 2.2: Module parameters converted for an array

Datasheet Values	Estimated Values
$I_{sc} \times N_{pp}$	$I_{ph} \times N_{pp}$
$V_{oc} \times N_{ss}$	$I_o \times N_{pp}$
$V_{mp} \times N_{ss}$	A
$I_{mp} \times N_{pp}$	$R_s \times N_{ss}/N_{pp}$
$N_s \times N_{ss}$	$R_{sh} \times N_{ss}/N_{pp}$

2.2.2 Temperature and irradiation dependance

The OCV and SCC vary linearly with temperature, are given as follows [23]:

$$V_{oc}(T) = V_{oc(STC)} + k_v(T - T_{STC}) \tag{2.14}$$

$$I_{sc}(T) = I_{sc(STC)}\left(1 + \frac{k_i}{100}(T - T_{STC})\right) \tag{2.15}$$

where k_i and k_v are the coefficients for SCC and OCV of the PV module respectively. The dark saturation current, which depends on temperature only, is given as follows [23]:

$$I_o(T) = I_{o(STC)}\left[\left(\frac{T}{T_{STC}}\right)^3 \exp\left\{\frac{1}{k}\left(\frac{E_{g(STC)}}{T_{STC}} - \frac{E_g}{T}\right)\right\}\right] \tag{2.16}$$

where $I_o(T_{STC})$ is the dark saturation current at standard temperature and the band gap energy E_g [82] of semiconductor is given as follows:

$$E_g(T) = E_{g0} - q\left(\frac{\alpha T^2}{T+\beta}\right) \tag{2.17}$$

where E_{g0}, α, and β are PV module material constants.

I_{ph} and SCC are directly proportional to the irradiance at a particular temperature, which are given by [10].

$$I_{ph}(G) = I_{ph}(G_{STC}) \times \left(\frac{G}{G_{STC}}\right) \tag{2.18}$$

$$I_{sc}(G) = I_{sc}(G_{STC}) \times \left(\frac{G}{G_{STC}}\right) \tag{2.19}$$

where G and G_{STC} are the irradiance under given conditions and at STC respectively.

Solar irradiation dependent OCV is given as follows [10]:

$$V_{oc}(G) = \ln\left(\frac{I_{ph}(G)R_{sh} - V_{oc}(G)}{I_o R_{sh}}\right) n_s \times V_t \tag{2.20}$$

2.3 Estimation of GSI

GSI (G_{TH}) in a certain location of the earth is estimated by taking ambient temperature (AT) and relative humidity (RH) data measured at meteorological station using empirical relations [37]. Solar radiation components are of two types, one is direct beam radiation (G_{BH}) and other is diffuse solar radiation (G_{DH}). The sum of these two radiations is called GSI and it is represented as follows:

$$G_{TH} = G_{BH} + G_{DH} \tag{2.21}$$

For the certain location on the earth's surface, latitude and longitude of the location can be found out from the atlas. Figure 2.1 shows the angle of location of panel on the globe. The angular distance (ϕ) between the equatorial plane and the normal to the location on the earth's surface is called as the latitude of the location. The intensity of GSI is decided by the angle between the sun's rays direction and the earth's surface. The angle between a normal line to the tangent plane to the earth's surface at the location of the module and the direction of the sun's ray is called as zenith angle (θ_z). Zenith

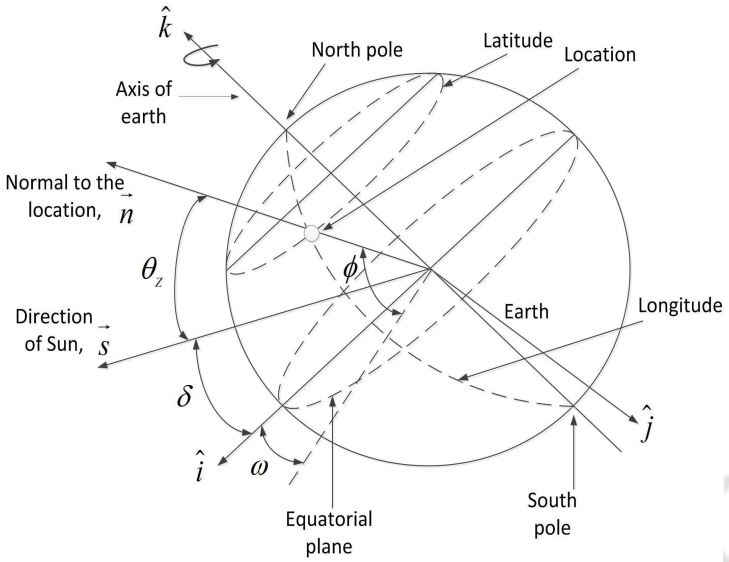

Figure 2.1: Location of panel on the globe [2].

angle, which is a function of the time of day, latitude and the time of the year, is calculated as follows:

$$\cos(\theta_z) = \sin(\phi)\sin(\delta) + \cos(\phi)\cos(\delta)\cos(\omega) \tag{2.22}$$

where ω and δ are hour angle and declination angle, respectively, which are given as follows [36, 83]:

$$\omega = 15 \times (ST - SN) \tag{2.23}$$

$$\delta = 23.45 \sin[360(\delta_n + 284)/365] \tag{2.24}$$

where ST is standard time, SN is solar noon, and δ_n is the calender day of the year.

Horizontal beam radiation is calculated by using (2.25)

$$G_{BH} = G_{PH} cos(\theta_z) \tag{2.25}$$

where G_{PH} is the beam received on perpendicular surface to incoming radiation. The model for G_{PH} proposed by Liu and Jordan is given as follows [84]:

$$G_{PH} = (G_{oh})(\tau^m) \tag{2.26}$$

where G_{oh} is the solar constant (1,360 W/m^2), τ is the atmospheric transmittance and m is the air mass

number. The air mass number (m) is calculated from the following expression [85].

$$m = (P_a)/(101.3 \times \cos(\theta_z)) \tag{2.27}$$

where P_a is the atmospheric pressure in kPa at the site, which is estimated as follows [85]:

$$P_a = 101.3 \times \{\exp -(a/8200)\} \tag{2.28}$$

where *'a'* is the elevation of the site in meter.

All of the beam radiation from the sun can not reach the earth's surface due to the presence of atmospheric gases, clouds and dust particles. Some of the beam radiation scattered towards earth is referred as diffuse radiation. Campbell and Norman [85] derived an empirical relationship based on the work of Liu and Jordan [84] for an estimation of diffuse radiation which is given as follows:

$$G_{DH} = 0.30 \times (1 - \tau^m)(G_{oh}) \cos(\theta_z) \tag{2.29}$$

Table 2.3: RH and atmospheric beam transmittance (τ) data

Serial No.	RH condition	τ value
1	RH=40	0.69
2	(40< RH ≤ 45)	0.67
3	(45< RH ≤ 55)	0.57
4	(55< RH ≤ 65)	0.47
5	(65< RH ≤ 75)	0.41
6	(75< RH ≤ 80)	0.3
7	(RH>80)	0.2

2.3.1 Determination of atmospheric beam transmittance

The percentage of the direct beam radiation passes through the atmosphere without being scattered is called atmospheric beam transmittance (τ). Spokas and Forcella used precipitation data to form decision matrix of atmospheric transmittance [36]. According to the RH values, the atmospheric beam transmittance is assigned in the decision matrix [37] as shown in Table 2.3. The value of τ is modified if $\Delta T < 10$ °C as given in (2.30) and in this condition, it is assumed that the site was not

near the poles [36].

$$\tau' = \tau/(11 - \Delta T) \tag{2.30}$$

The algorithm to determine beam transmittance was made based on decision matrix. Hourly atmospheric transmittance is determined by using the algorithm which is given in [37], and then hourly GSI is estimated using the hourly transmittance values.

2.3.2 Results and discussion of estimation of GSI

The meteorological data, such as longitude, latitude in radian, day length in hours, RH, and AT are collected from Regional Meteorological Center, Guwahati to estimate the GSI on a horizontal surface. We have taken Guwahati meteorological data, such as RH and AT on an hourly basis of each day for 12 months to estimate the GSI on an hourly basis of each day by using MATLAB program. In this work, 100 kW, PV panels installed horizontally in the Bijulee Bhawan, ASEB, Guwahati having longitude = 91.73°, latitude = 26.18° and elevation 55.5 m is considered.

The maximum GSI during the sunshine hours at midday (i.e., 12 o'clock) for monthly averaged daily in the month of March 2012 to February 2013, RH and AT is given in Table 2.4. It is observed from the Table that the solar irradiation is high in the month of March 2012 and less in the month of December 2012. Since the RH is low and temperature is high in the month of March 2012 as compared to all other months in a year is presented in Table 2.4, the GSI is high. The GSI is low in the month of December 2012 due to the RH is high and the temperature is low.

2.4 Estimation of MPP of a PV array

The values of the voltage and current at MPP operation under different temperature and irradiance conditions is calculated backwards from the estimated values of V_{oc}, I_{sc}, R_s, R_{sh} and V_t. To estimate V_{mp}, we can rewrite (2.9) as follows:

$$V_{mp} = (I_{sc} - I_{mp}) \times F - R_{sh} \times E \tag{2.31}$$

where

$$E = \left(I_{sc} - \frac{V_{oc} - I_{sc}R_s}{R_{sh}}\right)\left\{\exp\left(\frac{V_{mp} + I_{mp}R_s - V_{oc}}{n_s V_t}\right)\right\} \qquad \textit{and}$$

$$F = R_s + R_{sh}$$

Table 2.4: Estimated monthly averaged daily maximum GSI during sunshine hours

Month	Sunshine time at midday	RH %	AT (°C)	Gmax (W/m^2)
March-2012	12	39.87	28.82	907.54
April-2012	12	69.53	27.64	754.67
May-2012	12	68.80	29.78	808.92
June-2012	12	83.80	29.19	660.11
July-2012	12	78.48	30.53	779.13
August-2012	12	73.12	30.99	781.38
September-2012	12	77.72	28.91	664.19
October-2012	12	71.65	27.53	549.07
November-2012	12	62.17	23.52	500.36
December-2012	12	66.16	19.88	430.59
January-2013	12	58.74	18.88	570.41
February-2013	12	48.67	23.44	737.01

The values of I_{mp} and V_{mp} at different environmental conditions on hourly basis are calculated by solving two non-linear equations (2.10) and (2.31) using LM method. The LM algorithm [80], [86] is written as follows:

$$x_{i+1} = x_i - (\boldsymbol{J}^T(x_i)\boldsymbol{J}(x_i) + \lambda I)^{-1}\boldsymbol{J}^T(x_i)\boldsymbol{e}(x_i) \tag{2.32}$$

where x_i is the present weight, x_{i+1} is the next weight, $\boldsymbol{J}(x_i)^T\boldsymbol{J}(x_i)$ $(= \boldsymbol{H}(x_i))$ Hessian matrix evaluated at x_i, $e(x_i)$ is the error vector, and λ is combination coefficient and it is always positive. A flowchart for LM algorithms is shown in Figure 2.2. In this flowchart, $E(x_{i+1})$ and $E(x_i)$ are the present and the last total errors, respectively. The LM method behaves as two methods such as steepest descent and Gauss-Newton based on different orders of gradient. The LM method begins with the steepest descent to take advantage of its low sensitivity to initial values and when the calculated value close to the final solution, the LM method behaves Gauss-Newton as its advantage is allowing a fast convergence rate. The automatic switching sequence of LM method from steepest descent to Gauss-Newton is controlled by the parameter λ. When the LM method behaves as steepest descent, the parameter λ play a crucial rule and the Hessian matrix $(\boldsymbol{J}^T(x_i)\boldsymbol{J}(x_i) + \lambda I)$ in (2.32) becomes dominant in diagonal, but when the LM method behaves as Gauss-Newton stage, the parameter λ changes automatically and takes small value, this ensures that the Hessian $\boldsymbol{J}(x_i)^T\boldsymbol{J}(x_i)$ outweighs the matrix λI. If the error

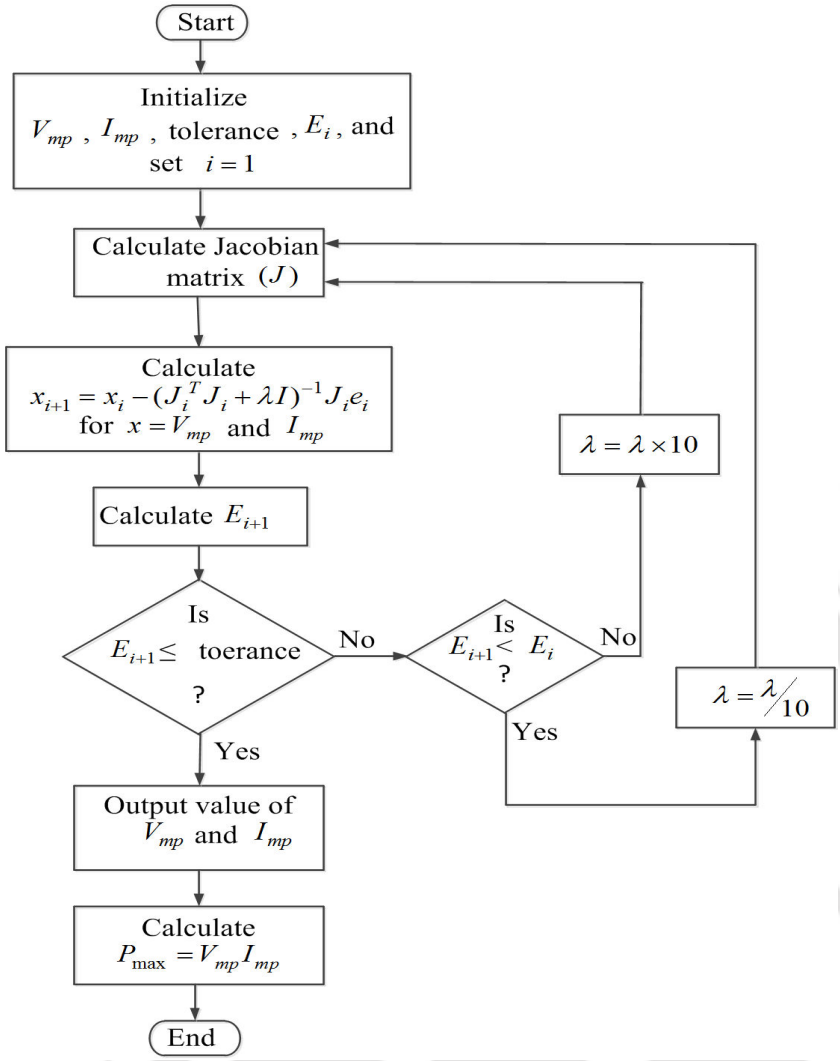

Figure 2.2: Algorithm for estimation of MPPT by using LM method.

is decreased after updated the above algorithm (2.32) then reduce λ value by a factor 10 to reduce the gradient descent and if the error is increased after updated the above the algorithm then increases λ value by a factor 10 to increase the gradient. Once the algorithm is converged, it will give voltage and current at MPP, in return, it will give maximum power (P_{max}) generation of a PV array on an hourly basis during sunshine hour which is expressed as follows:

$$P_{max} = V_{mp}I_{mp} \tag{2.33}$$

For estimation of maximum power of a PV array on hourly basis, the detail procedure is presented in the block diagram as shown in Figure 2.3.

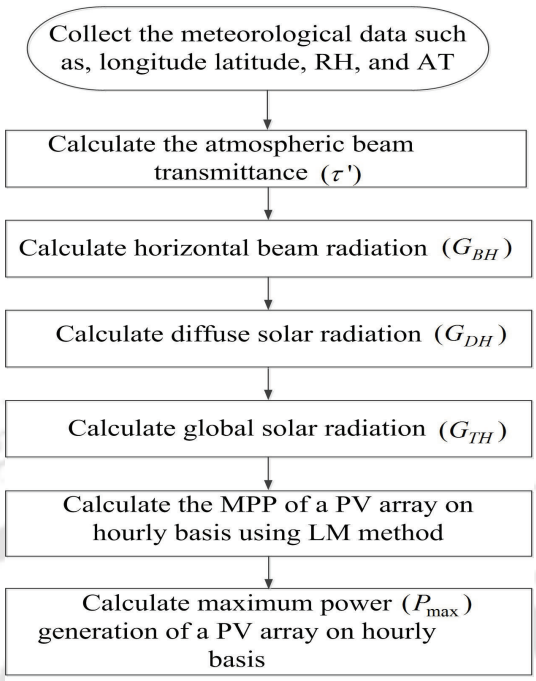

Figure 2.3: Conceptual flow for calculation of P_{max}.

2.4.1 Results and discussion of estimation MPP of a PV array

The variation of an actual power (P_{act}) and an estimated power (P_{est}) in kW with sunshine time in hours of March 2012 to February 2013 on monthly averaged daily and hourly basis is shown in Figure 2.4.

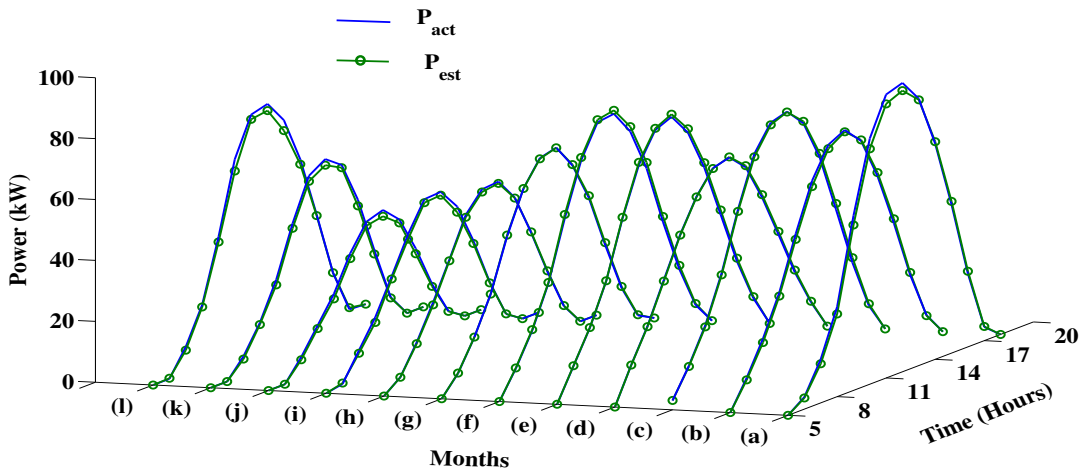

Figure 2.4: Power output of a PV array during sunshine hours for the month (a) March 2012, (b) April 2012, (c) May 2012, (d) June 2012, (e) July 2012, (f) August 2012, (g) September 2012, (h) October 2012, (i) November 2012, (j) December 2012, (k) January 2013 and (l) February 2013.

The actual maximum power of a PV array for corresponding GSI and AT in hourly basis during sunshine hours is calculated by plotting the P-V curve using (2.1) - (2.3). The peak value of power in P-V characteristics of a PV array in each sunshine hour are taken as actual maximum power. The MPP of a PV array in each hour is estimated by taking the irradiation and temperature dependant V_{oc} and I_{sc}. The MPP of a PV array is estimated by using LM method. It is observed that the estimated maximum power of a PV array on monthly averaged daily and hourly basis is nearly equal to the actual maximum power on an hourly basis of all the twelve month from March 2012 to February 2013. The maximum power generated in a month of March 2012 is more as compared to other months in a year from March 2012 to February 2013, and in December 2012, the maximum power generated by a PV array is low as seen from the Table 2.5. The power generation of a PV array mainly depends upon GSI. As the GSI in March 2012 is more as compared to other months, the power generation in this month is more and in the month of December 2012 the irradiation is low, so power generation is low. The percentage (%) error of an estimated maximum power ($P_{\max,(est)}$) in the monthly averaged daily

Table 2.5: Monthly averaged daily actual maximum power and estimated maximum power generation of the PV array

Month	Sunshine time at midday	P_{max} generation in monthly averaged daily		
		Max P_{act} (kW)	Max P_{est} (kW)	Relative error (%) (w.r.t. P_{act})
March 2012	12	94.82	92.31	2.64
April 2012	12	78.46	77.88	0.74
May 2012	12	83.60	83.46	0.16
June 2012	12	67.62	67.81	-0.27
July 2012	12	80.08	80.93	-1.06
August 2012	12	80.15	81.30	-1.44
September 2012	12	68.15	68.09	0.08
October 2012	12	56.09	55.51	1.02
November 2012	12	51.81	50.73	2.08
December 2012	12	44.97	42.91	4.57
January 2013	12	60.77	58.79	3.27
February 2013	12	78.00	75.81	2.80

and hourly basis with respect to (w.r.t.) actual maximum power ($P_{\max,(act)}$) is calculated as follows:

$$(\%)Error = \frac{P_{\max,(act)} - P_{\max,(est)}}{P_{\max,(act)}} \times 100 \tag{2.34}$$

The relative errors of $P_{\max,(est)}$ w.r.t. $P_{\max,(act)}$ in each sunshine hour of monthly averaged daily and hourly are minimal as shown in Table 2.5. It is investigated from the results that, the performance of the proposed method to estimate the maximum power of a PV array on an hourly basis is accurate, and it will help the PV plant promotors to estimate MPP of a PV array in real environmental condition for grid integration. The PV stations which are installed for grid integration, they can estimate the solar power on an hourly basis using the proposed numerical method. Thus it becomes helpful for integration of PV stations to the microgrid.

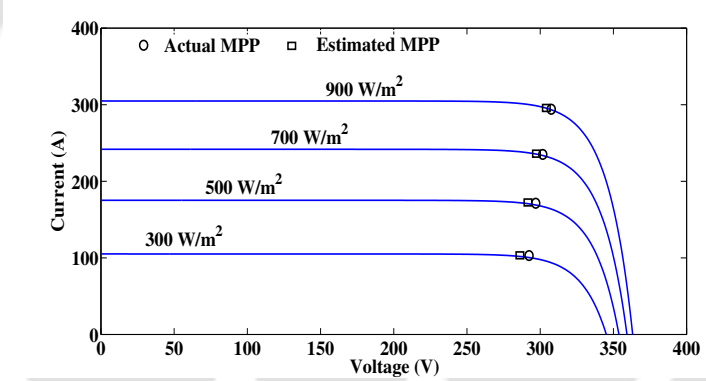

(a)

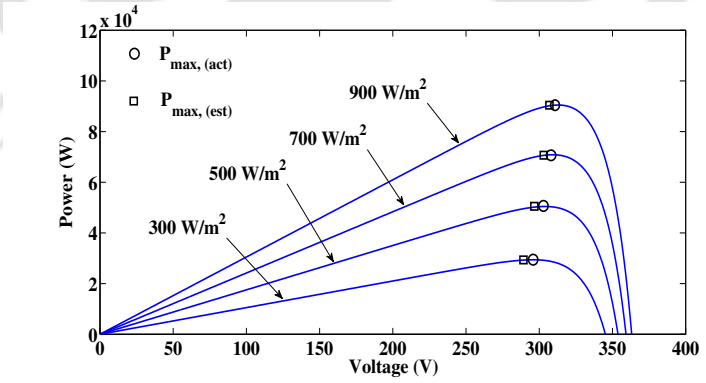

(b)

Figure 2.5: (a) I-V and (b) P-V characteristics of a 100 kW PV array at a temperature of 25 °C with varying irradiations.

For the demonstration of the proposed method to estimate the MPP of a 100 kW PV array under different environmental conditions is considered. The I-V and P-V characteristics of a PV array at a

temperature of 25 °C with varying irradiations are presented in Figure 2.5(a) and (b) respectively.

Table 2.6: MPP of a 100 kW PV array at a temperature of 25 °C with varying irradiations

Temperature (°C)	Irradiation (W/m^2)	V_{mp} (V)	I_{mp} (A)	$P_{max,(est)}$ (kW)	$P_{max,(act)}$ (kW)	(%) Error of $P_{max,(est)}$ w.r.t. $P_{max,(act)}$	Time taken to achieve $P_{max,(est)}$, t_{MPP} (s)
25	300	294.61	98.99	29.16	29.93	2.57	0.007623
	500	299.91	165.14	49.52	50.38	1.70	0.007658
	700	301.99	231.18	69.81	70.75	1.32	0.007493
	900	302.56	297.08	89.88	90.43	0.60	0.007757

It is observed that the $P_{max,(est)}$ by using LM algorithm varies from 29.16 to 89.88 kW and the $P_{max,(act)}$ obtained from the curve varies from 29.93 to 90.43 kW with the increase of solar irradiation as given in Table 2.6. The V_{mp} and I_{mp} of a PV array increases with an increase of solar irradiation, therefore the power generation of a PV array increases. It is observed that there is a minimal error between the $P_{max,(est)}$ and the $P_{max,(act)}$ under different operating conditions as given in Table 2.6 and therefore, the proposed method is more accurate.

A comparison of LM method with three different existing methods such as PO based on proportional-integral (PI), GA and GS in terms of optimal solution, i.e., MPP and time required to achieve the MPP (t_{MPP}) is carried out by Matlab simulation for a 250 W PV module as given in Table 2.1. The simulation results of above different methods for the MPP of a 250 W PV module at a temperature of 25 °C with varying irradiations are presented in Table 2.7. The $P_{max,(act)}$ of 201, 125.30, and 48.60 W under different solar irradiations, such as 800, 500, and 200 W/m^2, respectively, are obtained from the P-V characteristics of a module at a temperature of 25 °C. In PO based on PI method, the maximum power of 198.68, 122.76, and 46.86 W of a PV module are achieved after a time duration i.e., t_{MPP} of 0.25, 0.99, and 1.92 s with an irradiations of 800, 500, and 200 W/m^2, respectively, as shown in Figure 2.6(a). Considering the population size of 100, a crossover fraction of 0.811 and tournament function in GA method, the maximum power of 196.58, 122.52, and 45.89 W of a PV module are achieved after time duration i.e., t_{MPP} of 12.63, 32.65, and 58.64 s with an irradiations of 800, 500, and 200 W/m^2, respectively, as shown in Figure 2.6(b). From Table 2.7, it is observed that the maximum power obtained from the PV module by LM method is more or less same as the actual maximum power of the same module and also t_{MPP} is less as compared with the other existing methods under

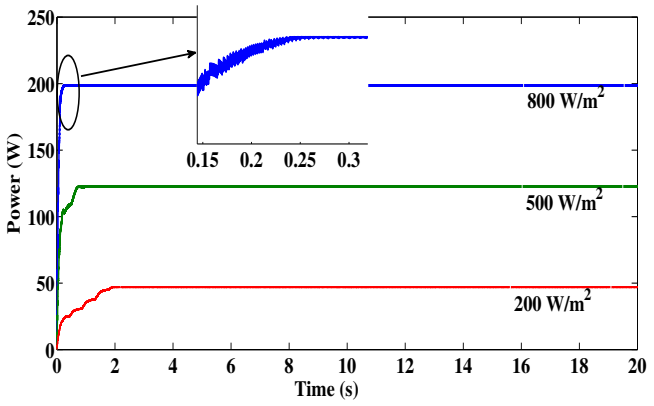

(a)

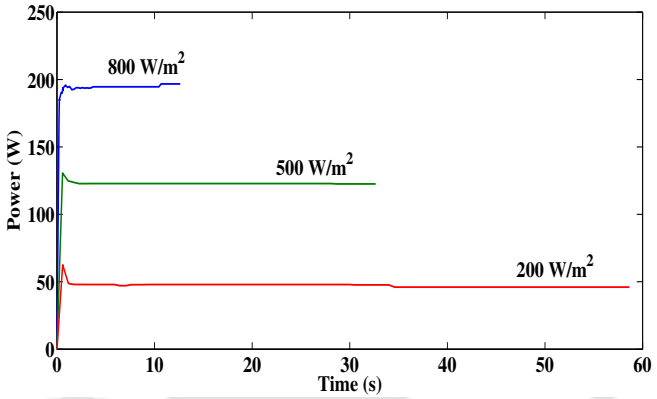

(b)

Figure 2.6: (a) Maximum power generation in PO based on PI method and (b) maximum power generation in GA method.

different environmental conditions. Hence, the estimation of MPP of a PV module by the proposed method is more accurate and computationally efficient.

For the demonstration of the tracking performance of different MPPT methods to estimate the MPP of a 250 W PV module under rapid change of solar irradiations at different instant of time are considered as shown in Figure 2.7(a). In the present analysis to obtain the output power variation of above mentioned PV module, due to sudden change of solar irradiation from 800 to 400 W/m^2 at 5 s, 400 to 600 W/m^2 at 15 s, 600 to 300 W/m^2 at 23 s, and 300 to 800 W/m^2 at 30 s, respectively, are considered. The $P_{max,(act)}$ of 201, 150, 99.60, and 74.50 W under different solar irradiations, such as 800, 600, 400, and 300 W/m^2, respectively, are obtained from the P-V characteristics of a module at a temperature of 25 °C. It is observed from Figure 2.7(b) that for a sudden change of solar irradiation from 800 to 400 W/m^2 at 5 s, the t_{MPP} in the PO based on PI, GS, and LM methods are 0.95, 0.1293,

Table 2.7: A comparison of MPP of a 250 W PV module at a temperature of 25 °C with varying irradiations

Different MPPT methods	Irradiation (W/m^2)	V_{mp} (V)	I_{mp} (A)	$P_{max,(est)}$ (W)	(%) Error of $P_{max,(est)}$ w.r.t. $P_{max,(act)}$	t_{MPP} (s)
PO based on PI	200	28.75	1.63	46.86	3.58	1.92
	500	29.87	4.11	122.76	2.02	0.99
	800	30.15	6.59	198.68	1.15	0.25
GA	200	27.48	1.67	45.89	5.57	58.64
	500	28.56	4.29	122.52	2.21	32.65
	800	28.74	6.84	196.58	2.19	12.63
GS	200	28.38	1.66	47.11	3.06	0.1241
	500	29.65	4.13	122.45	2.19	0.1436
	800	30.05	6.62	198.93	1.02	0.1102
LM	200	29.07	1.64	47.67	1.91	0.0074
	500	30.10	4.12	124.01	1.02	0.0072
	800	30.30	6.60	199.98	0.50	0.0076

and 0.0072 s, respectively. Similarly, the variation of power w.r.t. time and t_{MPP} for the rapid change of aforementioned irradiations at 15, 23, and 30 s, respectively, are presented in Fig. 2.7(b). The amount of energy loss during t_{MPP} by a given MPPT method is calculated by subtracting the amount of energy obtained from the actual maximum energy available during the above tracking duration. Hence, the percentage of energy loss during t_{MPP} is calculated as follows:

$$(\%)Energy \quad loss = \frac{Energy \quad loss \quad by \quad MPPT \quad method \quad during \quad t_{MPP}}{Actual \quad maximum \quad energy \quad available \quad during \quad t_{MPP}} \times 100 \qquad (2.35)$$

The simulation results of t_{MPP}, energy obtained, energy loss, and % of energy loss during t_{MPP} for three different MPPT methods during rapid change of aforementioned irradiation at 5, 15, 23, and 30 s are presented in Table 2.8. It is observed that t_{MPP} and the % of energy loss during t_{MPP} in LM method is less as compared with the other existing methods for the aforementioned rapid variation of solar irradiations. Therefore, the estimation of MPP of a PV module by the proposed method is more accurate and computationally efficient for rapid change of solar irradiation conditions.

2.5 Experimental validation

To validate the proposed LM algorithm for the estimation of MPP of a PV module, a laboratory scale experimental setup was developed on the roof of the Department of Electronics and Electrical Engineering, IIT Guwahati as shown in Figure 2.8. The experimental setup was prepared by taking

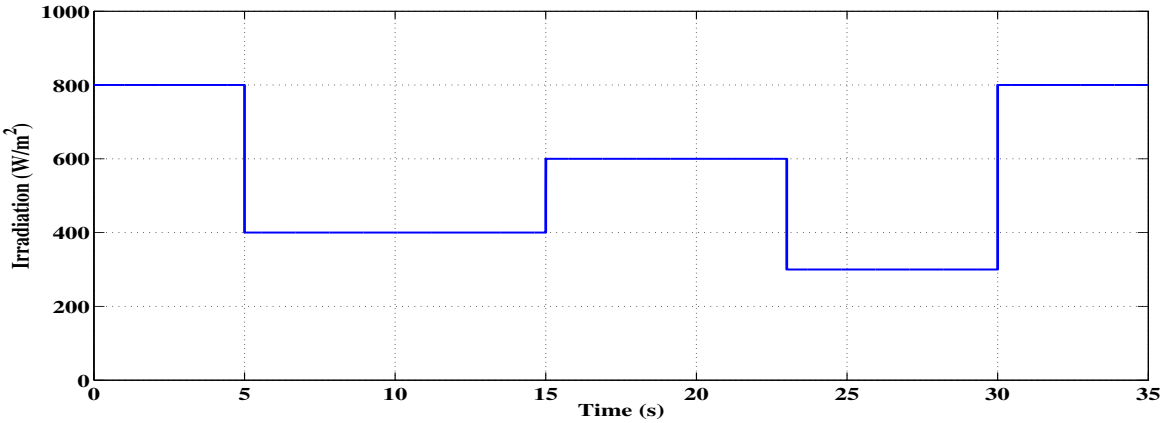

(a)

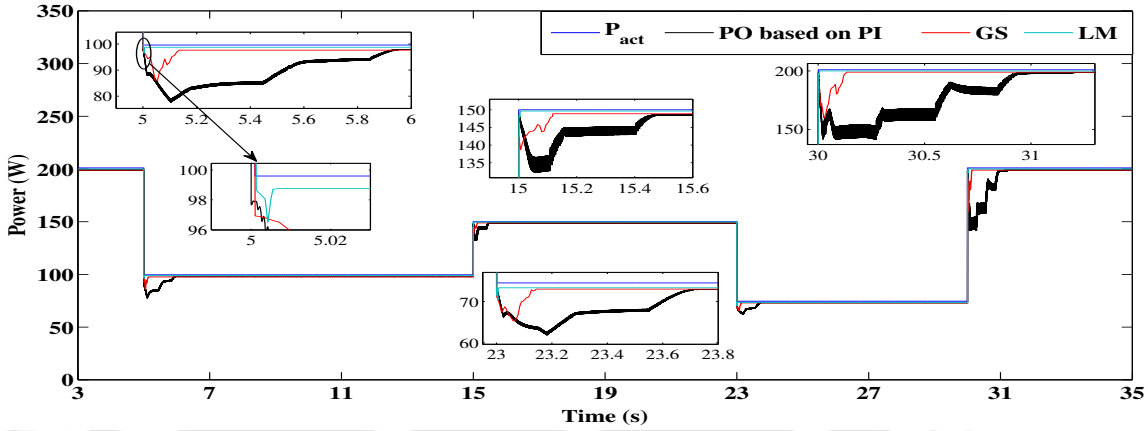

(b)

Figure 2.7: (a) Variation of solar irradiation w.r.t. time and (b) maximum power obtained during change of irradiation condition by PO based on PI, GS, and LM method.

a PV modules of rating 15 W, one rheostat (300 Ω, 2A), two multimeters, connecting wires, and the transparent sheets of different color to create the different intensity of solar irradiation. The datasheet values of a 15 W PV module provided by the manufacturer are I_{sc} = 0.92 A, V_{oc} = 21.0 V, V_{mp} = 17.60 V, I_{mp} = 0.85 A, and N_s = 36, k_i = 0.06 % and k_v = - 0.33 %. The power generated from a PV module is estimated from the current measured by multimeter connected in series with rheostat and the voltage measured by multimeter connected across the rheostat.

The level of solar irradiation at the time of the experiment (11:30 AM, 4th June 2015) is calculated by using (2.19) and the data sheet values of the module. The temperature was measured by the temperature sensor (i.e., 32 °C) at the time of experiment. The solar irradiation calculated at the time of performing an experiment was 910 W/m^2, and other different levels of solar irradiation, such as

Table 2.8: A comparison of tracking performance of different MPPT methods during rapid change of solar irradiation conditions

Solar irradiation variation in W/m^2	Different methods	t_{MPP} (s)	Energy obtained during t_{MPP} (J)	Energy loss during t_{MPP} (J)	(%) Energy loss
800 to 400	PO based on PI	0.95	82.42	12.20	12.89
	GS	0.1293	11.64	1.23	9.55
	LM	0.0072	0.6703	0.0468	6.52
400 to 600	PO based on PI	0.47	65.60	4.90	6.95
	GS	0.1179	16.76	0.92	5.20
	LM	0.0073	1.054	0.0410	3.74
600 to 300	PO based on PI	0.70	46.63	5.52	10.58
	GS	0.1462	9.92	0.97	8.90
	LM	0.0075	0.5294	0.0293	5.24
300 to 800	PO based on PI	1.22	202.29	42.93	17.50
	GS	0.1352	23.14	4.03	14.83
	LM	0.0074	1.3724	0.1150	7.73

Figure 2.8: Laboratory scale experimental setup.

820, 696, 560, 400, 340, and 188 W/m^2 are obtained by putting different thickness and colors of transparent sheets on the modules. The I-V and P-V characteristics of a 15 W PV module are shown in Figure 2.9(a) and (b) respectively. The $P_{max,(est)}$ of a PV module is closely equal to the $P_{max,(act)}$, but there is a small variation between measured and estimated maximum power as shown in Table 2.9. The small variation in power is due to the slight change in solar irradiation and temperature at the time of conducting the experiment and mismatch in the cell parameters.

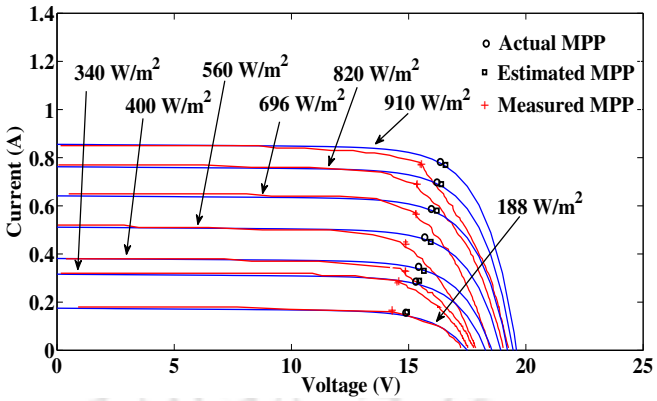

(a)

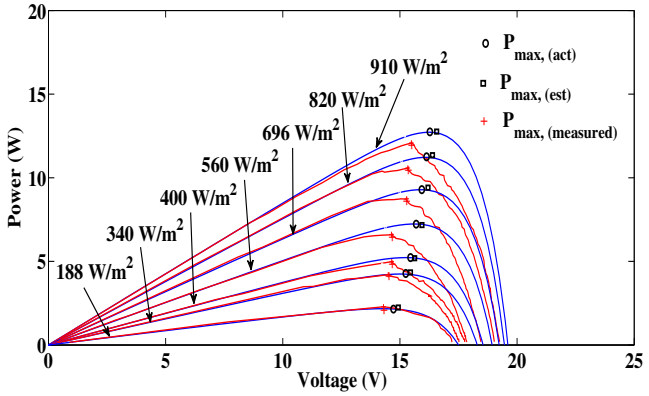

(b)

Figure 2.9: (a) I-V and (b) P-V curve of a PV module at a temperature of 32 °C with varying irradiations.

Table 2.9: MPP of a PV module at a temperature of 32 °C with varying irradiations

Temperature (°C)	Irradiation (W/m^2)	V_{mp} (V)	I_{mp} (A)	$P_{max,(est)}$ (W)	$P_{max,(measured)}$ (W)	$P_{max,(act)}$ (W)	(%) Error of $P_{max,(est)}$ w.r.t. $P_{max,(act)}$	(%) Error of $P_{max,(est)}$ w.r.t. $P_{max,(measured)}$
32	188	14.93	0.15	2.24	2.28	2.22	-0.90	1.75
	340	15.45	0.28	4.34	4.20	4.23	-0.02	-3.33
	400	15.63	0.33	5.19	4.95	5.22	0.57	-4.89
	560	15.94	0.45	7.17	6.61	7.23	0.82	-8.47
	696	16.20	0.58	9.41	8.74	9.28	-1.40	-7.66
	820	16.39	0.69	11.35	10.58	11.22	-1.15	-7.27
	910	16.57	0.77	12.76	12.08	12.72	-0.31	-5.62

2.6 Estimation of MPP of a PV array under PSC

Partial shading occurs due to the moving clouds or shadows of nearby trees or house. Under PSC, the modules of a PV array receive nonuniform solar irradiation, and therefore, there is a mismatch between the current of the module [16]. Since the shaded modules generate less current than the

unshaded modules and the current of shaded modules limits the output current of a PV array, the power generation of a PV array under partial shading reduces. For the demonstration of the proposed method to estimate the MPP, a 5 × 5 PV array is considered for SP connection of identical modules of rating 250 W as given in Table 2.1, under two different shading conditions. In the present study two different types of shading scenario (case-I and case-II) as shown in Figure 2.10(a) and (b) are considered. Since the I-V curve near the MPP is dominated by diode behavior, and so the R_s and R_{sh} are neglected in the present analytical analysis [87]. Therefore, the current flowing across each string of a SP connection (without bypass diode) for an ideal diode of a PV module [23] is given as follows:

$$I_j = I_{phj} - I_o \left\{ \exp\left(\frac{V}{N_s V_t}\right) - 1 \right\} \tag{2.36}$$

where 'j' is the number of strings (i.e. j = 1, 2, .., 5) in a PV array. I_{phj} is the lowest value of photo generated current of the modules connected in series of j^{th} string of a PV array under shading condition and I_{ph} is directly proportional to solar irradiation.

$$I = \sum_{j=1}^{5} I_{phj} - 5I_o \left\{ \exp\left(\frac{V}{NsV_t}\right) - 1 \right\} \tag{2.37}$$

The derivative of current in (2.37) w.r.t. voltage can be written as follows:

$$\frac{dI}{dV} = -\frac{5I_o}{N_s V_t} \exp\left(\frac{V}{N_s V_t}\right) \tag{2.38}$$

The power generation of the PV module at any point on the I-V curve is given as follows:

$$P = VI \tag{2.39}$$

Now the derivative of power w.r.t. voltage, (2.39) can be written as follows:

$$\frac{dP}{dV} = I + \left(\frac{dI}{dV}\right) V \tag{2.40}$$

Substituting (2.7) into (2.40), yield

$$\frac{dI}{dV} = -\frac{I_{mp}}{V_{mp}} \tag{2.41}$$

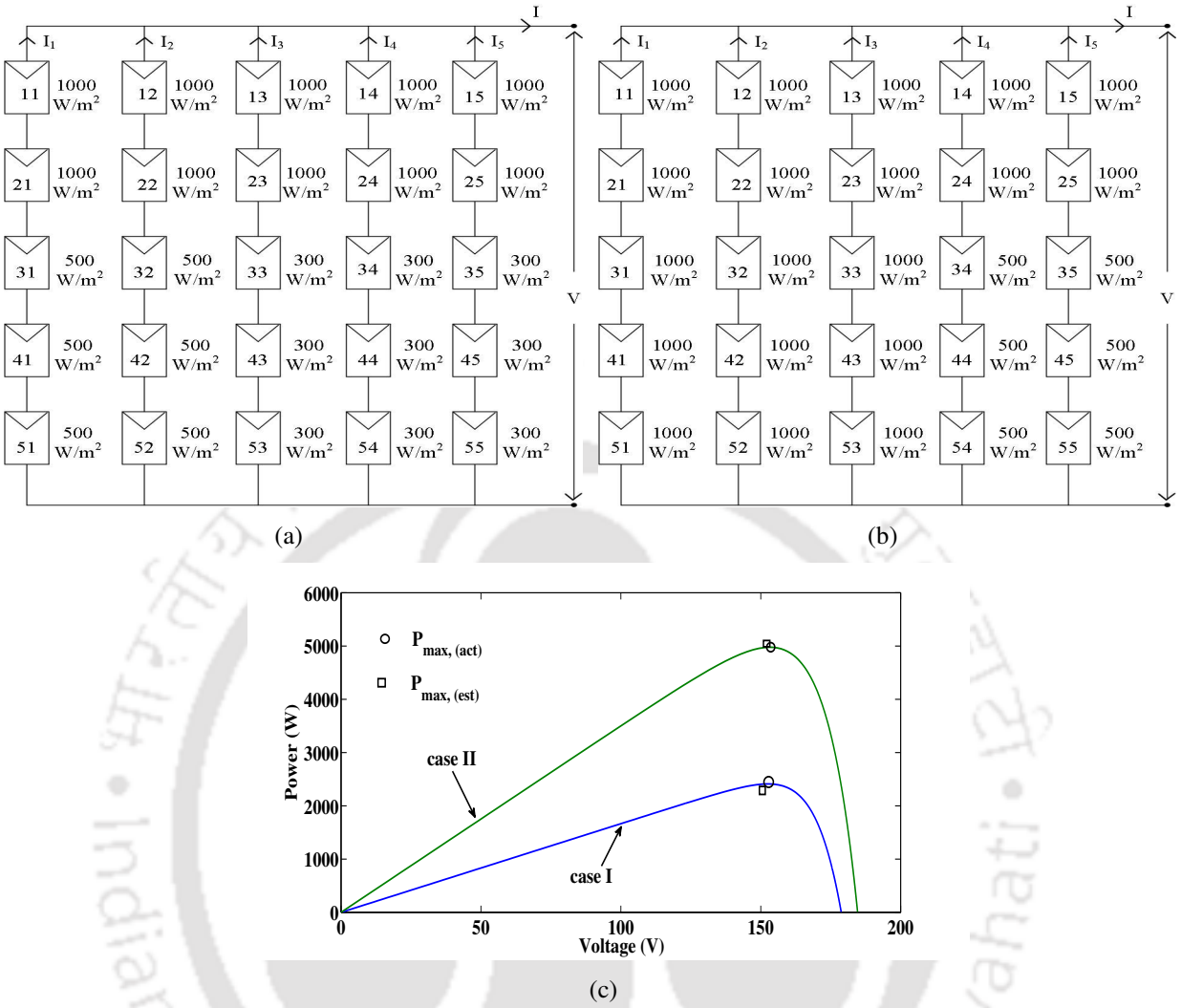

Figure 2.10: (a) case-I shading condition, (b) case-II shading condition and (c) P-V curve.

Substituting the value of $\frac{dI}{dV}$ from (2.41) in (2.38), the resulting equation is written as follows:

$$\frac{I_{mp}}{V_{mp}} = \frac{5I_o}{N_s V_t} \exp\left(\frac{V_{mp}}{N_s V_t}\right) \tag{2.42}$$

At MPP (2.37) can be written as follows:

$$I_{mp} = \sum_{j=1}^{5} I_{phj} - 5I_o \left\{\exp\left(\frac{V_{mp}}{N_s V_t}\right) - 1\right\} \tag{2.43}$$

The above two nonlinear equations (2.42) and (2.43) are solved by using LM algorithm to obtain two unknown parameters, i.e., V_{mp} and I_{mp} and then estimated $P_{max,(est)}$ is calculated by multiplying V_{mp} and I_{mp}.

In the first string, the current generated by the modules 31 (500 W/m^2), 41 (500 W/m^2), 51 (500

W/m^2) is the lower value than the current generated by the modules 11 (1000 W/m^2), 21 (1000 W/m^2) as shown in Figure 2.10(a). So the lowest current generated by the module (which receive low solar irradiation) is flowing in the string because of a series connection of the PV modules in a string. So the current flowing in the first and second string is the current generated by the modules receive low solar irradiation, i.e., 500 W/m^2 and similarly, the current flowing in the string third, fourth and fifth is the current generated by the modules receive low solar irradiation, i.e. 300 W/m^2. Thus the current generated by a PV array is the sum of the current of each strings. Neglecting the small variations in voltage of each module under PSC, the voltage of each string is consider to be V. Therefore, the voltage of an array is same as the string voltage.

The P-V curve of a PV array for the two different shading conditions (case-I and case-II) is plotted by using MATLAB simulation as shown in Figure 2.10(c). The $P_{\max,(est)}$ of the array is denoted by small square in the P-V curve. From Figure 2.10(c), it is observed that the $P_{\max,(est)}$ is more or less same as $P_{\max,(act)}$ and a minor deviation between the two powers is presented in Table 2.10.

Table 2.10: MPP of a PV array under two different shading conditions

Shading conditions	V_{mp} (V)	I_{mp} (A)	$P_{max,(est)}$ (W)	$P_{max,(act)}$ (W)	(%) Error
case-I	149.62	15.75	2357.0	2410.0	2.19
case-II	150.94	33.25	5019.0	4977.0	-0.84

2.7 Summary of the chapter

PV array modeling and MPP estimation are needed for the integration of solar power into the microgrid. Also, proper estimation of weather dependent GSI is essential for the estimation of MPP of a PV array. The monthly averaged daily and hourly GSI is estimated for a certain location on the surface of the earth by using empirical relations by taking RH and AT data. The important conclusions drawn from this work are reported below.

1. It is observed that when the RH is less and the temperature is more than 25 °C, the GSI is more i.e. in the month of Mar-2012.

2. The MPPT of a PV array is estimated numerically by using the LM algorithm based on the characteristic equation for different irradiation and temperature during sunshine hours of each day.

The $P_{\max,(est)}$ and $P_{max,(act)}$ of a PV array of monthly average daily and hourly basis are presented in power versus sunshine time in hours characteristics. It is observed that the deviation of the $P_{\max,(est)}$ of a PV array and the $P_{max,(act)}$ on an hourly basis is minimal.

3. The MPP results estimated by using the LM algorithm of a 15 W PV module under different environmental conditions are validated with the actual and experimental results. It is observed that the deviation of estimated MPP w.r.t. actual and measured MPP are minimal.

4. The MPPT of a PV array under PSC is estimated numerically by using the proposed algorithm and the estimated MPP results closely match with the actual MPP of a PV array.

Also a comparison of LM method with three different existing methods such as PO based on PI, GA and GS is presented. From the simulation results, it is observed that the accuracy of the proposed method is high and the time taken to achieve the MPP of a PV array is less as compared with the other methods. Therefore, the proposed method is robust, accurate and computationally efficient. Thus, this proposed numerical method will help the PV plant promoters to estimate the MPP of a PV array under uniform and nonuniform (partial shading) conditions.

In this chapter, the MPP of a PV array is estimated numerically by solving (2.10) and (2.31) using LM method. In the next chapter, instead of solving above two equations, a simple explicit expression of current (i.e., current is a function of voltage only) derived from an implicit current expression, is solved using bisection method (BM) for MPP tracking of an SDM PV module accurately and efficiently.

Note: This work, Numerical approach to estimate the maximum power point of a photovoltaic array has been published in IET Generation, Transmission & Distribution.

3

MPPT of a PV Module from Current-Voltage Explicit Expression

Contents

3.1 Introduction

The PV system converts light energy into electrical energy without any environmental pollution [78]. The output power of a PV source varies with different environmental conditions. The output current and voltage relationship of the PV array is highly nonlinear and depends on the solar irradiation and temperature conditions. Thus, an estimation of MPP of a PV array under DEC is not simple. Many researchers have proposed different methods to track the MPP of the PV array [38]. MPPT methods are used to track the MPP of a PV module at which the module operates and the MPP lies in the power region of the I-V or P-V curve [88]. In this power region, the MPP will deliver an actual maximum power from the PV module. The more popular MPPT techniques are fractional OCV (V_{frac}) and fractional SCC [53]. However, the accuracy of these methods are not good enough, and hence, power losses occur in these methods. The AI techniques such as neural fuzzy logic, neural network and GA [50–52] have been used for the MPPT of a PV module. However, the AI techniques are computationally demanding, and their practical implementation is difficult. Therefore, the implementation of AI techniques may not be the first choice for many applications. Some of the methods such as, PO [13], IC [89], and HCB [19] do not depend on the characteristics parameters of the PV module. However, the searching nature of these methods are slow to some extent, and hence, these methods are not suitable for the application purpose (i.e., solar car, moving broken clouds) due to the rapid change of environmental conditions.

In order to overcome the aforementioned limitations, a novel mathematical explicit function is derived from the implicit I-V function of the PV module to estimate the MPP of a module accurately with less computational cost. Since the explicit I-V function is used for the estimation of MPP of a PV module under DEC, it ensures simple, accuracy and computationally efficient. A comparative study of MPPT of a PV module in different existing methods for the steady and rapid change of solar irradiation conditions has been carried out, and it is observed that the proposed method is more accurate and computationally efficient. For validation of the proposed method, the maximum power obtained in the simulation and experimentally for a 250 W PV module under DEC are compared, and the results show that the performance of the proposed method is superior to the existing methods.

3.2 Parameters estimation of an SDM PV module

The datasheet values of the parameters of 250 W PV module are given in Table 3.1(a). The values of the unknown PV parameters such as V_t, R_s and R_{sh} are estimated at STC by solving (2.9)-(2.11) of Chapter 2 by using LM method as shown in Figure 3.1. The value of *'A'*, I_o, and I_{ph} are calculated from (2.2), (2.12) and (2.13), respectively. The estimated value of the module parameters such as I_{ph}, I_o, R_s, R_{sh}, and *'A'* are given in Table 3.1 (b).

Table 3.1: PV Parameters

(a) Datasheet values

Module Parameters	Actual Values
I_{sc}	7.60 A
V_{oc}	44.0 V
V_{MP}	36.0 V
I_{MP}	7.0 A
N_s	72
k_i	0.05 %
k_v	- 0.36 %

(b) Estimated values

Module Parameters	Estimated Values
I_{ph}	7.60 A
I_o	0.71404 μA
A	1.4717
R_s	0.1164 Ω
R_{sh}	566.0928 Ω

3.3 Conversion of implicit to explicit form of I-V characteristic of an SDM PV module

The implicit I-V relationship of an SDM is written as follows:

$$I_{pv} = I_{ph} + I_o - I_o \exp\left(\frac{V_{pv} + I_{pv}R_s}{N_s V_t}\right) - \frac{V_{pv} + I_{pv}R_s}{R_{sh}} \tag{3.1}$$

To convert the implicit function (3.1) into an explicit function, the third non-linear term is denoted by *'f'* as follows:

$$f = I_o \exp\left(\frac{V_{pv} + I_{pv}R_s}{N_s V_t}\right) \tag{3.2}$$

Hence, (3.1) is simplified as follows:

$$I_{pv} = I_{ph} + I_o - f - \frac{V_{pv}}{R_{sh}} - I_{pv}\frac{R_s}{R_{sh}} \tag{3.3}$$

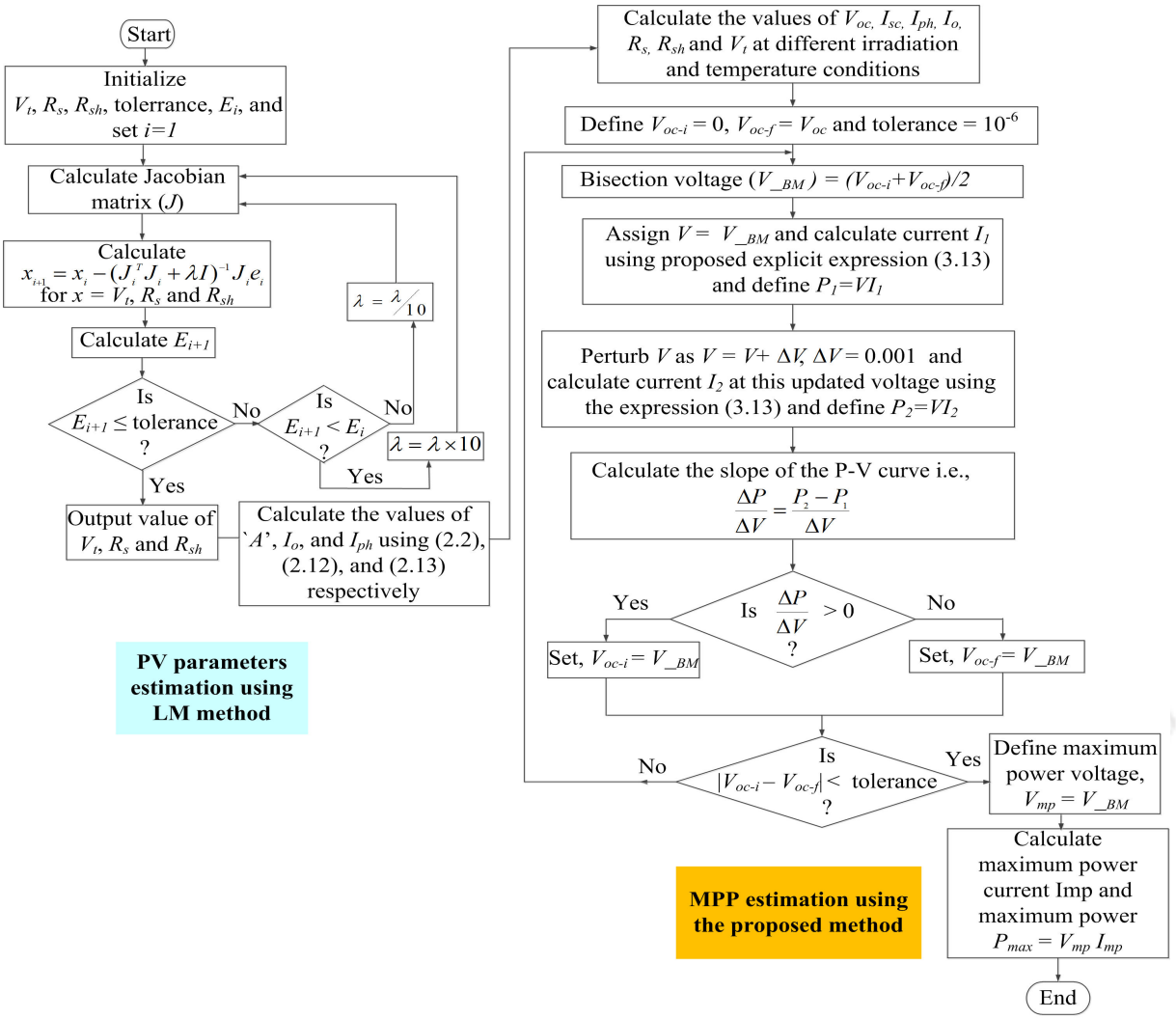

Figure 3.1: Algorithm for estimation of MPP using the proposed explicit expression.

Taking the first and second derivative of 'f' with respect to I_{pv}, (3.4), (3.5) are obtained as follows:

$$\frac{\partial f}{\partial I_{pv}} = I_o \frac{R_s}{N_s V_t} \exp\left(\frac{V_{pv} + I_{pv} R_s}{N_s V_t}\right) \tag{3.4}$$

$$\frac{\partial^2 f}{\partial I_{pv}^2} = I_o \left(\frac{R_s}{N_s V_t}\right)^2 \exp\left(\frac{V_{pv} + I_{pv} R_s}{N_s V_t}\right) \tag{3.5}$$

Since I_o and $\left(\frac{R_s}{N_s V_t}\right)^2$ are very very small, the value of $\frac{\partial^2 f}{\partial I_{pv}^2} \approx 0$ for the I_{pv} between 0 and I_{sc}. Therefore, f-I_{pv} characteristic of a PV module is approximated as a straight line for the current from 0 to I_{sc} at a constant value of voltage (at any voltage from 0 to V_{oc}). The f-I_{pv} characteristics in the afore-mentioned range of current for different value of voltage from 3/4(V_{oc}) to V_{oc} with the increment of 1/20(V_{oc}) for better visualization are plotted in Figure 3.2.

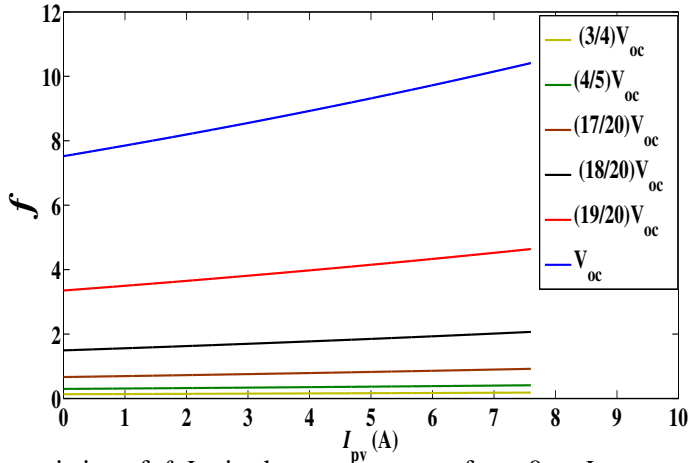

Figure 3.2: Linear characteristics of f-I_{pv} in the current range from 0 to I_{sc} at a constant value of voltage (at any voltage from 0 to V_{oc}).

Therefore, the function f, is defined as follows:

$$f = a(V_{pv})I_{pv} + b(V_{pv}) \tag{3.6}$$

Putting the conditions $I_{pv} = 0$ and $I_{pv} = I_{sc}$ in (3.6), (3.7) and (3.8) are obtained as follows:

$$f|_{I_{pv}=0} = b(V_{pv}) = I_o \exp\left(\frac{V_{pv}}{N_s V_t}\right) \tag{3.7}$$

$$f|_{I_{pv}=I_{sc}} = a(V_{pv})I_{sc} + b(V_{pv}) = I_o \exp\left(\frac{V_{pv} + I_{sc}R_s}{N_s V_t}\right) \tag{3.8}$$

Substituting $b(V_{pv})$ from (3.7) in (3.8)

$$I_o \exp\left(\frac{V_{pv} + I_{sc}R_s}{N_s V_t}\right) = a(V_{pv})I_{sc} + I_o \exp\left(\frac{V_{pv}}{N_s V_t}\right) \tag{3.9}$$

Simplifying (3.9), $a(V_{pv})$ is obtained as follows:

$$a(V_{pv}) = \left(\frac{I_o}{I_{sc}}\right)\exp\left(\frac{V_{pv}}{N_s V_t}\right)\left\{\exp\left(\frac{I_{sc}R_s}{N_s V_t}\right) - 1\right\} \tag{3.10}$$

Substituting $b(V_{pv})$ and $a(V_{pv})$ obtained from (3.7) and (3.10), respectively in (3.6), *'f'* is written as follows:

$$f = \left(\frac{I_o}{I_{sc}}\right)\exp\left(\frac{V_{pv}}{N_s V_t}\right)\left\{\exp\left(\frac{I_{sc}R_s}{N_s V_t}\right) - 1\right\} I_{pv} + I_o \exp\left(\frac{V_{pv}}{N_s V_t}\right) \tag{3.11}$$

After substituting (3.11) in (3.3), the current I_{pv} is written as follows:

$$I_{pv} = I_{ph} + I_o - \left(\frac{I_o}{I_{sc}}\right)\exp\left(\frac{V_{pv}}{N_s V_t}\right)\left\{\exp\left(\frac{I_{sc}R_s}{N_s V_t}\right) - 1\right\} I_{pv} - I_o \exp\left(\frac{V_{pv}}{N_s V_t}\right) - \frac{V_{pv}}{R_{sh}} - I_{pv}\frac{R_s}{R_{sh}} \tag{3.12}$$

Simplifying (3.12), the explicit expression of I_{pv} is obtained as follows:

$$I_{pv} = \frac{I_{ph} - I_o\left\{\exp\left(\frac{V_{pv}}{N_s V_t}\right) - 1\right\} - \frac{V_{pv}}{R_{sh}}}{\left(\frac{I_o}{I_{sc}}\right)\exp\left(\frac{V_{pv}}{N_s V_t}\right)\left\{\exp\left(\frac{I_{sc}R_s}{N_s V_t}\right) - 1\right\} + \frac{R_s}{R_{sh}} + 1} \tag{3.13}$$

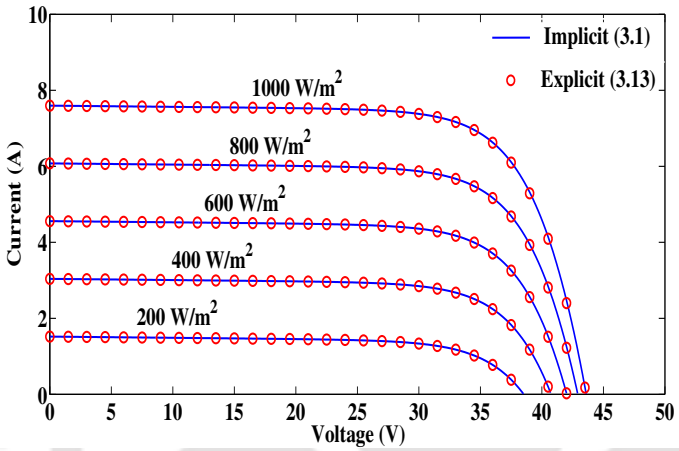

(a)

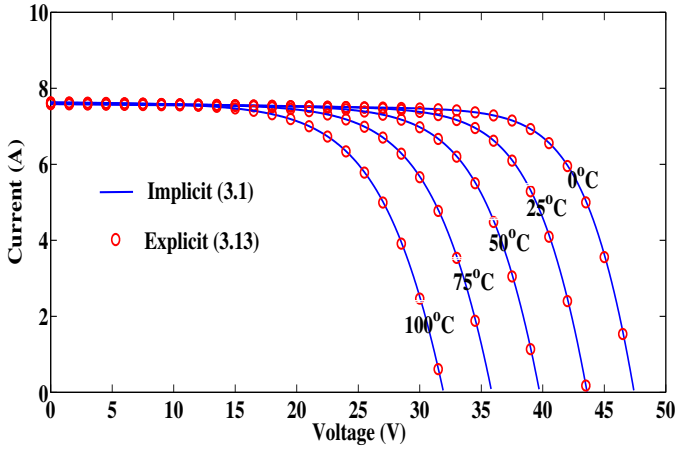

(b)

Figure 3.3: I-V characteristics of a 250 W PV module under (a) different irradiation with a fixed temperature of 25 °C and (b) different temperature with a fixed irradiation of 1000 W/m^2.

The explicit I-V function (3.13) is used to calculate the current at the estimated voltages in each step of bisection algorithm. In Figure 3.3(a) and (b), the I-V characteristics of a PV module under DEC obtained using the implicit (3.1) and explicit (3.13) relationships, respectively are plotted. It is

seen from the figures that the I-V characteristics of the module plotted using both the functions are closely matched. Therefore, the derived explicit I-V function (3.13) is similar nature as the implicit function (3.1). Since the derived I-V function (3.13) is an explicit form, the estimation of MPP of a PV module using this proposed method is simple, accurate and computationally efficient.

3.3.1 Proposed method

The main objective of the proposed method is to extract the P_{max} of a PV module using the explicit form of an I-V relationship given in (3.13). The algorithm of the proposed method to find the P_{max} of the module under DEC is shown in Figure 3.1 as explained bellow.

- In the present work, the estimated PV parameters such as I_{ph}, I_o, V_t, R_s, and R_{sh} are used for the estimation of MPP of a module by solving the proposed current explicit function (3.13) using bisection method (BM).
- For the estimation of MPP using BM, the initial voltage (V_{oc-i}), final voltage (V_{oc-f}) and the bisection voltage (V_{BM}) are assigned as 0, V_{oc}, and (V_{oc-i} + V_{oc-f})/2 respectively.
- The calculated current at voltage V_{BM} using the proposed explicit I-V characteristic is used to estimate the power, $P_1 = VI$, where $V = V_{BM}$ and I is the current at $V = V_{BM}$.
- The current and the power $P_2 = VI$ are estimated for the perturbed voltage i.e., $V = V + \Delta V$, ΔV = 0.001.
- The slope i.e., $\frac{\Delta P}{\Delta V}$ (= $\frac{P_2 - P_1}{\Delta V}$) of the P-V curve is calculated.
  - case 1: if $\frac{\Delta P}{\Delta V} > 0 \Rightarrow V_{BM} < V_{mp}, \therefore V_{oc-i} = V_{BM}$.
  - case 2: if $\frac{\Delta P}{\Delta V} < 0 \Rightarrow V_{BM} > V_{mp}, \therefore V_{oc-f} = V_{BM}$.
- The above mentioned steps are repeated until $|V_{oc-i} - V_{oc-f}| <$ tolerance.
- The converged algorithm estimates the V_{mp}.
- The I_{mp} and P_{max} (= $V_{mp}I_{mp}$) are estimated under DEC.

3.4 Other different MPPT methods

The different popular MPPT methods such as, V_{frac} [38] and PO [13] are explained as follows:

3.4.1 V_{frac} method

The V_{frac} method is a simplest method for MPPT and the MPP voltage of the PV module estimated using this method is equal to the fraction of open-circuit voltage as given bellow:

$$V_{mp} = kV_{oc} \tag{3.14}$$

where k is a constant of proportionality which depends on the irradiation and temperature varies from 0.71 to 0.78 [38]. In this method, the PV module is forced to operate at calculated maximum voltage using (3.14) and for that V_{oc} of the module is periodically measured. Hence, there is a power loss in this method.

3.4.2 PO method

The most popular MPPT algorithm is PO because it is easy for implementation. PO involves a

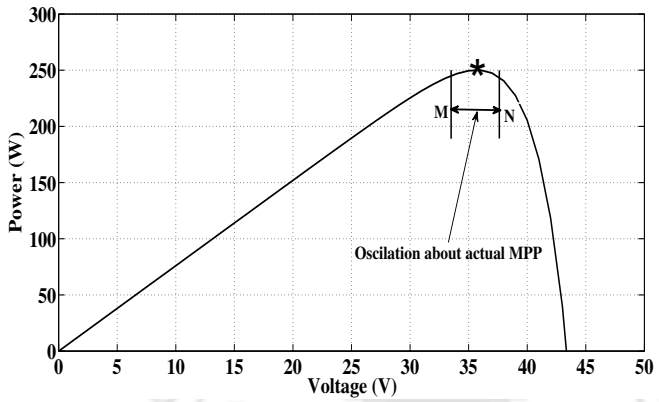

Figure 3.4: Oscillation about an actual MPP in PO method.

perturbation in the operating voltage of the PV module. If the direction of operating voltage perturbation is in the given direction and the power drawn from the module increases, then the operating point moves towards the MPP. Otherwise, if the operating voltage is perturbed in the reverse direction and the power drawn from the PV module decreases, the operating point moves away from the MPP. In this way, the operating point will reach at an actual MPP and will oscillate between the points M and N as shown in Figure 3.4.

3.5 Results and discussion

3.5.1 Simulation results

The P-V characteristics of a 250 W PV module under DEC as shown in Figure 3.5 and 3.6 are plotted using MATLAB, and the MPP of the module at different irradiation and temperature conditions are estimated using the proposed method. The actual MPP of a PV module for different irradiations and temperatures is calculated by plotting the I-V and P-V curve. The peak value of the power in P-V characteristics under DEC are taken as an actual maximum power, $P_{max,(act)}$. It is observed from the figures that the maximum power and V_{mp} of the module increase with the increase in solar irradiation and decrease in temperature. The MPP and the percentage of tracking efficiency (% η_{track}) of the module under DEC estimated using the proposed algorithm, PO method, V_{frac} and the estimated, actual values of P_{max} are given in Table 3.2 and 3.3. The maximum power of the PV module is obtained from the estimated V_{mp} and I_{mp} under DEC.

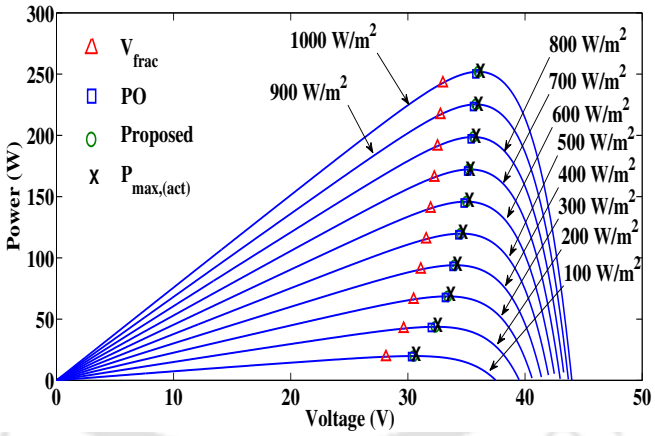

Figure 3.5: P-V curve of the PV module at standard temperature (25 °C) with varying irradiations.

The % η_{track} of a PV module is calculated using (3.15)

$$\%\eta_{track} = \left| \frac{P_{\max,(est)}}{P_{\max,(act)}} \right| \times 100 \tag{3.15}$$

It is observed from the tables that the tracking efficiency of the proposed method is always more than the different existing methods in different irradiations with a standard temperature 25 °C and different temperature with an irradiation of 1000 W/m^2.

For the demonstration of the tracking performance of different MPPT methods to estimate the

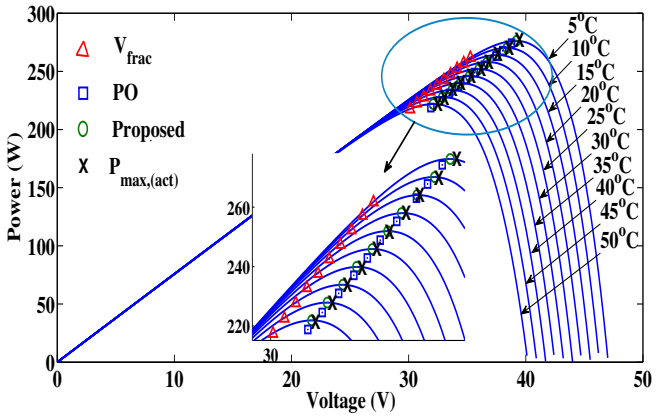

Figure 3.6: P-V curve of the PV module at an irradiance of 1000 W/m^2 with varying temperatures.

Table 3.2: MPP of a PV module under different irradiation at a temperature of 25 °C

Irradiation (W/m^2)	P_{max} in V_{frac} method (W)	P_{max} in PO method (W)	P_{max} in the proposed method (W)	$P_{mp,act}$ (W)	% η_{track} in V_{frac} method	% η_{track} in PO method	% η_{track} in the proposed method
100	19.12	19.39	19.80	19.89	96.12	97.48	99.54
200	42.08	43.20	43.64	43.76	96.16	98.72	99.72
300	65.85	67.72	68.36	68.63	95.94	98.67	99.60
400	90.50	93.08	93.95	94.08	96.19	98.93	99.86
500	115.19	118.85	119.54	119.87	96.09	99.14	99.72
600	140.21	144.76	145.74	145.93	96.08	99.19	99.86
700	165.49	170.93	172.16	172.29	96.05	99.21	99.92
800	191.00	197.17	198.36	198.70	96.12	99.22	99.82
900	216.67	223.56	225.05	225.32	95.86	99.21	99.88
1000	242.55	250.24	251.86	251.98	96.25	99.30	99.95

MPP of a 250 W PV module under the rapid change of solar irradiation conditions as shown in Figure 3.7(a) is considered. In the present analysis to obtain the output power variation of the above mentioned PV module, due to the rapid change of solar irradiation from 700 to 300 W/m^2 (first step) at 3 s, 300 to 500 W/m^2 (second step) at 8 s and 500 to 700 W/m^2 (third step) at 12 s are considered. In V_{frac}, PO and the proposed method, the variation of power with respect to time for the above mentioned solar irradiations during the total time duration from 0 to 15 s are presented in Figure 3.7(b). The $P_{max,(act)}$ of 172.30, 69.20 and 120.35 W under different solar irradiations such as, 700, 500, and 300 W/m^2, respectively, are obtained from the P-V characteristics of a PV module at a temperature of 25 °C. It is observed from Figure 3.7(b) that for a rapid change of solar irradiation

Table 3.3: MPP of a PV module under different temperature at an irradiation of 1000 W/m^2

Temperature (°C)	P_{max} in V_{frac} method (W)	P_{max} in PO method (W)	P_{max} in the proposed method (W)	$P_{max,act}$ (W)	% η_{track} in V_{frac} method	% η_{track} in PO method	% η_{track} in the proposed method
5	261.70	274.24	275.79	276.20	94.75	99.29	99.85
10	257.12	267.80	269.84	270.15	95.17	99.13	99.88
15	252.29	263.03	263.97	264.12	95.52	99.58	99.94
20	247.41	255.22	257.68	258.10	95.85	98.88	99.83
25	242.55	248.91	251.86	251.98	96.25	98.78	99.98
30	237.63	242.90	245.69	245.91	96.63	98.77	99.91
35	232.82	237.07	239.56	239.97	97.02	98.79	99.82
40	227.71	231.01	233.79	233.94	97.33	98.74	99.93
45	222.57	224.56	227.78	227.98	97.62	98.49	99.91
50	217.46	218.83	221.81	221.99	97.95	98.57	99.91

in each steps, the computational time to obtain MPP (t_{MPP}) in the proposed method is less than PO but sightly more than V_{frac} method. However, the accuracy of the V_{frac} method for the estimation of MPP of a PV module is worse. Also it is observed from the figure that the accuracy of the proposed method is high as compared to the other existing methods for the aforementioned rapid variation of solar irradiations. Therefore, the estimation of MPP of a PV module by the proposed method is more accurate and computationally efficient for rapid change of solar irradiation conditions.

3.5.2 Experimental validation of the proposed method

3.5.2.1 Design of the boost converter

For the practical implementation of the MPPT of a PV module by using the proposed method under DEC, a boost converter is designed considering the better efficiency of the converter during the operation at any level of solar irradiation. The inductor of the converter is designed in such a way that the boost converter operates in continuous conduction mode of 1 % inductor current ripple under the rated power of the module. The mathematical expression for the inductor in the boost converter is given as follow:

$$L = \frac{V_i D}{\Delta I_L f_s} \tag{3.16}$$

where V_i = input voltage, D = duty cycle, ΔI_L = 1% inductor current ripple under the rated power of the module and f_s = switching frequency. Equating the input power ($V_i I_i$) with the output power

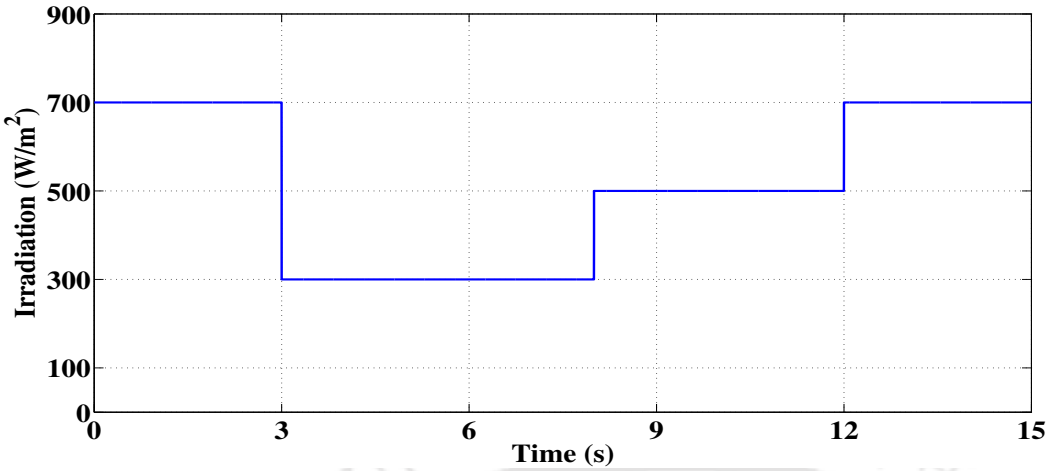

(a)

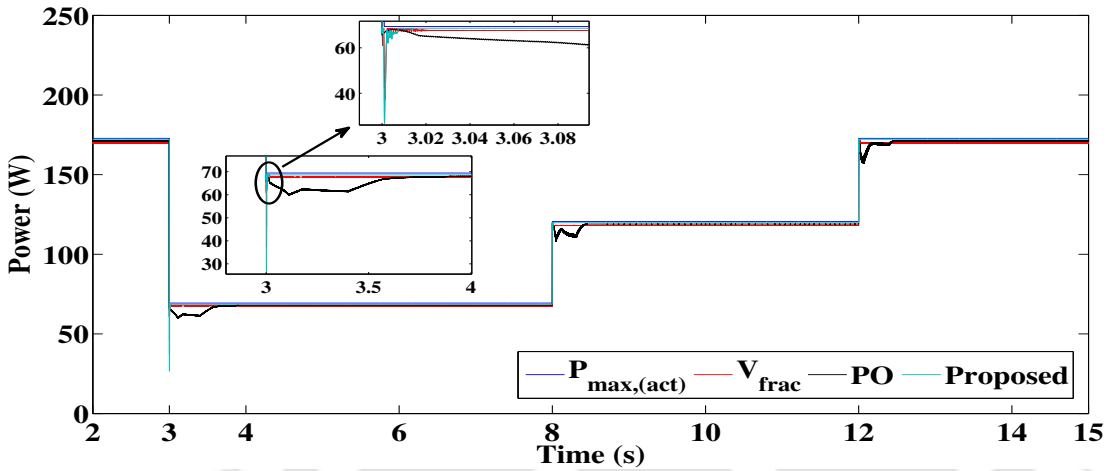

(b)

Figure 3.7: (a) Rapid change of solar irradiation at different instant of time and (b) maximum power obtained from a 250 W PV module during rapid change of solar irradiation conditions by V_{frac}, PO, and proposed method.

($\frac{V_o^2}{R_{eq(bulb)}}$), the expression for the output voltage (V_o) of the system is derived as follows:

$$V_o = \sqrt{V_i I_i R_{eq(bulb)}} \tag{3.17}$$

where I_i is the input current to the system and $R_{eq(bulb)}$ is the equivalent resistance of the two parallelly connected bulbs acting as a load. The D of the boost converter is given as follows:

$$D = 1 - \frac{V_i}{V_o} \tag{3.18}$$

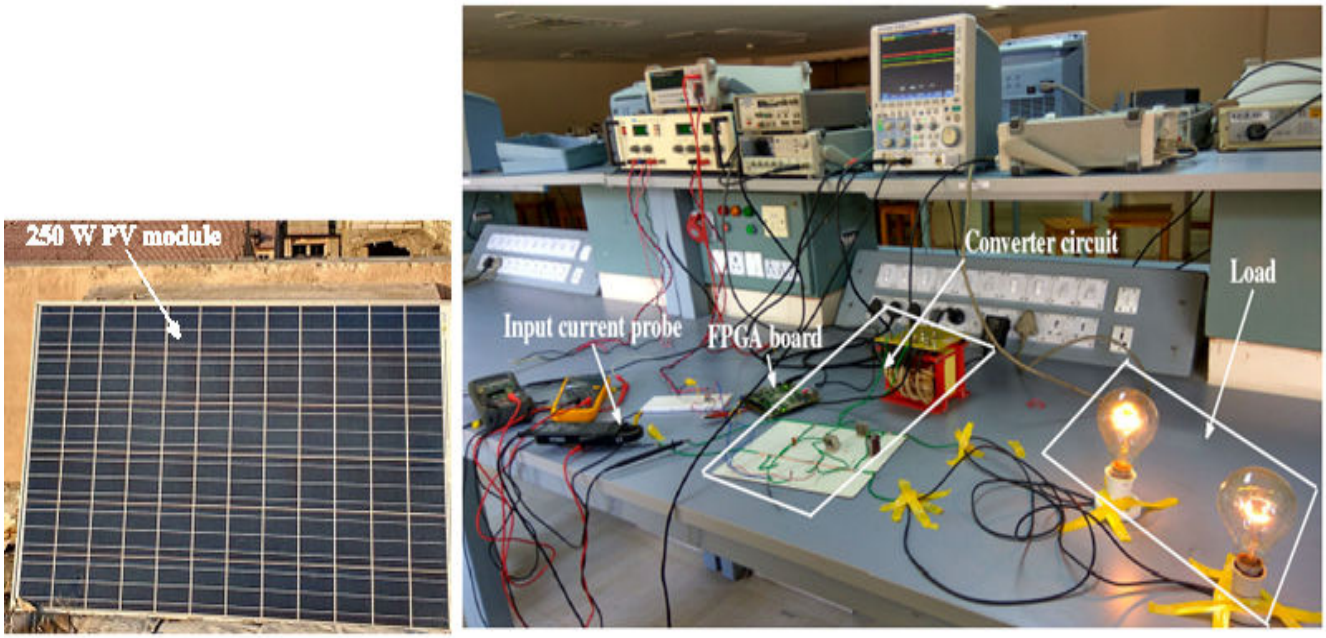

Figure 3.8: Laboratory scale experimental setup.

Substituting (3.17) in (3.18), the D is written as follows:

$$D = 1 - \frac{V_i}{\sqrt{V_i I_i R_{eq(bulb)}}} \tag{3.19}$$

After substituting (3.19) in (3.16), the L of the boost converter is written as follows:

$$L = \frac{V_i\left(1 - \sqrt{\frac{V_i}{I_i R_{eq(bulb)}}}\right)}{\Delta I_L f_s} \tag{3.20}$$

Also the output capacitor is designed in such a way that the output voltage ripple is negligible and the mathematical expression for the output capacitor is given [90] as follows:

$$C_o = \frac{I_o D}{f_s \Delta V_o} \tag{3.21}$$

3.5.2.2 Experimental analysis

The complete experimental setup in the laboratory to estimate the MPP is shown in Figure 3.8. It consists of a 250 W PV module which is feeding to two 200 W incandescent bulbs through a dc/dc boost converter. The nominal parameters of the converter used in the present experiment are given in Table 3.4. The proposed algorithm for the estimation of MPP of a module as explained in Fig. 3.1 is

written in the FPGA board, XILINX Spartan-6 (the FPGA program is given in Appendix A).

Table 3.4: Bosst converter parameters

Parameter	Value
Inductance (L)	20 mH
Input capacitance (C_i)	100μF
Output capacitance (C_o)	100μF
Converter switching frequency (f_s)	20 kHz

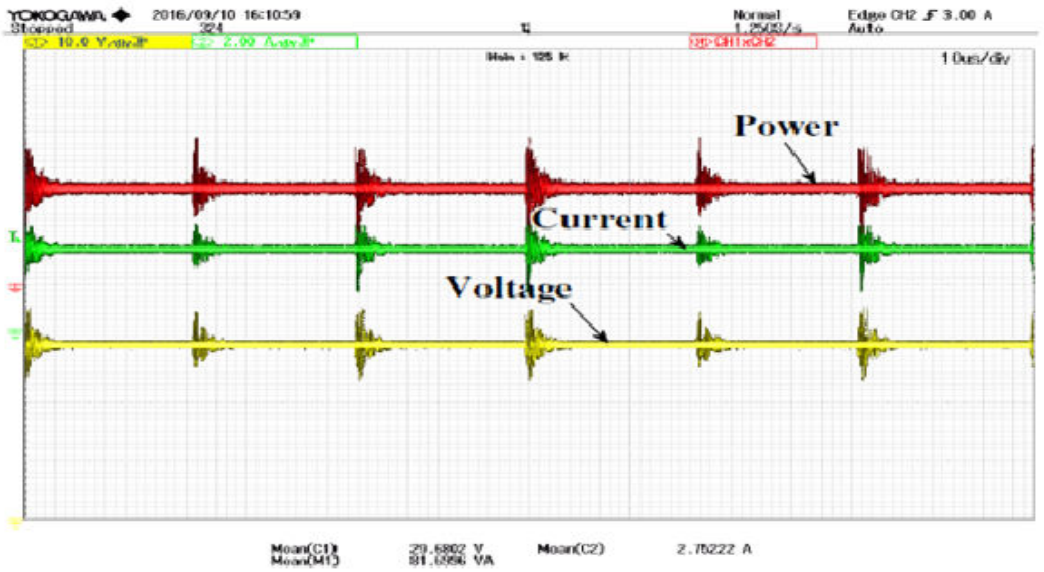

Figure 3.9: Steady-state behavior of the proposed method at an irradiation of 394 W/m^2 [Channel (CH)1: V_{mp} = 29.6802 V, CH2: I_{mp} = 2.75222 A and CH3: P_{max} = 81.6996 W].

The prime objective of this study is to analyze the accuracy of the proposed technique to estimate the MPP of a PV module under DEC. To study the performance of the proposed technique, the V_{mp}, I_{mp}, and P_{max} of the module obtained experimentally for the solar irradiation of 394 and 716 W/m^2 are presented in Figure 3.9 and 3.10 respectively. The P_{max} obtained experimentally and by using the proposed method for the solar irradiation of 394 and 716 W/m^2 are given in Table 3.5.

The (%) deviation between the P_{max} obtained experimentally and by simulation using the proposed technique is calculated as follows:

$$(\%)Deviation = \frac{P_{\max,(est)} - P_{\max,(experimental)}}{P_{\max,(est)}} \times 100 \tag{3.22}$$

Since the (%) deviation between the P_{max} obtained experimentally and by simulation using the

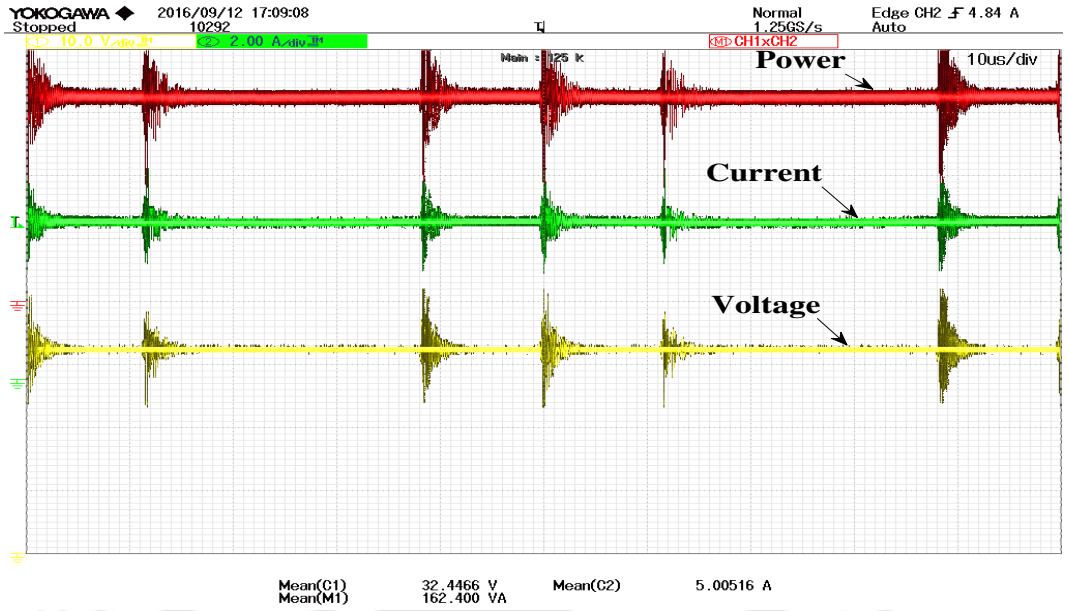

Figure 3.10: Steady-state behavior of the proposed method at an irradiation of 716 W/m^2 [Channel (CH)1: V_{mp} = 32.4466 V, CH2: I_{mp} = 5.00516 A and CH3: P_{max} = 162.400 W].

proposed technique is less than 4% (3.22) as seen from Table 3.5. So the proposed technique for the estimation of P_{max} of a module is accurate.

Table 3.5: MPP of a PV module under DEC

DEC		Experimental Results			Simulation Results			Deviation
Irradiation (W/m^2)	Temperature (°C)	V_{mp} (V)	I_{mp} (A)	P_{max} (W)	V_{mp} (V)	I_{mp} (A)	P_{max} (W)	in (%)
394	30	29.68	2.75	81.69	30.82	2.76	85.06	3.96
716	35	32.44	5.00	162.40	33.75	5.00	168.75	3.76

3.6 Summary of the chapter

In this work, the implicit function of an I-V relationship of a PV module is converted into an explicit function such that the estimation of MPP of a PV module is simple, accurate and computationally efficient. The BM is used for the estimation of MPP from the explicit I-V function of a single diode PV module under DEC. A comparison of the proposed method with different existing methods for the estimation of MPP of a PV module is carried out by using MATLAB program. It is observed that the estimated MPP of a module using the proposed technique is more or less same as an actual MPP value under DEC and also, the tracking efficiency of the proposed method is more as compare to other MPPT methods. The tracking performance such as accuracy and computational time of the

proposed technique is better as compared to other different existing methods for the rapid change of solar irradiation conditions. The deviation between the P_{max} obtained experimentally and by using an explicit expression of current for DEC are within the limit. Since the estimation of MPP of a PV module using an explicit expression of current is simple, accurate and computationally efficient, it is useful for the PV professional in domestic and commercial applications.

Since the accuracy of MPP of a DDM PV module is higher than SDM module under low irradiation level, a robust algorithm for the estimation of MPP of a DDM PV module based on its characteristic equation under DEC is presented in the next chapter.

4

Estimation of MPP of a Double Diode Model PV Module

Contents

4.1 Introduction

Photovoltaic (PV) source is more promising as compared to other renewable energy sources to fulfil the present energy demand [78, 91]. Nowadays, the installation of PV plants in residential and commercial use is promoted by the development of technology [92, 93]. Proper modeling of the PV cells and the modules are required for understanding of the behavior of the PV systems and also it is essential for the grid integration. Many researchers have designed the PV cells and modules SDM and DDM. The SDM of the PV module is most widely used because of its accuracy and low computational cost. But since the recombination losses are not taken into account, its accuracy at open circuit voltage (OCV) highly diminishes at low solar irradiation level [29]. The DDM PV module is used to improve the modeling accuracy by connecting another diode in parallel with SDM. Since DDM takes into account the recombination losses, it is more accurate than the SDM at low solar irradiation for representing the cell behaviors [11, 28, 30–33]. Therefore, the DDM circuit is most useful for PV module and it is considered for the present study. However, the estimation of PV parameters of the DDM is a challenging problem because of solving the number of non-linear equations. To reduce the complexity of solving non-linear equations, many researchers have assumed that the diode quality factors of two diodes with a reasonable accuracy based on Shockley's diffusion theory are A_1=1 and A_2=2 [28, 94, 95].

MPPT of a PV array is required for the integration of solar power to the grid. Since the output I-V characteristic of a PV array is non-linear in nature and it varies with solar irradiation and temperature and hence MPPT of a PV array is not simple. Many researchers have used three different methods such as direct, artificial intelligence, and indirect method to track the MPP of a PV array as discussed in Chapter 2. An analytical method for estimation of MPP based on mean value theorem (MVT) has been proposed in [54] which does not require any iteration scheme. However, the periodic measurement of the OCV by power interruption is still needed, which is the disadvantage of this method. An analytical expression of MPP voltage and current for an ideal SDM PV module based on several assumptions for the estimation of maximum power under DEC has been proposed by Saloux *et al.* [96]. For the direct MPP calculation of the SDM under different operating conditions, an accurate and computationally efficient explicit expression in terms of five parameters of the SDM using

the Lambert W function has been proposed [97]. However, the explicit expression of MPP voltage and current of the DDM using Lambert W function method is difficult due to the complexity of the DDM. In the present work, the LM algorithm for the estimation of MPP of a DDM PV module is categorized into the indirect methods. A non-linear least square (NLS) method based on trust region reflective algorithm has been proposed to estimate the PV module parameters [57], but it may fail to converge at an optimum point. In recent contribution, GS method is used for the estimation of the PV parameters of an SDM of a module using datasheet values, and the MPP of a PV array under DEC are estimated by using modified GS method [10]. However, modified GS method may converge at the wrong point in some cases.

Considering the aforementioned limitations, this section presents the estimation of MPP of a DDM PV module based on its characteristic equation by using the robust LM algorithm for DEC, assuming the diode quality factors of two diodes as 1 and 2 respectively. A comparison of LM method with six different existing MPPT methods such as GA, PS, MVT, Saloux, NLS, and GS is presented under DEC. It is observed that the accuracy of LM method is more as compared to other methods and the time taken to obtain MPP (t_{MPP}) of a DDM PV module is low for different operating conditions but slightly more than the two explicit methods such as MVT and Saloux. However, the accuracy of the estimation of the MPP of a module in MVT and Saloux methods is less as compared to other methods. Thus, the performance of the proposed method to estimate the MPP of a DDM PV module is more accurate and computationally efficient.

In Section 4.2, the parameters of a DDM PV module at STC and for DEC are estimated. The effect of solar irradiation and temperature on the PV parameters is analyzed in this section. The estimation of MPP of a DDM PV module is presented in Section 4.3. The details of modeling of a PV array is explained and the simulation results of MPP of a PV array are validated with the experimental results under DEC and presented in Section 4.4. Finally the conclusion is presented in Section 4.5.

4.2 Parmeters estimation of a DDM PV module

In this work a DDM is presented which accounts the recombination loss in the depletion region of a PV array to estimate the MPP accurately. Figure 1.3(b) shows an electrical equivalent circuit of the DDM PV module. The output current of the PV module is given as follows:

$$I_{pv} = I_{ph} - I_{o1}\left\{\exp\left(\frac{V_{pv} + I_{pv}R_s}{A_1 N_s V_t}\right) - 1\right\} - I_{o2}\left\{\exp\left(\frac{V_{pv} + I_{pv}R_s}{A_2 N_s V_t}\right) - 1\right\} - \frac{V_{pv} + I_{pv}R_s}{R_{sh}} \tag{4.1}$$

where I_{o1} and I_{o2} are the dark saturation currents, A_1 and A_2 are the diode quality factor of two diodes and $V_t(= \frac{kT}{q})$. Substituting the values of $A_1 = 1$ and $A_2 = 2$ and putting the three important points such as $(V_{oc}, 0)$, $(0, I_{sc})$, and (V_{mp}, I_{mp}) in (4.1), (4.2)-(4.4) are obtained as follows:

$$I_{ph} = \frac{V_{oc}}{R_{sh}} + I_{o1}\left\{\exp\left(\frac{V_{oc}}{N_s V_t}\right) - 1\right\} + I_{o2}\left\{\exp\left(\frac{V_{oc}}{2N_s V_t}\right) - 1\right\} \tag{4.2}$$

$$I_{sc} = I_{ph} - I_{o1}\left\{\exp\left(\frac{I_{sc}R_s}{N_s V_t}\right) - 1\right\} - I_{o2}\left\{\exp\left(\frac{I_{sc}R_s}{2N_s V_t}\right) - 1\right\} - \frac{I_{sc}R_s}{R_{sh}} \tag{4.3}$$

$$I_{mp} = I_{ph} - I_{o1}\left\{\exp\left(\frac{V_{mp} + I_{mp}R_s}{N_s V_t}\right) - 1\right\} - I_{o2}\left\{\exp\left(\frac{V_{mp} + I_{mp}R_s}{2N_s V_t}\right) - 1\right\} - \frac{V_{mp} + I_{mp}R_s}{R_{sh}} \tag{4.4}$$

To obtain five parameters, two more equations are required. The power generation of the PV module at any point on the I-V curve is given as follows:

$$P = V_{pv} I_{pv} \tag{4.5}$$

The derivative of power w.r.t. voltage at MPP is as follows:

$$\left.\frac{dP}{dV_{pv}}\right|_{V_{pv}=V_{mp}, I_{pv}=I_{mp}} = 0 \tag{4.6}$$

Taking the derivative of power w.r.t. voltage, (4.5) can be written as follows:

$$\frac{dP}{dV_{pv}} = I_{pv} + \left(\frac{dI_{pv}}{dV_{pv}}\right) V_{pv} \tag{4.7}$$

Substituting (4.6) into (4.7), yield

$$\frac{dI_{pv}}{dV_{pv}} = -\frac{I_{mp}}{V_{mp}} \tag{4.8}$$

Also the derivative of current in (4.1) w.r.t. voltage can be written as follows:

$$\frac{dI_{pv}}{dV_{pv}} = -\left(1 + R_s\frac{dI_{pv}}{dV_{pv}}\right)\left\{\frac{I_{o1}}{N_sV_t}\exp\left(\frac{V_{pv}+I_{pv}R_s}{N_sV_t}\right) + \frac{I_{o2}}{2N_sV_t}\exp\left(\frac{V_{pv}+I_{pv}R_s}{2N_sV_t}\right) - \frac{1}{R_{sh}}\right\} \tag{4.9}$$

Substituting the value of $\frac{dI}{dV}$ from (4.8) in (4.9), the resulting equation can be written as follows:

$$\frac{I_{mp}}{V_{mp}} = \left(1 - R_s\frac{I_{mp}}{V_{mp}}\right)\left\{\frac{I_{o1}}{N_sV_t}\exp\left(\frac{V_{mp}+I_{mp}R_s}{N_sV_t}\right) + \frac{I_{o2}}{2N_sV_t}\exp\left(\frac{V_{mp}+I_{mp}R_s}{2N_sV_t}\right) + \frac{1}{R_{sh}}\right\} \tag{4.10}$$

Substituting I_{ph} from (4.2) in (4.3) and (4.4), the equations are obtained as follows:

$$I_{sc} = I_{o1}\left\{\exp\left(\frac{V_{oc}}{N_sV_t}\right) - \exp\left(\frac{I_{sc}R_s}{N_sV_t}\right)\right\} + I_{o2}\left\{\exp\left(\frac{V_{oc}}{2N_sV_t}\right) - \exp\left(\frac{I_{sc}R_s}{2N_sV_t}\right)\right\} + \frac{V_{oc}-I_{sc}R_s}{R_{sh}} \tag{4.11}$$

$$\begin{aligned} I_{mp}\left(1 + \frac{R_s}{R_{sh}}\right) &= I_{o1}\left\{\exp\left(\frac{V_{oc}}{N_sV_t}\right) - \exp\left(\frac{V_{mp}+I_{mp}R_s}{N_sV_t}\right)\right\} \\ &+I_{o2}\left\{\exp\left(\frac{V_{oc}}{2N_sV_t}\right) - \exp\left(\frac{V_{mp}+I_{mp}R_s}{2N_sV_t}\right)\right\} + \frac{V_{oc}-V_{mp}}{R_{sh}} \end{aligned} \tag{4.12}$$

Four unknown PV parameters such as I_{o1}, I_{o2}, R_s, and R_{sh} are presented in three equations such as (4.10), (4.11), and (4.12). In order to estimate the four PV parameters, the equation derived from the derivative of current w.r.t. voltage at SCC in the I-V curve is considered and it is expressed as follows [11]:

$$\left.\frac{dI_{pv}}{dV_{pv}}\right|_{(V_{pv}=0, I_{pv}=I_{SC})} = -\frac{1}{R_{sh}} \tag{4.13}$$

Putting (4.13) in (4.9) and taking some assumption [98], the equation obtained is given as follows:

$$(R_{sh} - R_s)\left\{\frac{1}{R_{sh}} + \frac{I_{o1}}{N_sV_t}\exp\left(\frac{I_{sc}R_s}{N_sV_t}\right) + \frac{I_{o2}}{2N_sV_t}\exp\left(\frac{I_{sc}R_s}{2N_sV_t}\right)\right\} - 1 = 0 \tag{4.14}$$

Solving the equations (4.10), (4.11), (4.12), and (4.14) using NR method, the unknown PV parameters such as I_{o1}, I_{o2}, R_s, and R_{sh} are obtained. Then the value of I_{ph} is obtained by using the estimated PV parameters value in (4.2). The datasheet values of the PV module and the estimated PV parameters value of the module at STC are given in Table 4.1.

Table 4.1: PV parameters

(a) Datasheet values

Module Parameters	Actual Values
I_{sc}	8.76 A
V_{oc}	37.30 V
V_{mp}	30.30 V
I_{mp}	8.25 A
N_s	60
k_i	0.05 %
k_v	−0.36 %

(b) Estimated values

Model Parameters	Estimated Values
I_{ph}	8.76 A
I_{o1}	0.2687 nA
I_{o2}	.7289 μA
R_s	0.2929 Ω
R_{sh}	733.982 Ω

4.2.1 Temperature and solar irradiation dependance PV parameters

The SCC and OCV of the PV module vary linearly with temperature [12] and the relationship are given as follows:

$$I_{sc}(T) = I_{sc(STC)}\left\{1 + \frac{k_i}{100}(T - T_{STC})\right\} \tag{4.15}$$

$$V_{oc}(T) = V_{oc(STC)} + k_v(T - T_{STC}) \tag{4.16}$$

The dark saturation currents I_{o1} and I_{o2} of two diodes mainly depend on the temperature and these are given as follows [34]:

$$I_{o1} = I_{o1(STC)}\left[\left(\frac{T}{T_{STC}}\right)^3 \exp\left\{\frac{1}{k}\left(\frac{E_{g(STC)}}{T_{STC}} - \frac{E_g}{T}\right)\right\}\right] \tag{4.17}$$

$$I_{o2} = I_{o2(STC)}\left[\left(\frac{T}{T_{STC}}\right)^{5/2} \exp\left\{\frac{1}{2k}\left(\frac{E_{g(STC)}}{T_{STC}} - \frac{E_g}{T}\right)\right\}\right] \tag{4.18}$$

where E_g is the band gap energy of the material at STC and for silicon cell its value is 1.121 eV. E_g depends on cell temperature and is given as follows:

$$E_g = E_{g(STC)}\{1 - 0.0002677(T - T_{STC})\} \tag{4.19}$$

The R_s and R_{sh} of the PV module at all operating conditions are given as follows [99]:

$$R_s = R_{s(STC)} \tag{4.20}$$

$$R_{sh} = R_{sh(STC)} \frac{G_{STC}}{G} \tag{4.21}$$

The photo-generated current of the PV modules depends on the temperature and solar irradiation and is given as follows [12], [81]:

$$I_{ph} = I_{ph(STC)} \left[\frac{G}{G_{STC}} \{1 + k_i (T - T_{STC})\} \right] \tag{4.22}$$

where $I_{ph(STC)}$ is the photo generated current at STC and k_i is the temperature coefficient of the PV module. The SCC depends on solar irradiation and is given as follows:

$$I_{sc}(G) = \left(\frac{G}{G_{STC}} \right) I_{sc(STC)} \tag{4.23}$$

where $I_{sc(STC)}$ is the short circuit current at STC. For solar irradiation dependance, the OCV of the double-diode PV module from (4.2) is written as follows:

$$V_{oc}(G) = R_{sh} I_{ph}(G) - I_{o1} R_{sh} \left[\exp\left\{ \frac{V_{oc}(G)}{N_s V_t} \right\} - 1 \right] - I_{o2} R_{sh} \left[\exp\left\{ \frac{V_{oc}(G)}{2 N_s V_t} \right\} - 1 \right] \tag{4.24}$$

For the estimation of V_{oc} under different irradiation conditions, NR method is used to solve the above non-linear equation.

4.3 Estimation of MPP of a DDM PV module

The estimation of MPP of the module at a given environmental conditions is required for integration of PV power with the power grid. In this work, a novel approach is used to estimate the MPP of a DDM PV module at given environmental conditions by using the estimated PV parameters, such as R_s, R_{sh}, V_{oc}, and I_{sc} . For the estimation of MPP of a DDM PV module, first the V_{oc} and I_{sc} under given environmental condition are estimated. To estimate the V_{mp} and I_{mp} at a particular solar irradiation and temperature, two equations in terms of unknown variables V_{mp} and I_{mp} are required. Since the values of I_{o1} and I_{o2} are very small as shown in Table 4.1 (b), the Jacobian matrix may close to

singular. Therefore, by taking the approximation $\exp(\frac{V_{oc}}{N_s V_t}) \gg \exp(\frac{I_{sc}R_s}{N_s V_t})$ and $\exp(\frac{V_{oc}}{2N_s V_t}) \gg \exp(\frac{I_{sc}R_s}{2N_s V_t})$ in the PV module [11], (4.11) can be expressed as follows:

$$I_{sc} = I_{o1}\exp\left(\frac{V_{oc}}{N_s V_t}\right) + I_{o2}\exp\left(\frac{V_{oc}}{2N_s V_t}\right) + \frac{V_{oc} - I_{sc}R_s}{R_{sh}} \tag{4.25}$$

The expression of I_{o1} and I_{o2} obtained by solving (4.25) and (4.12) are given as follows:

$$I_{o1} = \frac{Q\exp\left(-\frac{V_{oc}}{2N_s V_t}\right) - R\exp\left(-\frac{V_{mp}+I_{mp}R_s}{2N_s V_t}\right)}{\exp\left(\frac{V_{oc}}{2N_s V_t}\right) - \exp\left(\frac{V_{mp}+I_{mp}R_s}{2N_s V_t}\right)} \tag{4.26}$$

$$I_{o2} = \frac{Q\exp\left(-\frac{V_{oc}}{N_s V_t}\right) - R\exp\left(-\frac{V_{mp}+I_{mp}R_s}{N_s V_t}\right)}{\exp\left(-\frac{V_{oc}}{2N_s V_t}\right) - \exp\left(-\frac{V_{mp}+I_{mp}R_s}{2N_s V_t}\right)} \tag{4.27}$$

where

$$Q = \left(1 + \frac{R_s}{R_{sh}}\right)I_{sc} - \frac{V_{oc}}{R_{sh}} \quad and$$

$$R = \left(1 + \frac{R_s}{R_{sh}}\right)\left(I_{sc} - I_{mp}\right) - \frac{V_{mp}}{R_{sh}}$$

Substituting I_{o1} and I_{o2} obtained from (4.26) and (4.27) in (4.10) and (4.14), the equations are obtained as follows:

$$\left(\frac{Q_1}{R_{sh}} - \frac{I_{mp}}{V_{mp}}\right)\{2 - \exp(Q_2) - \exp(-Q_2)\} + \frac{Q_1}{N_s V_t}\left\{-(\frac{Q}{2} + R)\exp(-Q_2) + \frac{Q}{2}\exp(-2Q_2) - \frac{R}{2}\exp(Q_2) + \frac{3R}{2}\right\} = f_1(V_{mp}, I_{mp}) = 0 \tag{4.28}$$

where

$$Q_1 = \left(1 - \frac{I_{mp}}{V_{mp}}\right) \quad and$$

$$Q_2 = \left(\frac{V_{oc} - V_{mp} - I_{mp}R_s}{2N_s V_t}\right)$$

$$\frac{R_{sh}-R_s}{N_sV_t}\left\{Q\exp(2Q_3)+(Q+R)\exp\left(\frac{I_{sc}R_s}{N_sV_t}-Q_4+\frac{V_{oc}}{2N_sV_t}\right)+R\exp\left(\frac{I_{sc}R_s}{N_sV_t}-2Q_4\right)+\frac{Q}{2}\exp(Q_3)\right.$$
$$-\frac{R}{2}\exp\left(\frac{V_{oc}+I_{sc}R_s}{2N_sV_t}-2Q_4\right)-\frac{Q}{2}\exp\left(Q_4+\frac{I_{sc}R_s}{2N_sV_t}-\frac{V_{oc}}{N_sV_t}\right)+\frac{R}{2}\exp\left(\frac{I_{sc}R_s}{2N_sV_t}-Q_4\right)\Big\}$$
$$-\frac{R_s}{R_{sh}}\{2-\exp(-Q_5)-\exp(Q_5)\}=f_2(V_{mp},I_{mp})=0 \tag{4.29}$$

where

$$Q_3=\frac{I_{sc}R_s-V_{oc}}{2N_sV_t},$$

$$Q_4=\frac{V_{mp}+I_{mp}R_S}{2N_sV_t} \quad and$$

$$Q_5=\frac{V_{mp}-V_{oc}+I_{mp}R_S}{2N_sV_t}$$

The above two nonlinear equations (4.28) and (4.29) are solved by using LM algorithm to obtain two unknown parameters i.e., V_{mp} and I_{mp}. The LM algorithm [80], [86] to obtain the unknown parameters is expressed as follows:

$$x_{i+1}=x_i-(\boldsymbol{J}^T(x_i)\boldsymbol{J}(x_i)+\lambda I)^{-1}\boldsymbol{J}^T(x_i)\boldsymbol{e}(x_i) \tag{4.30}$$

where x_i is the present weight, x_{i+1} is the next weight, $\boldsymbol{J}(x_i)^T\boldsymbol{J}(x_i)$ $(=\boldsymbol{H}(x_i))$ Hessian matrix evaluated at x_i, $\boldsymbol{e}(x_i)$ is the error vector, and λ (>0) is the combination coefficient. A flowchart for LM algorithms is shown in Figure 4.1. In this flowchart, $E(x_{i+1})$ and $E(x_i)$ are the present and the last total error respectively.

The LM method behaves as the combination of SD and GN based on different orders of gradient. The LM method begins with the SD to take the advantage of its low sensitivity to initial values and when the calculated value close to the final solution, it behaves as GN for the fast convergence. The automatic switching sequence of LM method from SD to GN is controlled by the parameter λ. When the LM method behaves as SD, the parameter λ play a crucial rule and the Hessian matrix

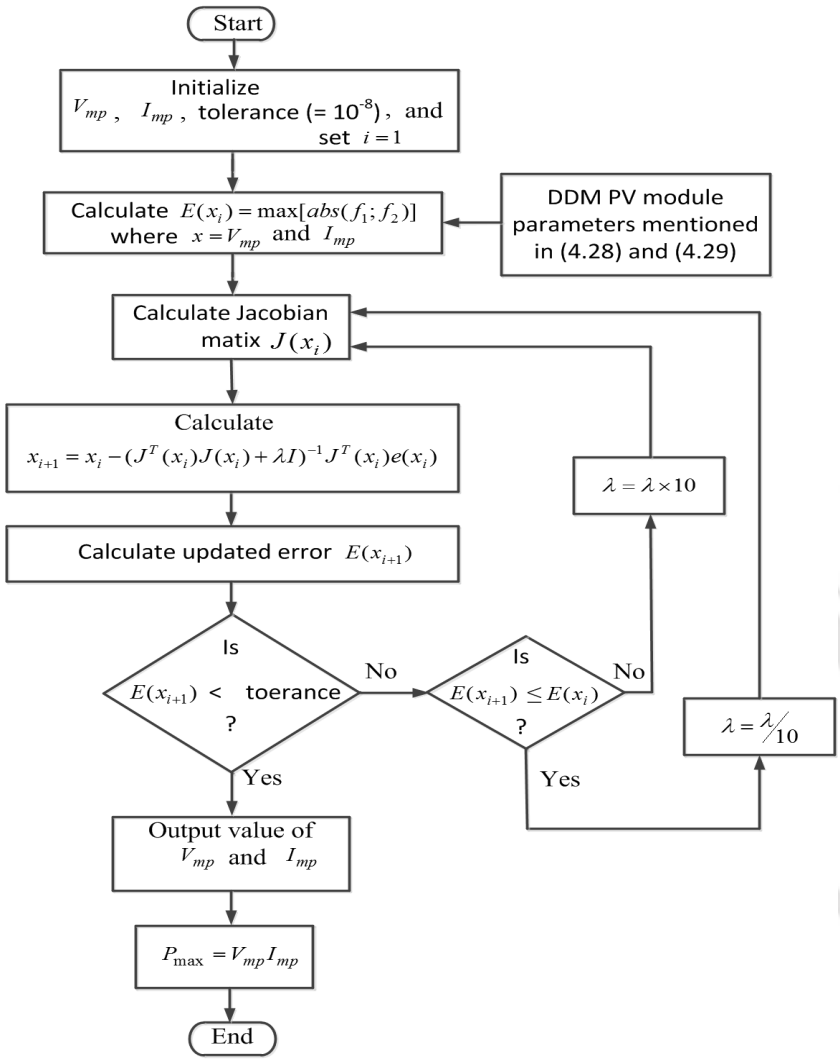

Figure 4.1: Algorithm for estimation of MPP of a DDM PV module by using LM method.

$(\boldsymbol{J}^T(x_i)\boldsymbol{J}(x_i) + \lambda I)$ in (4.30) becomes dominant in diagonal but when the LM method behaves as GN stage, the parameter λ changes automatically and takes small value, this ensures that the Hessian $\boldsymbol{J}(x_i)^T\boldsymbol{J}(x_i)$ outweighs the matrix λI. If the error is decreased after updating the algorithm given in (4.30), then λ is decreased by a factor of 10 for decreasing the gradient descent. Otherwise, if the error is increased, then λ is increased by a factor of 10 for increasing the gradient. Once the algorithm has converged, it will give voltage and current at MPP, in return it will give the P_{max} generation of a DDM PV module.

4.4 Results and discussion

In a large PV plant, an array is formed by connecting the modules in series and parallel and the parameters of an array are estimated from the parameters of the DDM PV modules. In the present analysis, a 60 kW, 10×24 PV array (number of modules in series i.e., N_{ss} = 10, number of strings in parallel i.e., N_{pp} = 24) is designed by taking 240 modules of same rating as given in Table 4.1. The array parameters estimated from the module parameters at STC are presented in Table 4.2.

Table 4.2: PV array parameters are estimated from module parameters

Datasheet Values	Estimated Values
$I_{sc} \times N_{pp}$	$I_{ph} \times N_{pp}$
$V_{oc} \times N_{ss}$	$I_{o1} \times N_{pp}$
$V_{mp} \times N_{ss}$	$I_{o2} \times N_{pp}$
$I_{mp} \times N_{pp}$	$R_s \times N_{ss}/N_{pp}$
$N_s \times N_{ss}$	$R_{sh} \times N_{ss}/N_{pp}$

4.4.1 MPP estimation of a PV array

The present LM algorithm is validated by comparing the simulation result with an experimental result for a 5×5 PV array of rating 75 W at fixed temperature with different irradiation. Further, the present algorithm is utilized to simulate 60 kW PV array based on DDM at standard temperature with different irradiation and at standard irradiation with different temperature. The I-V and P-V characteristics of a 60 kW PV array under DEC are analyzed, and an actual MPP of a PV array is estimated from the above characteristics. By using the proposed algorithm, the MPP of the same array is also estimated and compared with an actual MPP. The peak value of power in P-V characteristics of a PV array is taken as an $P_{max,(act)}$ and the MPP of a PV array under DEC is estimated using LM algorithm by taking the irradiation and temperature dependant V_{oc} and I_{sc}.

The I-V and P-V characteristics of a 60 kW PV array for varying irradiation from 200 to 800 W/m^2 at standard temperature of 25 °C are presented in the Figure 4.2(a) and (b) respectively. It is observed that the $P_{max,(est)}$ of a PV array by using LM algorithm varies from 11.411 to 48.064 kW and the $P_{max,(act)}$ obtained from the curve varies from 11.510 to 49.150 kW with the increase of solar

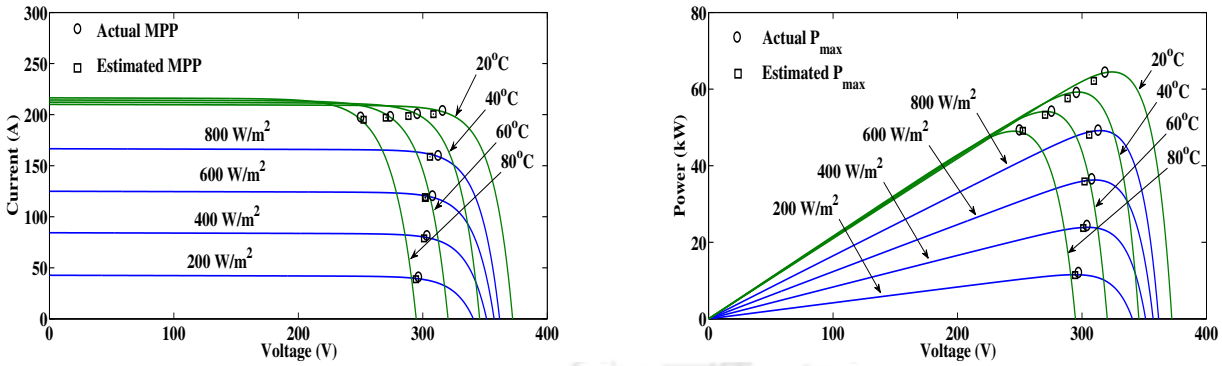

(a) (b)

Figure 4.2: (a) I-V and (b) P-V curves of a PV array at standard temperature (25 °C) with varying irradiations and at an irradiance of 1000 W/m^2 with varying temperature respectively.

irradiation as given in Table 4.3. The I-V and P-V characteristics of the same PV array for varying temperature from 20 to 80 °C at standard irradiation of 1000 W/m^2 are presented in the Figure 4.2(a) and (b) respectively. It is observed that the $P_{max,(est)}$ and $P_{max,(act)}$ vary from 61.776 to 49.429 kW and 63.150 to 49.770 kW respectively, with an increment of temperature as given in Table 4.3. The (%) error in $P_{max,(est)}$ w.r.t. $P_{max,(act)}$ of a PV array under aforementioned environmental conditions is calculated as follows:

$$(\%)Error = \left| \frac{P_{\max,(act)} - P_{\max,(est)}}{P_{\max,(act)}} \right| \times 100 \tag{4.31}$$

Table 4.3: MPP of a PV array under DEC

Different irradiation at a temperature of 25 °C						Different temperature at a standard irradiation of 1000 W/m^2					
Irradiation (W/m^2)	V_{mp} (V)	I_{mp} (A)	$P_{max,(est)}$ (kW)	$P_{max,(act)}$ (kW)	(%) error of $P_{max,(est)}$	Temperature (°C)	V_{mp} (V)	I_{mp} (A)	$P_{max,(est)}$ (kW)	$P_{max,(actual)}$ (kW)	(%) error of $P_{max,(est)}$
200	293.97	38.82	11.411	11.510	0.86	20	308.76	200.08	61.776	63.150	2.17
400	301.05	78.79	23.719	23.890	0.71	40	289.44	198.62	57.488	59.190	2.87
600	302.06	118.78	35.878	36.260	1.05	60	271.41	197.05	53.481	54.030	1.016
800	302.79	158.74	48.064	49.150	2.20	80	252.58	195.70	49.429	49.770	0.68

It is observed from Table 4.3 that the relative errors of the $P_{max,(est)}$ by the proposed method w.r.t. the $P_{max,(act)}$ of a PV array under DEC are minimal. In order to evaluate the accuracy of the proposed method, the estimation of MPP of a PV array is carried out for different operating conditions i.e., non-STC. For this analysis, the solar irradiation is varied from 100 to 900 W/m^2 with the increment of 100 W/m^2 and the temperature is varied from 20 to 140 °C with the increment of 20 °C. The deviation of $P_{max,(est)}$ from $P_{max,(act)}$ of a PV array under different operating conditions is presented

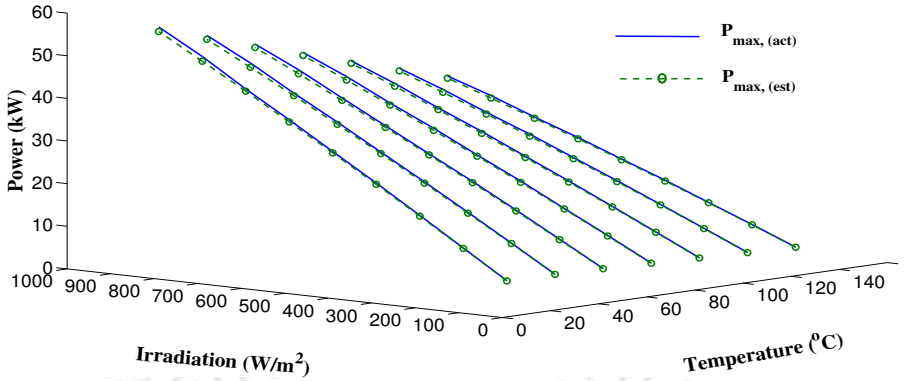

Figure 4.3: Comparison of $P_{max,(est)}$ using the proposed method with $P_{max,(act)}$ under different operating conditions.

Table 4.4: (%) Error of $P_{max,(est)}$ in the proposed method under different operating conditions

Irradiation (W/m^2)	(%) error at 20 °C	(%) error at 40 °C	(%) error at 60 °C	(%) error at 80 °C	(%) error at 100 °C	(%) error at 120 °C	(%) error at 140 °C
100	1.22	1.13	1.08	1.11	0.93	1.07	0.98
200	0.83	0.93	0.95	1.07	0.73	0.88	0.87
300	1.08	1.18	1.22	0.78	0.94	0.87	0.58
400	1.13	1.30	1.30	1.47	1.28	1.20	1.35
500	0.98	1.07	0.87	1.12	1.19	1.18	0.85
600	1.33	1.46	1.10	1.64	1.52	1.65	1.28
700	1.16	1.35	1.43	1.27	1.18	1.33	1.03
800	2.22	2.13	2.00	1.95	1.76	1.96	1.81
900	1.86	1.74	1.61	1.53	1.37	1.60	1.42

in Figure 4.3. It is observed from Figure 4.3 that the $P_{max,(est)}$ closely matches with $P_{max,(act)}$ of an array under different operating conditions. From Table 4.4, it is observed that the % error of $P_{max,(est)}$ w.r.t. $P_{max,(act)}$ of an array is minimal under different operating conditions. Therefore, the proposed algorithm is robust and accurate to estimate the MPP of an array for any operating condition.

A comparison of LM method with different existing methods such as GA, PS, MVT, Saloux, NLS and GS in terms of optimal solution i.e., MPP and execution time to obtain the MPP i.e., t_{MPP} is carried out by Matlab simulation for a 250 W DDM PV module as given in Table 4.1. The simulation results of above different methods for the MPP of a 250 W DDM PV module at a temperature of 25 °C with varying irradiations are presented in Table 4.5.

The $P_{max,(act)}$ of 176.80, 125.70, and 74.20 W under different solar irradiations such as, 700, 500, and 300 W/m^2, respectively, are obtained from the P-V characteristics of a DDM PV module at a

Table 4.5: A comparison of MPP of a 250 W DDM PV module at a temperature of 25 °C with varying irradiations

Different MPPT methods	Irradiation (W/m^2)	V_{mp} (V)	I_{mp} (A)	$P_{max,(est)}$ (W)	(%) Error of $P_{max,(est)}$ w.r.t. $P_{max,(act)}$	t_{MPP} (s)
GA	300	27.80	2.55	70.89	4.46	56.64
	500	29.12	4.23	123.17	2.01	43.08
	700	29.21	5.93	173.21	2.03	36.67
PS	300	28.81	2.48	71.44	3.71	2.7961
	500	29.37	4.19	123.06	2.10	3.0284
	700	29.77	5.84	173.85	1.66	2.8589
MVT	300	29.00	2.44	70.76	4.63	0.01135
	500	29.54	4.10	121.11	3.65	0.01337
	700	29.92	5.77	172.63	2.35	0.01012
Saloux	300	30.15	2.59	78.08	5.22	0.00981
	500	30.28	4.29	129.90	3.34	0.00866
	700	30.37	6.02	182.82	3.40	0.00852
NLS	300	29.68	2.45	72.71	2.00	0.400136
	500	30.04	4.11	123.46	1.78	0.410115
	700	30.16	5.78	174.27	1.43	0.37728
GS	300	29.12	2.47	71.92	3.07	0.17425
	500	29.60	4.13	122.24	2.75	0.18316
	700	30.10	5.79	174.27	1.43	0.15924
LM	300	29.87	2.45	73.18	1.37	0.01978
	500	30.21	4.11	124.16	1.22	0.02018
	700	30.29	5.78	175.07	0.97	0.01979

temperature of 25 °C. Considering the population size of 100, a crossover fraction of 0.845 and tournament function in GA method, the maximum power of 173.21, 123.17, and 70.89 W of a DDM PV module are achieved after time duration i.e., t_{MPP} of 36.67, 43.08, and 56.64 s with an irradiations of 700, 500, and 300 W/m^2, respectively as shown in Figure 4.4. From Table 4.5, it is observed that the GA method has highest computational cost among all the aforementioned existing methods. The explicit methods such as MVT and Saloux require less execution time but high % error of $P_{max,(est)}$ among all the methods. However, it is also observed that the maximum power obtained from the DDM PV module by LM method is more or less same as the actual maximum power of the same module for different solar irradiations. The proposed method has low t_{MPP} which is slightly more than the t_{MPP} of MVT and Saloux methods. In Figure 4.5, the P-V characteristic of the module is plotted for the solar irradiation of 700 W/m^2 and the $P_{max,(est)}$ for an aforementioned methods are denoted in the P-V characteristic for further study of the accuracy of the LM method. This figure shows that the

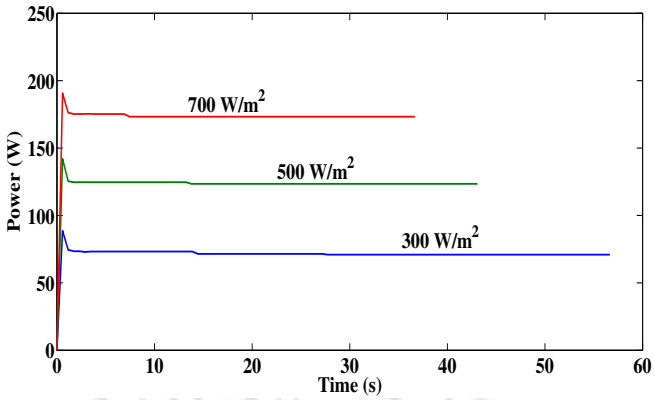

Figure 4.4: Maximum power generation of a 250 W DDM PV module in GA method under DEC.

$P_{max,(est)}$ using LM method is more or less same as $P_{max,(act)}$ whereas there is a significant deviation of $P_{max,(est)}$ w.r.t. $P_{max,(act)}$ in other methods. Therefore, the estimation of MPP of a DDM PV module by the proposed method under DEC is more accurate and computationally efficient.

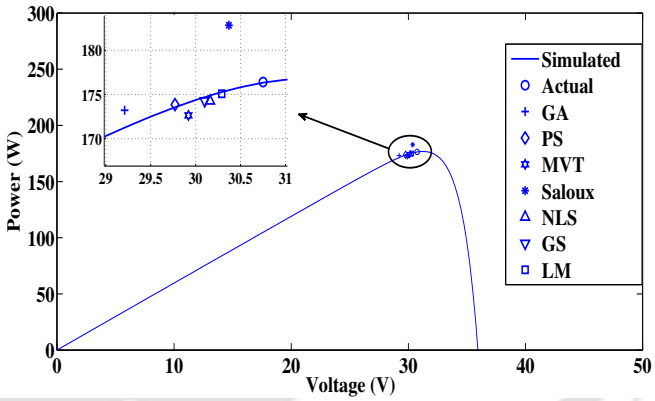

Figure 4.5: $P_{max,(est)}$ using different methods at an irradiation of 700 W/m^2 and temperature of 25 °C .

4.4.2 Experimental validation

To verify the simulation results, an experiment is performed in the Department of Electronics and Electrical Engineering, IIT Guwahati by taking the same rating of 3 W PV modules, two current and voltage sensors, one rheostat (1000 Ω, 2A), and the transparent papers of different thickness to set the different intensity of solar irradiance as shown in Figure 4.6(a). The datasheet values of a 3 W PV module provided by the manufacturer are I_{sc} = 0.37 A, V_{oc} = 10.60 V, V_{mp} = 8.70 V, I_{mp} = 0.34 A, and N_s = 18, k_i = 0.05% and k_v = - 0.35%. The power generated from a 5 × 5 PV array is measured by considering the current and voltage sensor data.

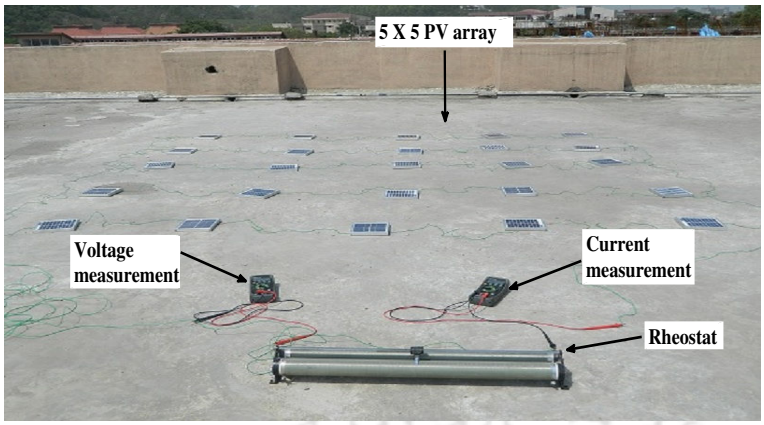

(a)

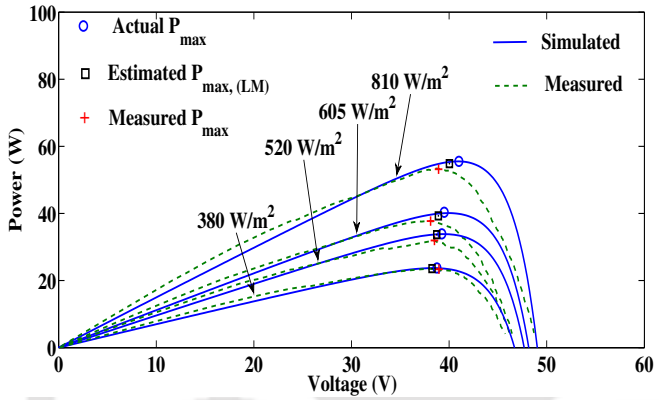

(b)

Figure 4.6: (a) Laboratory scale experimental setup, and (b) P-V curve of a PV array at a temperature of 38 °C with varying irradiations.

The level of solar irradiance while performing the experiment (10:30 AM, 9th April 2016) is calculated by using (4.23) and the data sheet values of the module provided by the manufacturer. The temperature was measured by the temperature sensor (i.e., 38 °C) at the time of experiment. The calculated solar irradiance while conducting the experiment is 810 W/m^2, and other different levels of solar irradiance, such as 605, 520, and 380 W/m^2 are obtained by using different thickness of transparent paper on the modules. The P-V characteristics of a 5 × 5 PV array of 75 W rating are presented in Figure 4.6(b). It is seen from Figure 4.6(b) that there is a deviation between the simulated and measured P-V curve of a PV array for lower voltage range from 0 to 30 V and high voltage range from 40 to 50 V. The reasons for the deviation between the two curves are as follows: (i) the solar irradiation may be changing slightly while performing an experiment, (ii) at lower voltage range i.e. 0 to 30V before MPP, the variation in load resistance (rheostat) is not smooth whereas, at the MPP

Table 4.6: Comparison of $P_{max,(est)}$ with $P_{max,(measured)}$ and $P_{max,(act)}$ of a 5×5 PV array under different irradiation at a temperature of 38 °C

Irradiation (W/m^2)	$P_{max,(est)}$ in GA (W)	$P_{max,(est)}$ in PS (W)	$P_{max,(est)}$ in MVT (W)	$P_{max,(est)}$ in Saloux (W)	$P_{max,(est)}$ in NLS (W)	$P_{max,(est)}$ in GS (W)	$P_{max,(est)}$ in LM (W)	$P_{max,(measured)}$ (W)	$P_{max,(act)}$ (W)
380	22.78	22.85	22.46	25.06	23.10	23.02	23.57	23.38	23.75
520	30.56	30.75	30.54	34.48	31.44	30.88	32.79	31.95	33.91
605	36.78	37.27	36.99	41.40	38.11	37.00	39.28	38.42	40.35
810	52.05	52.69	52.01	57.21	53.09	52.74	54.51	53.68	55.52

region, the resistance is varied precisely to obtain the correct MPP of an array and (iii) since the current changes significantly with small change in voltage at higher voltage range i.e. 40 to 50 V after MPP in the I-V curve, the variation in electrical load i.e., rheostat is not smooth enough to collect the current and voltage experimental data precisely. However, if the I-V curve of the PV array is obtained using an electronic load (6063B 250 Watt DC Electronic Load by Agilent) instead of electrical load, then the measured I-V curve can closely match with the simulated I-V curve of an array. Hence, the P-V curves obtained experimentally will be more or less same as the simulated P-V curve.

The deviation of the $P_{max,(est)}$ in LM method from $P_{max,(act)}$ and $P_{max,(measured)}$ of a PV array are minimal compared to other methods as given in Table 4.6. The (%) error of $P_{max,(est)}$ w.r.t. $P_{max,(measured)}$ and $P_{max,(actual)}$ in LM method are always less as compared with other existing methods for different irradiation conditions as shown in Figure 4.7.

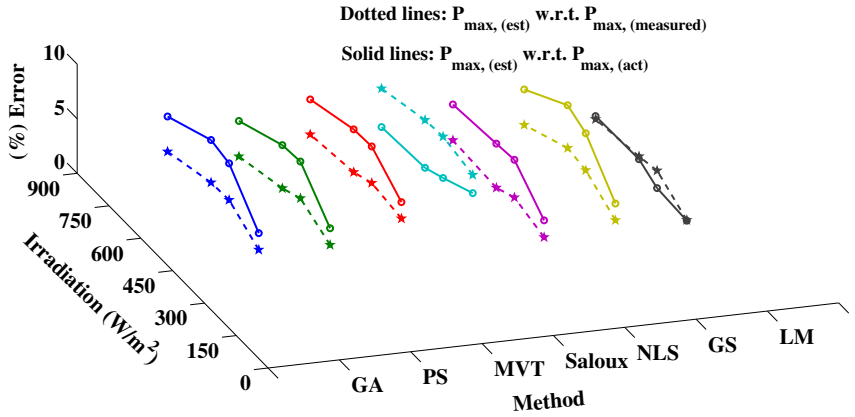

Figure 4.7: (%) Error of $P_{max,(est)}$ w.r.t. $P_{max,(measured)}$ and $P_{max,(act)}$ in different methods for different irradiation condition.

The small variation in maximum power is due to the little variation in solar irradiance and ambient

temperature while performing the experiment and discrepancy in the PV cell parameters. Fluke model 175 multimeters which has an accuracy of 1% in DC current and 0.15% in DC voltage has been used for the measurement of current and voltage of an array. Therefore, the total measurement error of ±1.15% is introduced in the present measurement of power generation of a PV array under DEC. Considering the error of ±1.15%, the measured power of an array at an irradiation of 380 W/m^2 will vary from 23.11 to 23.64 W as given in Table 4.7. The power generation of an aforementioned PV array in GA, PS, MVT, Saloux, NLS, GS, and LM methods by MATLAB simulink will vary from 22.55 to 23.00 W, 22.58 to 23.11 W, 22.20 to 22.71 W, 24.77 to 25.34 W, 22.83 to 23.36 W, 22.78 to 23.25 W, and 23.33 to 23.80 W respectively as given in Table 4.7. Hence, the maximum measurement error introduced in the present analysis by considering the maximum measured power of 23.64 W with minimum estimated power of 22.55 W in GA, 22.58 W in PS, 22.20 W in MVT, 22.94 W in NLS, and 22.78 W in GS are 4.61%, 4.48%, 6.09%, 3.42%, and 3.63% respectively. Similarly the maximum measurement error of 8.80% is introduced in Saloux method by considering the maximum estimated power of 25.34 W in Saloux with minimum measured power of 23.11 W. However, the maximum measurement error of 2.89% which is well within the limit, is introduced in LM method by considering the maximum estimated power of 23.80 W in LM with minimum measured power of 23.11 W. In the same way, the maximum measurement error introduced in aforesaid methods for the solar irradiation of 520, 605, and 810 W/m^2 can be estimated.

Table 4.7: Maximum measurement error in the power generation of a 5 × 5 PV array in different methods for the irradiation of 380 W/m^2

(%) Uncertainty in measurement	$P_{max,(est)}$ in GA (W)	$P_{max,(est)}$ in PS (W)	$P_{max,(est)}$ in MVT (W)	$P_{max,(est)}$ in Saloux (W)	$P_{max,(est)}$ in NLS (W)	$P_{max,(est)}$ in GS (W)	$P_{max,(est)}$ in LM (W)	$P_{max,(measured)}$ (W)
+1.15 corrected	22.55	22.58	22.20	24.77	22.83	22.78	23.33	23.11
Actual measurement	22.78	22.85	22.46	25.06	23.10	23.02	23.57	23.38
-1.15 corrected	23.00	23.11	22.71	25.34	23.36	23.25	23.80	23.64

As seen from Figure 4.6(b), there is a deviation between the simulated and measured P-V curves. Therefore, for further validation of the accuracy of a DDM, a number of experiments under DEC are performed precisely by considering a 15 W PV module (specification of the module mentioned in Chapter 2). The I-V and P-V characteristics of the module obtained experimentally and by simulation

are presented in Figure 4.8(a) and (b) respectively. It is seen from the figures that I-V and P-V curves obtained experimentally and by simulation are closely matched under DEC. The MPP obtained experimentally and estimated using LM method of a DDM module under different irradiation at a temperature of 29 °C are presented in Table 4.8. It is observed from the table that the % error of $P_{max,(est)}$ w.r.t. $P_{max,(measured)}$ under DEC is minimal. Thus, it validates the accuracy of a DDM PV module and the proposed method.

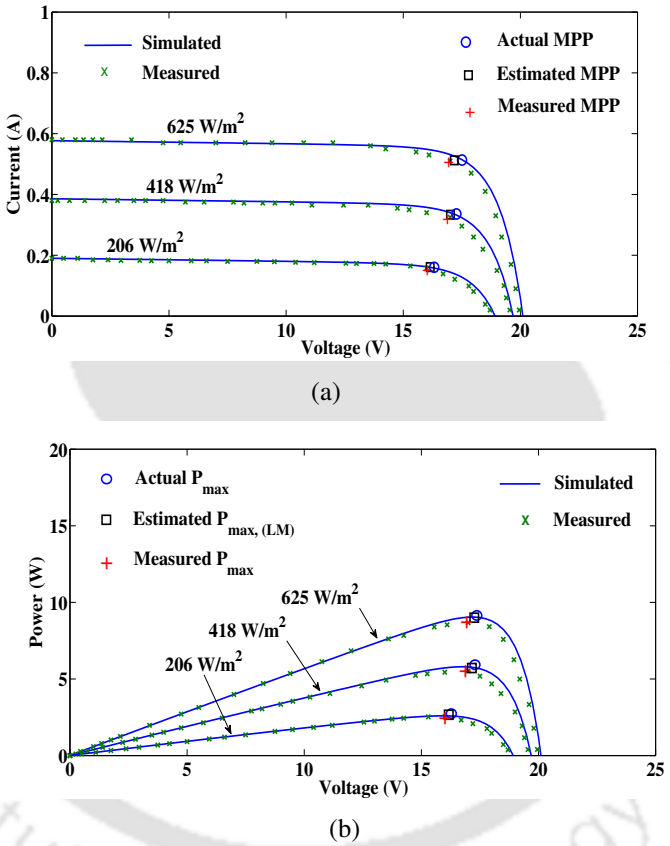

Figure 4.8: (a) I-V curve and (b) P-V curve of a 15 W PV module at a temperature of 29 °C with varying irradiations.

Table 4.8: MPP of a 15 W PV module at a temperature of 29 °C with varying irradiations

Temperature (°C)	Irradiation (W/m^2)	V_{mp} (V)	I_{mp} (A)	$P_{max,(est)}$ (W)	$P_{max,(measured)}$ (W)	(%) Error of $P_{max,(est)}$ w.r.t. $P_{max,(measured)}$
29	206	16.08	0.16	2.57	2.52	1.98
	418	16.91	0.34	5.74	5.52	3.98
	625	17.25	0.52	8.97	8.67	3.46

4.5 Summary of the chapter

In this chapter, a model based MPP estimation of a PV module has been presented. The estimation of MPP of a DDM PV module based on its characteristic equation is carried out by using the LM method under DEC. The parameters of a DDM PV module are estimated by using data sheet values at STC provided by the manufacturer and also the effect of solar irradiation and temperature on the parameters are presented. MATLAB platform is used for the demonstration of the proposed method to estimate the MPP of a DDM PV array under DEC and also partial shading conditions. It is observed that the estimated MPP of a PV array is more or less same as the actual MPP of an array. A comparative study between LM method with six different existing methods such as GA, PS, MVT, Saloux, NLS, and GS is presented under DEC. From the simulation results, it is observed that the accuracy of the proposed method is high as compared to other methods. The execution time to obtain the MPP of a 250 W DDM PV module in the LM method is low and slightly higher than the two explicit methods such as MVT and Saloux. However, the accuracy of the estimation of the MPP of a DDM PV module in MVT and Saloux methods is less as compared with other methods. For further validation of the proposed method, the estimated MPP at non-STC are compared with the MPP obtained experimentally for a 75 W PV array. It is observed that the difference between the estimated, measured, and an actual MPP of a PV array is minimal. Therefore, the proposed method for the estimation of MPP of a DDM PV module is simple, robust, accurate and computationally efficient. Hence, the proposed method can be used in industry for simple and accurate estimation of MPP of a DDM PV module.

Since the PV systems are susceptible to large amounts of power losses due to partial shading on an array, in the next chapter, for the enhancement in the power generation of an array, a Futoshiki puzzle pattern for the rearrangement of the modules in the TCT configuration under PSC has been proposed.

Note: This work, Estimation of maximum power point of a double diode model photovoltaic module has been published in IET Power Electronics.

5

Maximizing the Power Generation of a Partially Shaded PV Array

Contents

5.1 Introduction

PV power system is growing rapidly in the present scenario because of the solar energy source is free from environmental pollution and has low maintenance. At the present scenario, among all the renewable energy sources, the impact of the solar energy to meet the energy demand of the society is high [39, 100–102]. However, the major issues of a PV system are high installation cost, and low energy efficiency [103–106] but it is expected that, with the development of the technology, the installation cost of a PV system will decrease in future.

Partial shading is one of the causes of decrease of the power generation of a PV array. It occurs due to the moving clouds, deposition of sand or dust, and shadows of nearby trees or house. The modules of a PV array receive nonuniform solar irradiation under PSC, and hence, there is a mismatch between the modules current [16]. As the shaded modules generate less current than the unshaded modules and the current of shaded modules limits the output current of a PV array, the power generation of a PV array under partial shading reduces. The modules of a PV array receive different levels of solar irradiation under PSC, which may give multiple local-maxima in P-V characteristic [59]. Different MPPT algorithms are used to track the LMPP of an array [107], and also different methods are proposed to track the GMPP of an array [48, 61–63, 108].

As discussed in Chapter 1, four different types of topology of a PV array, such as SP, BL, TCT and HC exist and the power generation in the TCT configuration is higher than the other three configurations under PSC. The PEE is proposed for the enhancement of the power generation of a PV array under PSC [3]. However, the practical implementation of PEE in a large PV plant, a large number of sensors, switches and a complex control algorithm are required. The power generated by the PV array is enhanced using the EAR technique under PSC [76–78]. In EAR technique, electrical connection of PV modules is changed dynamically according to the shading condition. Therefore, during the practical implementation of a large PV system, a large number of sensors and switches are required for changing the electrical connections of PV modules. In order to eliminate the above limitations, in this work, a Futoshiki configuration technique is proposed to change the physical location of the modules of a PV array in TCT configuration without changing the electrical connection of the modules. This configuration enables the distribution of shading effect over the entire array, and reduces the shading

of the modules in the same row, which ensures the enhancement of the power generation of a PV array under PSC. The performance of a 5×5 PV array under different shading conditions demonstrated that the power output of the Futoshiki configuration with respect to the TCT configuration has increased.

This chapter is organized as follows: Section 5.2 describes details of the TCT and Futoshiki configuration of a PV array. The simulation results and experimental results of a 5 × 5 PV array under different shading conditions are presented in Section 5.3. The conclusion of the present work is presented in Section 5.4.

5.2 Description of Different PV Array Configuration

5.2.1 Electrical modeling of a PV module

The detail explanation of an electrical equivalent model of an SDM PV module is provided in Section 2.2 of Chapter 2.

5.2.2 TCT configuration of a PV array

The specification of the PV module (make: Askhay Solar Pvt. Ltd, India) at STC as shown in Table 5.1, is considered for the study.

Table 5.1: Datasheet values of PV module at STC

Parameters	Values
PV Power	3W
V_{oc}	10.60V
I_{sc}	0.37A
I_{mp}	0.34A
V_{mp}	8.70V
N_s	18

The TCT configuration of a 5 × 5 PV array (25 numbers of SDM module as shown in Figure 1.3(a)) is shown in Figure 5.1(a). The current produced by a module which depends on the solar irradiation G is calculated as follows [67]:

$$I = K_G I_m = (G/G_{STC}) \times I_m \tag{5.1}$$

where I_m is the current generated by the module at STC.

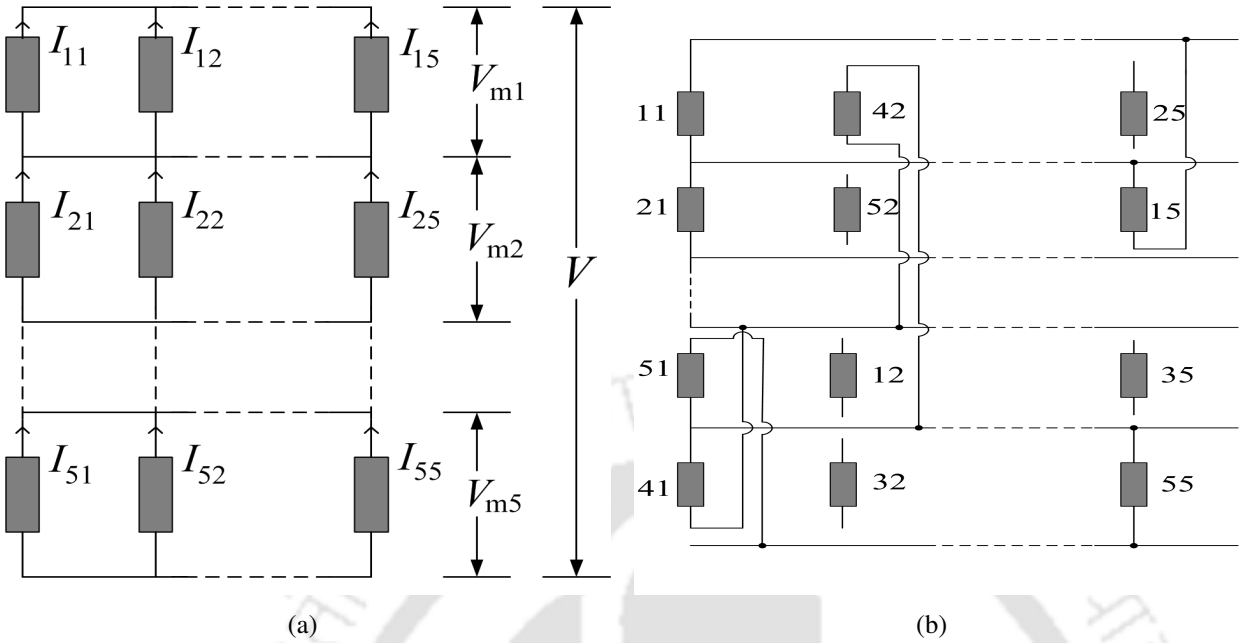

Figure 5.1: (a) TCT and (b) Futoshiki configuration of a PV array.

Using Kirchhoff's voltage law, the voltage of the array is calculated using the following equation:

$$V = \sum_{x=1}^{5} V_{mx} \tag{5.2}$$

where V_{mx} is the voltage of the x^{th} row of a PV array.

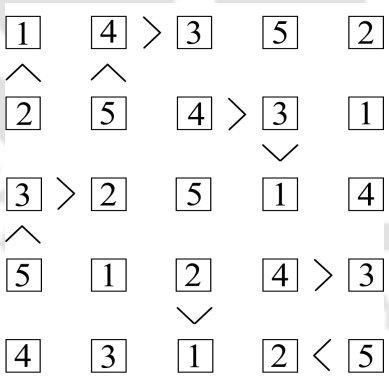

Figure 5.2: Futoshiki arrangement of a 5 × 5 grid.

5.2.3 Futoshiki configuration of a PV array

Futoshiki is a logic based puzzle for a $n \times n$ square grid. In this puzzle, the number 1 to n is placed in such a way that, each row and column of a square grid contains the digit 1 to n without repeating any number. During the placement of the digits in the square grid, the digit must respect

Table 5.2: Different configuration of a 5 × 5 PV array

(a) TCT

11	12	13	14	15
21	22	23	24	25
31	32	33	34	35
41	42	43	44	45
51	52	53	54	55

(b) Futoshiki

11	42	33	54	25
21	52	43	34	15
31	22	53	14	45
51	12	23	44	35
41	32	13	24	55

the initially specified inequality constraint between two adjacent numbers, and hence the puzzle has a unique solution. Linear programming approach (LPA) is used to generate the proper logic Futoshiki puzzle, which always contains a unique solution [109]. A Futoshiki puzzle pattern of a 5×5 PV array is shown in Figure 5.2. In this pattern, the row position of a 5 × 5 PV array is arranged using the digits 1 to 5, as shown in Table 5.2(b), and this arrangement shows that there is no repetition of digits 1 to 5 in each row and each column of a PV array. During PSC, the shaded modules in a PV array will be dispersed in such a way that, for any Futoshiki puzzle patterns, the low current in the row and the output voltage of an array will remain the same. Therefore, the output power, i.e., the product of low current and output voltage, will remain the same. Therefore, in the present analysis, a particular Futoshiki puzzle pattern has been chosen. The modules of a PV array in TCT configuration (Figure 5.1(a)), are rearranged using the Futoshiki configuration technique, without changing the electrical connection of the modules under PSC, as shown in Figure 5.1(b). In this arrangement, the module 42 (fourth row, second column) is physically placed on the first row second column, and the module 15 is physically placed on the second row fifth column of a PV array without changing the electrical connections. The modules of the same row in the TCT configuration are moved to different rows in the proposed configuration of the array without changing the column position. Thus, it enables to decrease the shading effect in the same row and to enhance the current in the same row. Hence, bypass panels are reduced, and the power generated by a PV array is increased under PSC. The voltage and current equations of the proposed configuration remain same as in the TCT configuration, because the electrical connection of a PV array is unchanged.

The shading effect is distributed in both the EAR and the proposed method. However, the practical implementation of reconfiguration method requires a number of sensors, switches, and a control algo-

rithm, because the electrical connection of the modules is changed dynamically according to shading conditions. However, the practical implementation of the proposed method does not require sensors, switches, and a control algorithm, because the electrical connection of the PV modules remains fixed. For the practical implementation of the Futoshiki configuration for the enhancement of the power generation in shading condition, the modules of a PV array in TCT configuration need to be rearranged once only, because of the same configuration holds effective for any shading condition. This rearrangement of the modules is carried out only once by the PV plant installer at the time of installation. As an illustration of the proposed method, a 1 MW, 750 V, 25 × 160 PV array which can be integrated with the microgrid or the distribution network is constructed by assembling 160 numbers of 6.25 kW, 150 V, 5 × 5 sub-array arranged using the proposed method. Hence, this large PV system is viewed as a 5 × 32 array, as shown in Figure 5.3. At the time of installation, the modules of all sub-array, i.e., 5 × 5 PV array, are rearranged using the proposed technique. Whenever shading occurs in a 25 × 160 PV array, the shade is dispersed in the sub-array which ensures the enhancement of the power generation. Therefore, the proposed technique can be applied for large square or rectangular PV array for the enhancement of the power generation compared with the TCT configuration during shading condition.

Table 5.3: Solar irradiation on hourly basis during sunshine hours

Sunshine hours	5	6	7	8	9	10	11	12	13	14	15	16	17	18
USI (W/m^2)	40	150	250	400	560	700	800	900	800	650	450	250	100	10
SSI (W/m^2)	16	60	100	160	224	280	320	360	320	260	180	100	40	4

For the validation of power enhancement of a PV array in the proposed configuration with respect to the TCT configuration in a real time scenario, the monthly averaged daily on an hourly basis solar irradiation during the sunshine time in hours (5 to 18 h) in the month of May-2012 of Guwahati city as shown in Table 5.3, is considered. Matlab platform is used for different intensity of shading modules of a PV array, and the effect of power generation of a PV array is demonstrated. Assuming some of the modules of a PV array receive 40% of unshaded solar irradiation (USI) (i.e., shaded solar irradiation (SSI)) in the presence of neighborhood obstacle, the shaded modules for each hour from 9

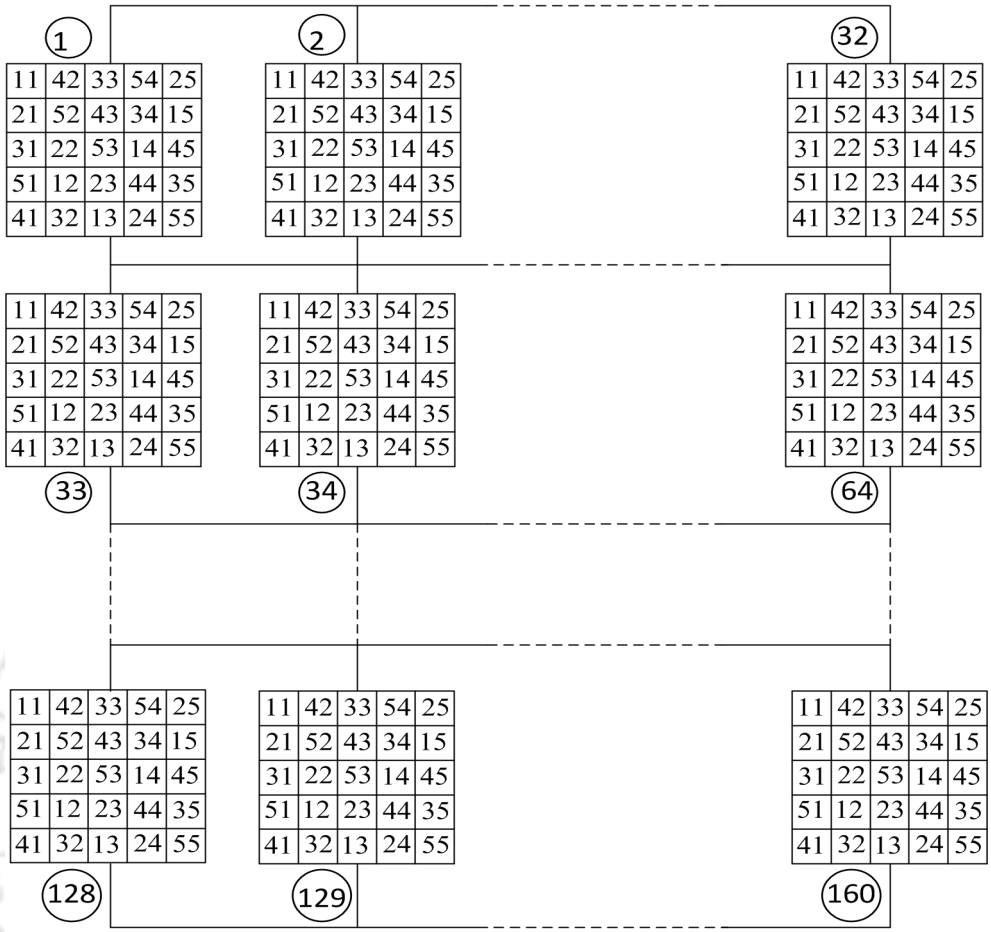

Figure 5.3: A 1 MW, 750 V 25×160 large PV array assembled by a 6.25 kW, 150 V 5×5 sub-array arranged by the proposed method.

to 15 h is represented by different symbols, as shown in Figure 5.4.

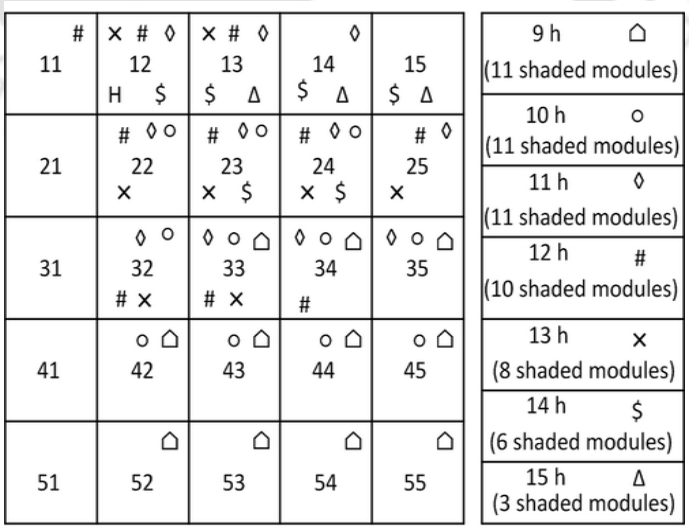

Figure 5.4: PSC occur on a 5×5 PV array an hourly basis during sunshine hours.

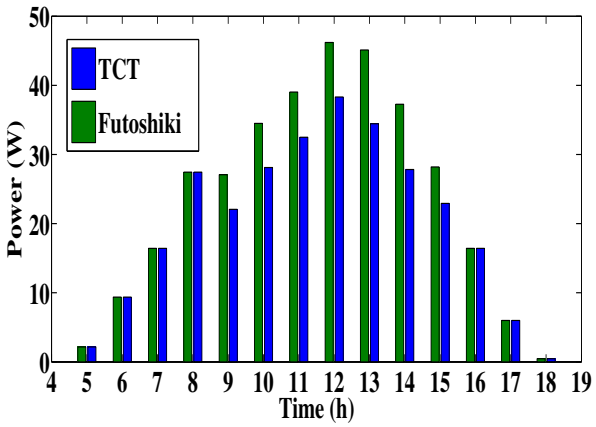

Figure 5.5: Power versus sunshine hours of a PV array.

From Figure 5.5, it is seen that there is a significant power enhancement in the proposed configuration with respect to the TCT configuration of a PV array under different types of shading conditions from 9 to 15 h. Therefore, in this work, four different standard shading conditions, such as SW, LW, SN, and LN [1] are taken for the estimation of power output of a PV array by using the proposed method, as shown in Figure 1.11.

5.3 Results and discussion

A 5 × 5 PV array is considered for TCT connection under four different standard shading conditions, for the demonstration of the proposed method for shade dispersion. The location of GMPP, calculated theoretically, simulated by using MATLAB simulink, and estimated experimentally, is compared for both the TCT and Futoshiki configurations. P-V and mismatch loss (ML) - shading factor (SF) characteristics of a 5 × 5 PV array for TCT and Futoshiki configuration are plotted in four different shading conditions.

5.3.1 Theoretical and simulation results for power enhancement

5.3.1.1 SW shading condition

In SW shading condition, three different types of solar irradiation, such as 950, 600, and 220 W/m^2, are received by the modules of a PV array, as shown in Table 5.4. It is necessary to calculate the current across each row of a PV array, to determine the location of GMPP. In the calculation of current, it is assumed that all the modules of a PV array are producing the same current I_m at STC. As all the modules of rows 1-3 receive the same irradiation of 950 W/m^2, so the current across the rows

1-3 in TCT (Table 5.4(a)) configuration is calculated as follows:

$$I_{R3} = I_{R2} = I_{R1} \quad = \quad 5 \times \frac{950}{1000} I_m = 4.75 I_m \tag{5.3}$$

In rows 4 and 5 of a PV array, the first three and next two modules receive solar irradiation of 600 and 220 W/m^2, respectively. Therefore, the current across the rows 4 and 5 is calculated as follows:

$$I_{R5} = I_{R4} \quad = \quad 3 \times 0.6 I_m + 2 \times 0.22 I_m = 2.24 I_m \tag{5.4}$$

The shading pattern of Futoshiki configuration [Table 5.4(b), physically placed] is same as shade

Table 5.4: Shading pattern for different configurations in SW shading condition.

950 W/m^2 600 W/m^2 220 W/m^2

(a) TCT

11	12	13	14	15
21	22	23	24	25
31	32	33	34	35
41	42	43	44	45
51	52	53	54	55

(b) Futoshiki

11	42	33	54	25
21	52	43	34	15
31	22	53	14	45
51	12	23	44	35
41	32	13	24	55

(c) Shade dispersion with Futoshiki

11	12	13	14	15
21	22	23	24	25
31	32	33	34	35
41	42	43	44	45
51	52	53	54	55

Table 5.5: Location of GMPP in TCT and Futoshiki configuration for SW shading condition

TCT configuration			Futoshiki configuration		
$*I_R$	Array Voltage (V)	Array Power (P)	$*I_R$	Array Voltage (V)	Array Power (P)
I_{R5} $2.24I_m$	$5V_m$	$11.20V_mI_m$	I_{R5} $3.67I_m$	$5V_m$	$18.35V_mI_m$
I_{R4} $2.24I_m$	$4V_m$	$8.96V_mI_m$	I_{R4} $3.67I_m$	$4V_m$	$14.68V_mI_m$
I_{R3} $4.75I_m$	$3V_m$	$14.25V_mI_m$	I_{R3} $3.67I_m$	$3V_m$	$11.01V_mI_m$
I_{R2} $4.75I_m$	$2V_m$	$9.50V_mI_m$	I_{R2} $3.67I_m$	$2V_m$	$7.34V_mI_m$
I_{R1} $4.75I_m$	V_m	$4.75V_mI_m$	I_{R1} $4.05I_m$	V_m	$4.05V_mI_m$

$*I_R$ is the row current of a PV array which are bypassed in increasing order and V_m is the voltage of each module at STC.

dispersion with Futoshiki configuration [Table 5.4(c), electrically connected] because the rearrangement of Futoshiki configuration is called shade dispersion with Futoshiki configuration. The current across each row of a PV array for shade dispersion with Futoshiki configuration is calculated using

the following equations:

$$\begin{aligned} I_{R1} &= 3 \times 0.95I_m + 2 \times 0.6I_m = 4.05I_m \\ I_{R2} &= 3 \times 0.95I_m + 0.6I_m + 0.22I_m = 3.67I_m \\ I_{R5} &= I_{R4} = I_{R3} = I_{R2} \end{aligned} \tag{5.5}$$

The power enhancement in the proposed configuration with respect to TCT configuration in PSC is calculated as follows:

$$\%P(enhancement) = \frac{P_{\max,(Futoshiki)} - P_{\max,(TCT)}}{P_{\max,(TCT)}} \times 100 \tag{5.6}$$

The voltages and row currents of a PV array in TCT and Futoshiki configuration are given in Table 5.5. To obtain the GMPP of a PV array, the row having less solar irradiation, i.e., low current, is bypassed in increasing order of the module current. If any row of the PV array is not bypassed, then the voltage of the array is 5Vm, neglecting small variation of voltage in each row. If the PV modules of one row are bypassed, then the voltage of the array is 4Vm, neglecting diode voltage. According to the number of bypassed rows, the voltage of the array is calculated, which is given in Table 5.5. It is demonstrated that the location of GMPP occurred at reduced voltage level, and it is far away from MPP voltage when rows 4 and 5 are bypassed in the TCT configuration of a PV array. Whereas, in the proposed configuration, the location of GMPP occurred at the MPP voltage of an array. The generation of power at GMPP is 14.25 and $18.35V_mI_m$ in TCT and Futoshiki configuration, respectively. Thus, the power enhancement theoretically calculated in the proposed configuration with respect to TCT configuration is 28.77%. To verify the theoretical results, the P-V characteristics of a PV array is simulated using MATLAB, and the simulation results are shown in the Figure 5.6.

From the Figure 5.6, it is seen that the maximum power produced for TCT and Futoshiki configuration is 40.07 and 53.93 W, respectively. Hence, the maximum power produced in Futoshiki configuration is 34.58% higher than the TCT configuration. It is observed that, the GMPP occurs at low voltage in TCT configuration, is shifted to MPP voltage of a PV array in the proposed arrangement. The power produced in the proposed configuration is higher than TCT, because of shading effects are distributed over the array.

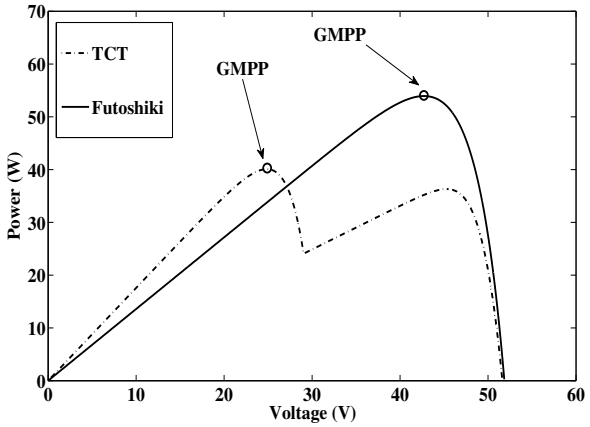

Figure 5.6: Simulated P-V curve for SW shading condition.

5.3.1.2 LW shading condition

In LW shading pattern, four different types of solar irradiation, such as 950, 760, 600, and 220 W/m^2, are received by the modules of a PV array. The shading pattern of TCT, Futoshiki, and shade dispersion with Futoshiki configuration is shown in Table 5.6.

Table 5.6: Shading pattern for different configurations in LW shading condition

950 W/m^2 760 W/m^2 600 W/m^2 220 W/m^2

(a) TCT

11	12	13	14	15
21	22	23	24	25
31	32	33	34	35
41	42	43	44	45
51	52	53	54	55

(b) Futoshiki

11	42	33	54	25
21	52	43	34	15
31	22	53	14	45
51	12	23	44	35
41	32	13	24	55

(c) Shade dispersion with Futoshiki

11	12	13	14	15
21	22	23	24	25
31	32	33	34	35
41	42	43	44	45
51	52	53	54	55

Table 5.7: Location of GMPP in TCT and Futoshiki configuration for LW shading condition

TCT configuration				Futoshiki configuration			
*I_R		Array Voltage (V)	Array Power (P)	*I_R		Array Voltage (V)	Array Power (P)
I_{R5}	$1.86I_m$	$5V_m$	$9.30V_mI_m$	I_{R2}	$3.10I_m$	$5V_m$	$15.50V_mI_m$
I_{R4}	$1.86I_m$	$4V_m$	$7.44V_mI_m$	I_{R1}	$3.29I_m$	$4V_m$	$13.16V_mI_m$
I_{R3}	$4.37I_m$	$3V_m$	$13.11V_mI_m$	I_{R5}	$3.48I_m$	$3V_m$	$10.44V_mI_m$
I_{R2}	$4.37I_m$	$2V_m$	$8.74V_mI_m$	I_{R4}	$3.48I_m$	$2V_m$	$6.96V_mI_m$
I_{R1}	$4.37I_m$	V_m	$4.37V_mI_m$	I_{R3}	$3.48I_m$	V_m	$3.48V_mI_m$

The current across each row, voltage, and power of a PV array is given in Table 5.7. It is seen from Table 5.7 that the power generated at GMPP in TCT and Futoshiki configuration is 13.11 and $15.50 V_m I_m$, respectively. Hence, the power enhancement theoretically calculated for the proposed configuration with respect to the TCT is 18.23%. The maximum power generated for the TCT and proposed configuration is 36.60 and 47.52 W, respectively, as seen from the Figure 5.7. Therefore, the maximum power generated in the proposed configuration is 29.83% higher than the TCT configuration. It is observed that the GMPP occurs at lower voltage in TCT configuration, but in Futoshiki configuration, the GMPP coincides with MPP voltage of a PV array.

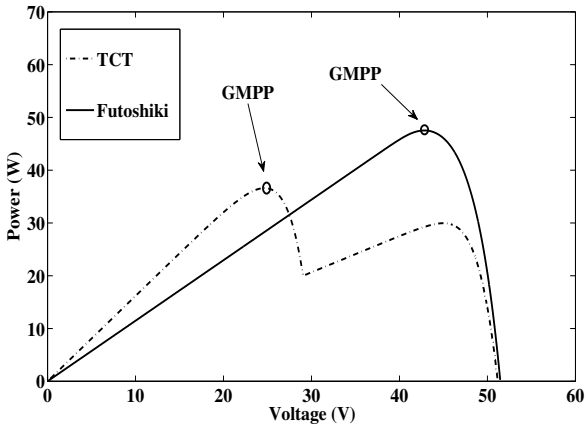

Figure 5.7: Simulated P-V curve for LW shading condition.

5.3.1.3 SN shading condition

In SN shading pattern, three different types of solar irradiation, such as 950, 600, and 520 W/m^2, are received by the modules of a PV array. The shading pattern of TCT, Futoshiki, and shade dispersion with Futoshiki configuration is shown in Table 5.8.

The location of GMPP theoretically calculated in the TCT and proposed configuration is shown in the Table 5.9. The power generated at GMPP in the TCT and proposed configuration is 19.45 and $21.60 V_m I_m$, respectively. Hence, the power enhancement theoretically calculated for the proposed configuration with respect to TCT configuration is 11.05%.

From Figure 5.8, it is seen that the maximum power generated for TCT and Futoshiki configuration is 62.06 and 64.87 W, respectively. Therefore, the maximum power generated in the proposed configuration is 4.52% higher than TCT configuration.

Table 5.8: Shading pattern for different configurations in SN shading condition

950 W/m^2 600 W/m^2 520 W/m^2

(a) TCT

11	12	13	14	15
21	22	23	24	25
31	32	33	34	35
41	42	43	44	45
51	52	53	54	55

(b) Futoshiki

11	42	33	54	25
21	52	43	34	15
31	22	53	14	45
51	12	23	44	35
41	32	13	24	55

(c) Shade dispersion with Futoshiki

11	12	13	14	15
21	22	23	24	25
31	32	33	34	35
41	42	43	44	45
51	52	53	54	55

Table 5.9: Location of GMPP in TCT and Futoshiki configuration for SN shading condition

TCT configuration			Futoshiki configuration		
$*I_R$	Array Voltage (V)	Array Power (P)	$*I_R$	Array Voltage (V)	Array Power (P)
I_{R4} $3.89I_m$	$5V_m$	$19.45V_mI_m$	I_{R4} $4.32I_m$	$5V_m$	$21.60V_mI_m$
I_{R5} $4.05I_m$	$4V_m$	$16.20V_mI_m$	I_{R3} $4.32I_m$	$4V_m$	$17.28V_mI_m$
I_{R3} $4.75I_m$	$3V_m$	$14.25V_mI_m$	I_{R5} $4.4I_m$	$3V_m$	$13.20V_mI_m$
I_{R2} $4.75I_m$	$2V_m$	$9.50V_mI_m$	I_{R2} $4.4I_m$	$2V_m$	$8.80V_mI_m$
I_{R1} $4.75I_m$	V_m	$4.75V_mI_m$	I_{R1} $4.75I_m$	V_m	$4.75V_mI_m$

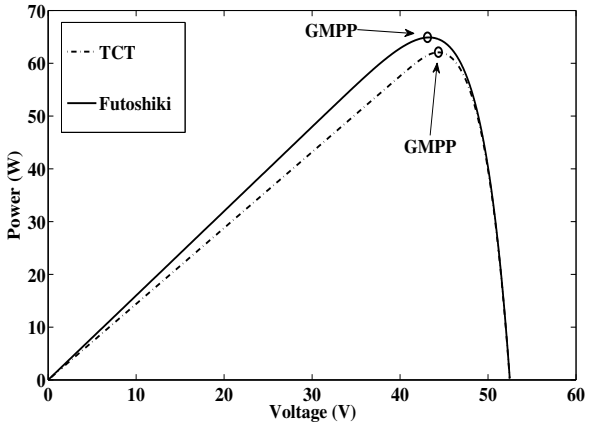

Figure 5.8: Simulated P-V curve for SN shading condition.

5.3.1.4 LN shading condition

In LN shading pattern, three different types of solar irradiation, such as 950, 650, and 520 W/m^2, are received by PV modules.The shading pattern of TCT, Futoshiki, and shade dispersion with Futoshiki configuration is shown in Table 5.10. The location of GMPP of the TCT and proposed configuration is shown in the Table 5.11. The power generated at GMPP in the TCT and proposed configu-

Table 5.10: Shading pattern for different configurations in LN shading condition

950 W/m^2 650 W/m^2 520 W/m^2

(a) TCT

11	12	13	14	15
21	22	23	24	25
31	32	33	34	35
41	42	43	44	45
51	52	53	54	55

(b) Futoshiki

11	42	33	54	25
21	52	43	34	15
31	22	53	14	45
51	12	23	44	35
41	32	13	24	55

(c) Shade dispersion with Futoshiki

11	12	13	14	15
21	22	23	24	25
31	32	33	34	35
41	42	43	44	45
51	52	53	54	55

ration is 19.45 and 20.10V_mI_m, respectively. Hence, the power enhancement theoretically calculated for the proposed configuration with respect to TCT configuration is 3.34%.

Table 5.11: Location of GMPP in TCT and Futoshiki configuration for LN shading condition

TCT configuration			Futoshiki configuration		
$*I_R$	Array Voltage (V)	Array Power (P)	$*I_R$	Array Voltage (V)	Array Power (P)
I_{R5} 3.89I_m	5V_m	19.45V_mI_m	I_{R4} 4.02I_m	5V_m	20.10V_mI_m
I_{R4} 3.89I_m	4V_m	15.56V_mI_m	I_{R3} 4.02I_m	4V_m	16.08V_mI_m
I_{R3} 4.15I_m	3V_m	12.45V_mI_m	I_{R1} 4.15I_m	3V_m	12.45V_mI_m
I_{R2} 4.15I_m	2V_m	8.30V_mI_m	I_{R5} 4.32I_m	2V_m	8.64V_mI_m
I_{R1} 4.75I_m	V_m	4.75V_mI_m	I_{R2} 4.32I_m	V_m	4.32V_mI_m

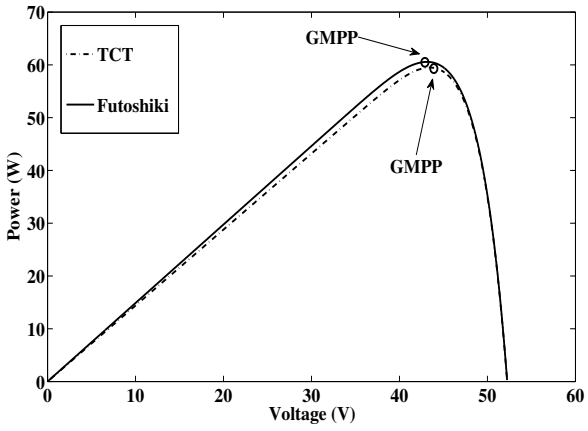

Figure 5.9: Simulated P-V curve for LN shading condition.

From the Figure 5.9, it is seen that the maximum power generated for TCT and Futoshiki configuration is 59.41 and 60.56 W, respectively. Therefore, the maximum power produced in Futoshiki

configuration is 1.93% higher than the TCT configuration. In Futoshiki configuration, there may be multiple peaks in the P-V curve, however, in the present work, it is not visible, because the distribution of shadow over each row of the PV array is nearly equal.

5.3.2 Experimental results for power enhancement

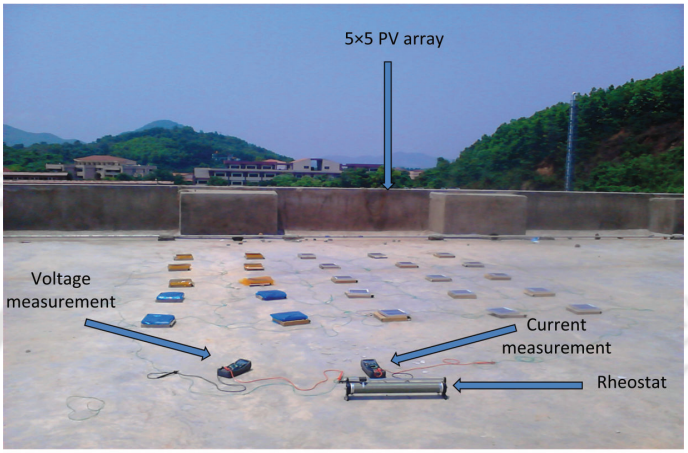

Figure 5.10: Laboratory scale experimental setup.

A laboratory scale experimental setup was developed on the roof of the Department of Electronics and Electrical Engineering, IIT Guwahati to validate the results obtained theoretically and by the MATLAB simulation for TCT and Futoshiki configuration under PSC as shown in Figure 5.10. The experimental setup was prepared by taking twenty-five numbers of the same rating PV modules as given the Table 5.1, one rheostat (300 Ω, 2A), two multimeters, connecting wires, and the transparent papers of different colors to create the partial shading environment.

The power generation of a PV array is calculated by multiplying the row current which is same as the array current measured by the multimeter connected in series with rheostat, and the array voltage measured by the multimeter connected across the rheostat. The level of solar irradiation at the time of the experiment (11:00 A.M., May 25, 2014) is calculated by using (5.1) and the data sheet values of the module. The solar irradiation calculated at the time of performing an experiment was 950 W/m^2, and other different levels of solar irradiation, such as 760, 650, 600, 520, and 220 W/m^2, are obtained by putting different thickness and colors of transparent sheets on the modules. The same level of irradiation is also achieved using the measured and the data sheet values of SCC [12]. These different levels of irradiations are used to calculate the GMPP of a 5×5 PV array. The experimental results are

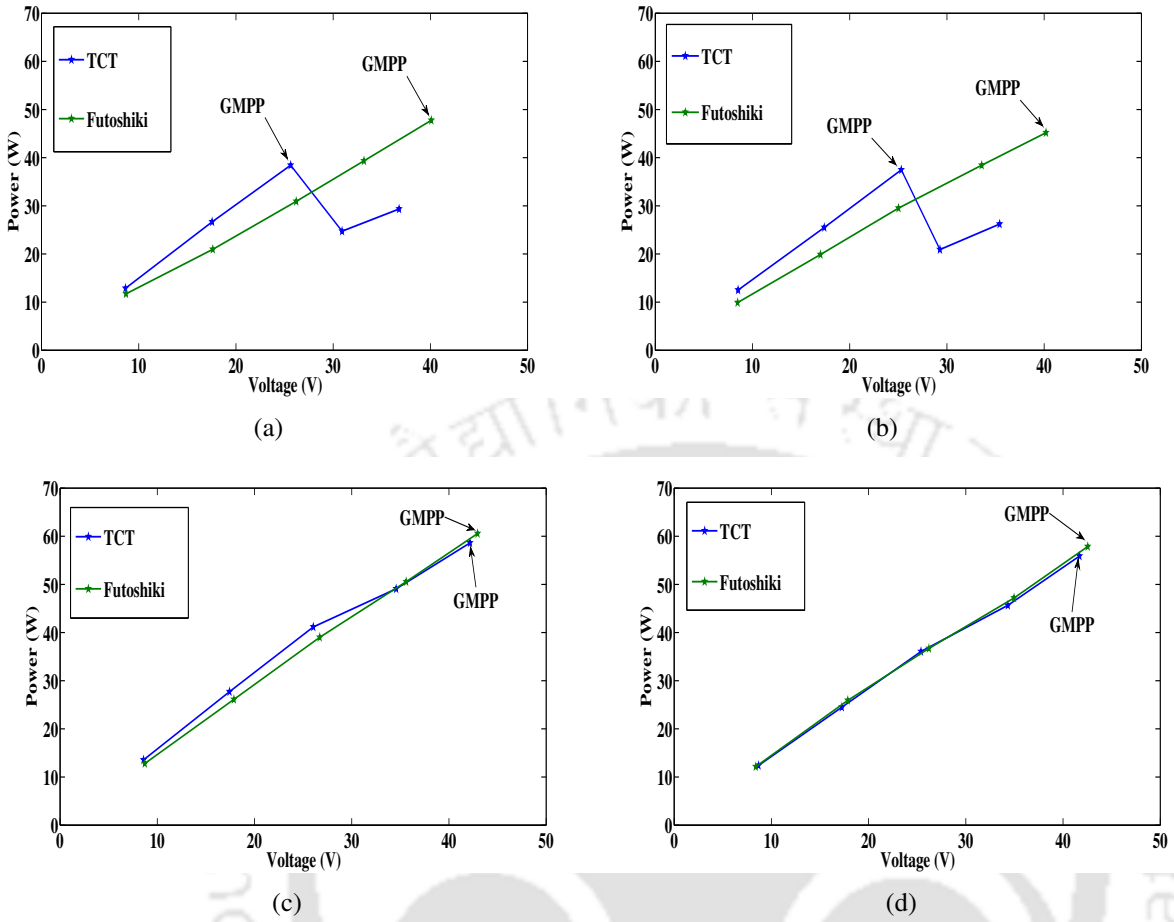

Figure 5.11: Experimentally obtained GMPP for (a) SW, (b) LW, (c) SN, and (d) LN shading conditions.

obtained after bypassing one by one row of a PV array in the increasing order of the row currents as GMPP is achieved theoretically. The experimentally obtained P-V characteristics for a 5×5 PV array for TCT and Futoshiki configuration for four different shading conditions are explained in Figure 5.11.

The power generation of a 5×5 PV array obtained theoretically, experimentally, and by simulation in TCT and Futoshiki configuration for four different shading conditions is shown in Table 5.12. It is observed that, there is a significant enhancement in the power generation of a PV array for SW and LW shading conditions. There is a minor deviation of the power generation in the experimental result from the theoretical and simulation result under four different shading conditions as given in Table 5.12. The deviation is due to the slight change in the solar irradiation at the time of conducting the experiment and mismatch in the cell parameters.

In SW shading condition, the generation of power at GMPP in TCT and Futoshiki configuration

Table 5.12: Comparison of power generated in TCT and Futoshiki configuration for different shading conditions

shading conditions	TCT (Max Power)			Futoshiki (Max Power)			Power Enhancement (%)		
	Theoretical	Simulated (W)	Experimental (W)	Theoretical	Simulated (W)	Experimental (W)	Theoretical	Simulated	Experimental
SW	$14.25V_mI_m$	40.07	38.44	$18.35V_mI_m$	53.93	47.76	28.77	34.58	24.24
LW	$13.11V_mI_m$	36.60	37.47	$15.50V_mI_m$	47.52	45.18	18.23	29.83	20.57
SN	$19.45V_mI_m$	62.06	58.62	$21.6V_mI_m$	64.87	60.57	11.05	4.52	3.32
LN	$19.45V_mI_m$	59.41	55.88	$20.1V_mI_m$	60.56	57.86	3.34	1.93	3.54

is 38.44 and 47.76 W, respectively. Hence, the power enhancement in Futoshiki configuration with respect to TCT configuration is 24.24%. In LW shading condition, the power generated at GMPP in TCT and Futoshiki configuration is 37.47 and 45.18 W, respectively. Hence, the enhancement in the power generation in Futoshiki configuration with respect to TCT is 20.57%. As seen from Figure 5.11(a) and 5.11(b), in the TCT configuration of SW and LW shading condition, the fourth and fifth points of P-V curve are not nearly equal to 4 and $5V_m$, because the modules of entire fourth row and fifth row of the PV array are shaded. The mismatch is due to shading effect over the PV array. For both SW and LW shading conditions, in TCT configuration, the GMPP occurred at the reduced voltage level, whereas in Futoshiki configuration, GMPP and MPP coincide with each other, as shown in Figure 5.11(a) and 5.11(b). In SN shading condition, the power generated at GMPP in TCT and Futoshiki configuration is 58.62 and 60.57 W, respectively. Therefore, the power enhancement in Futoshiki configuration with respect to TCT is 3.32%. In LN shading condition, the power generated at GMPP in TCT and Futoshiki configuration is 55.88 and 57.86 W, respectively. Thus, the power enhancement in Futoshiki configuration with respect to TCT is 3.54%. For both SN and LN shading conditions, the GMPP and MPP coincide with each other for both TCT and Futoshiki configuration, as shown in Figure 5.11(c) and (d).

There may be a slight change of solar irradiation and small mismatch in the cell parameters of a PV array at the time of conducting the experiment. Fluke model 175 multimeters having an accuracy of 0.15% in DC voltage and 1% in DC current are used to measure the array voltage and current. Hence, the total measurement error introduced in the present measurement is ±1.15%. Considering the error of ±1.15%, the measured power of a 5×5 PV array in Futoshiki configuration under SW

shading condition will vary from 47.21 to 48.30 W, as given in Table 5.13. Since there is an error of 1% in the current measurement, an error of ±1% will be introduced in the solar radiation. Therefore, the power generation of an aforementioned PV array by MATLAB simulink will vary from 54.46 to 53.39 W, as given in Table 5.13. Hence, the maximum measurement error introduced in the present analysis by considering the maximum simulated power, i.e., 54.46 W and minimum measured power, i.e., 47.21 W is 13.31%, whereas the maximum actual measurement errors in power generation for SW, LW, SN and LN shading conditions are 11.44%, 4.92%, 6.62%, and 4.45%, respectively. The PV modules as given in Table 5.1, are used to obtain the power generation of a PV array in Futoshiki configuration. Before measuring the power generation of an array, the SCC and OCV of an individual modules are measured. It is observed that there is a 2.70% and 1.88% change in SCC and OCV, respectively, from its data sheet values. Considering the uncertainty of ±2.70% in SCC and ±1.88% in OCV, the power generation of an array obtained from MATLAB simulink will vary from 56.67 to 51.26 W, as given in Table 5.14. Therefore, the maximum parameter error introduced in the present analysis by considering maximum simulated power, i.e., 56.67 W and minimum measured power, i.e., 47.21 W, is 16.7%. The maximum measurement and parameter errors obtained for an array are well within the limit.

Table 5.13: Maximum measurement error in power generation of a 5 × 5 PV array in Futoshiki configuration in SW shading condition

(%) Uncertainty in measurement	Simulation Max Power (W)	Experimental Max Power (W)
+1.15 corrected	53.39	47.21
Actual measurement	53.93	47.76
-1.15 corrected	54.46	48.30

Taking same rating of PV module, as specified in Table 5.1, a 5 × 5 PV array is considered for the comparison between the proposed and EAR methods by using MATLAB simulink under four standard shading conditions, as shown in Table 5.4, Table 5.6, Table 5.8, and Table 5.10, respectively. It is observed that the power generation in the proposed method is same as EAR method under four different shading conditions and the power generation in both the methods is always higher than the

Table 5.14: Maximum parameter error in power generation of a 5 × 5 PV array in Futoshiki configuration in SW shading condition

(%) Uncertainty in PV module parameters	Simulation Max Power (W)	Experimental Max Power (W)
Error in SCC = -2.7, error in OCV = -1.88	51.26	47.21
Error in SCC = 0, error in OCV = 0	53.93	47.76
Error in SCC = +2.7, error in OCV = +1.88	56.67	48.30

TCT configuration, as shown in Table 5.15. The practical implementation of EAR technique in a large PV system requires a large number of sensors and switches for changing the electrical connections of the PV modules dynamically. Hence, the practical implementation of EAR scheme is more expensive and complex. However, the implementation of the proposed configuration to estimate the power generation of a PV array is economical and simpler.

Table 5.15: Comparison of power generated in TCT, EAR, and Futoshiki configuration for different shading conditions

Different shading conditions	TCT Max Power (W)	EAR Max Power (W)	Futoshiki Max Power (W)
SW	40.07	53.93	53.93
LW	36.60	47.52	47.52
SN	62.06	64.87	64.87
LN	59.41	60.56	60.56

An analytic expression for power generation of a $M \times N$ PV array for TCT and proposed configuration is analyzed. The current across each row of an array in TCT configuration is calculated as follows:

$$I_R = \sum_{i=1}^{N} \frac{G_i}{G_{STC}} I_m \tag{5.7}$$

where N is a number of modules in a particular row. Since the equivalent circuit of of TCT configuration is a single string where the modules are connected in series, the lowest value of row current is flowing in an array (provided no rows are bypassed). Thus, the lowest value of row current '$min(I_R)$' of an array is considered for the calculation of power generation of an array. The voltage of

an array is calculated as follows:

$$V = \sum_{j=1}^{M} V_{mj} \tag{5.8}$$

where M is the number of rows of an array.

The analytical expression for the power generation of a PV array is expressed as follows:

$$P = V \times min(I_R) = \sum_{j=1}^{M} \sum_{i=1}^{N} V_{mj}(\frac{G_i}{G_{STC}})I_m \tag{5.9}$$

For the validation of (5.9), the shading condition of a 5×5 PV array at 9 h, as shown in Figure 5.4, is considered.

The lowest value of the current generated in the fifth row, which is equal to the fourth row, is flowing in the TCT configuration of a PV array, as shown in Table 5.16(a). Therefore, $min(I_R)$ of a PV array is calculated as follows:

$$min(I_R) = 4 \times 0.224I_m + 0.560I_m = 1.45I_m \tag{5.10}$$

The power generated by a PV array in the TCT configuration is calculated as follows:

$$P_{TCT} = 5V_m \times 1.45I_m = 7.25V_mI_m \tag{5.11}$$

The lowest value of the current generated in first row is flowing in the Futoshiki configuration with shade dispersion of a PV array at 9 h as shown in Table 5.16(c). Therefore, $min(I_R)$ of a PV array is calculated as follows:

$$min(I_R) = 3 \times 0.224I_m + 2 \times 0.560I_m = 1.79I_m \tag{5.12}$$

The power generated by a PV array in the Futoshiki configuration is calculated as follows:

$$P_{Futoshiki} = 5V_m \times 1.79I_m = 8.95V_mI_m \tag{5.13}$$

The power enhancement of a 5×5 PV array in Futoshiki configuration with respect to TCT configuration at 9 h is 22.93%. Similarly, the power generation of a 5×5 PV array in TCT and Futoshiki configuration from 10 to 15 hrs are presented in Table 5.17. From Table 5.17, it is observed that there

Table 5.16: Shading pattern for different configurations at 9 h

560 W/m^2 224 W/m^2

(a) TCT

11	12	13	14	15
21	22	23	24	25
31	32	33	34	35
41	42	43	44	45
51	52	53	54	55

(b) Futoshiki

11	42	33	54	25
21	52	43	34	15
31	22	53	14	45
51	12	23	44	35
41	32	13	24	55

(c) Shade dispersion with Futoshiki

11	12	13	14	15
21	22	23	24	25
31	32	33	34	35
41	42	43	44	45
51	52	53	54	55

Table 5.17: Power generation of an array under different shading conditions

Sunshine hours	9	10	11	12	13	14	15
TCT configuration	$7.25V_mI_m$	$9.10V_mI_m$	$10.40V_mI_m$	$11.70V_mI_m$	$10.40V_mI_m$	$8.45V_mI_m$	$7.20V_mI_m$
Futoshiki configuration	$8.95V_mI_m$	$11.20V_mI_m$	$12.80V_mI_m$	$14.40V_mI_m$	$15.20V_mI_m$	$12.35V_mI_m$	$9.90V_mI_m$
Power enhancement (%)	23.44	23.07	23.07	23.07	46.15	46.15	37.5

is a significant enhancement of power generation in Futoshiki configuration with respect to TCT configuration of a PV array under different shading conditions from 9 to 15 h of a day. Hence, the analytical expression is given in (5.9) for the calculation of power generation of a PV array is holding true for any shading conditions.

5.3.3 Mismatch loss (ML)

When the PV plants operate under unfavorable conditions, there will be a power loss in the modules, and this loss is called mismatch ML. There are two types of ML in a PV array, such as internal and external. The internal ML occurs due to the variation in PV source parameters of a module, such as R_S, R_{sh}, V_t, and I_o, due to changes of its physical conditions, and external ML occurs due to change of solar irradiation, i.e., partial shading. This chapter is focusing on the external ML, which is calculated as follows:

$$ML = P_1 - P_2 \tag{5.14}$$

where P_1 is the sum of the maximum power of an individual modules of the array, and P_2 is the total power generated by the same array when the modules are connected electrically. The opacity of a shadow which varies between 0 to 1 is called SF, and is expressed as follows [3]:

$$SF = 1 - {}^{G}/_{G_{STC}} = 1 - K_G \tag{5.15}$$

In this work, the ML is calculated by taking the same shading pattern for SW shading condition, as

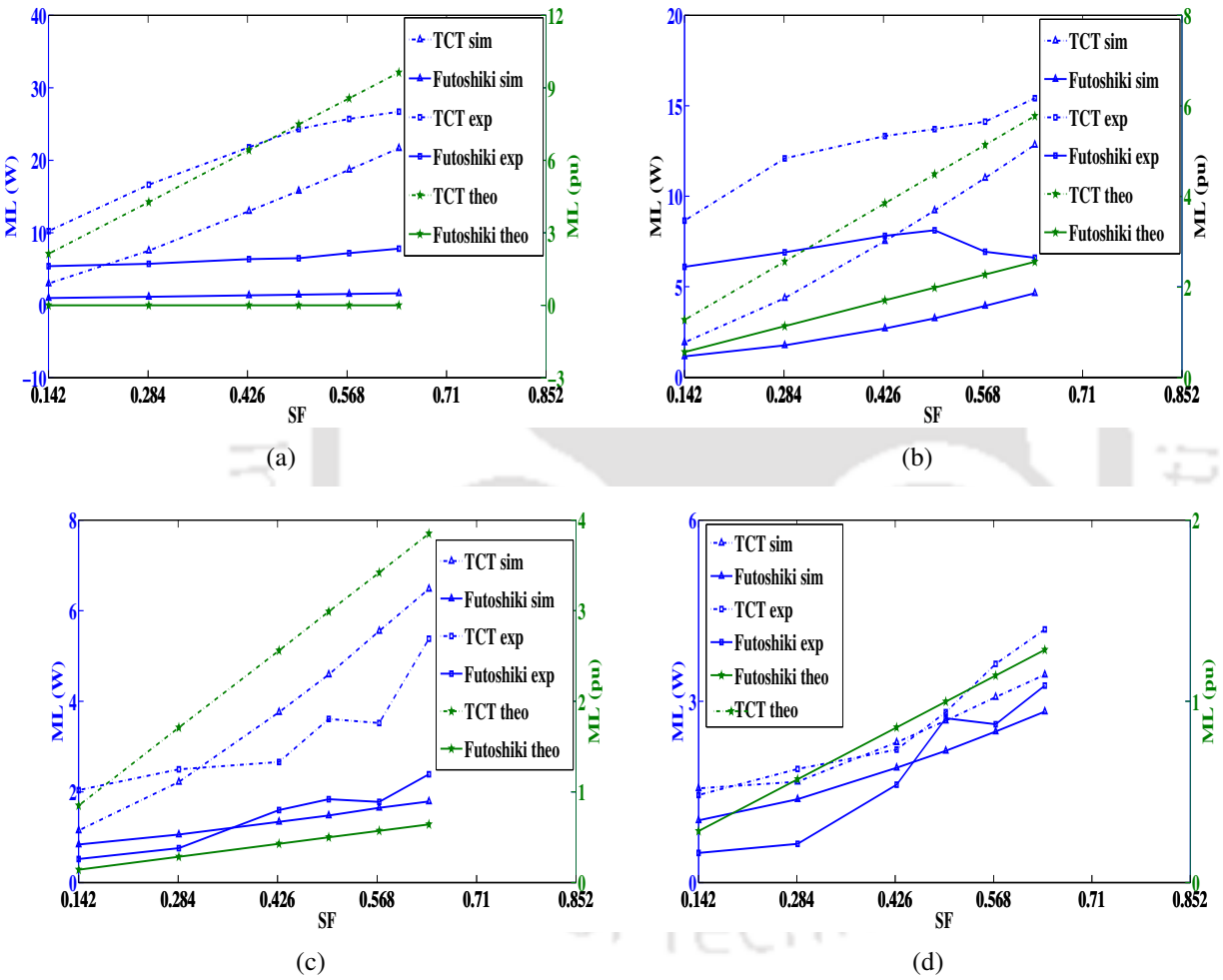

Figure 5.12: Simulation (sim), theoretical (theo) and experimental (exp) results for (a) SW, (b) LW, (c) SN, and (d) LN shading conditions.

shown in Table 5.4. To calculate the ML, the maximum power is calculated assuming all the shaded modules are shaded by the same solar irradiation. The sum of the maximum power of the individual modules (not connected electrically) of a 5×5 array under SW shading condition can be calculated

as follows:

$$P_1 = (15 + 10K_G)V_m I_m \tag{5.16}$$

The total power generated by the same array in the TCT configuration in SW shading condition is calculated (provided no rows are bypassed) as follows:

$$P_2 = 25K_G V_m I_m \tag{5.17}$$

Therefore, ML in the TCT configuration in SW shading condition is calculated as follows:

$$ML\,(TCT) = P_1 - P_2 = 15(1 - K_G)V_m I_m \tag{5.18}$$

$$ML\,(TCT)\ in\ p.u. = 15(1 - K_G) = 15SF \tag{5.19}$$

Similarly, the total power generated by the same array in shade dispersion with Futoshiki configuration in SW shading condition is calculated as follows:

$$P_3 = (15 + 10K_G)V_m I_m \tag{5.20}$$

Hence, the ML in the above configuration is calculated as follows:

$$ML\,(Futoshiki) = P_1 - P_3 = 0 \tag{5.21}$$

$$ML\,(Futoshiki)\ in\ p.u. = 0 \tag{5.22}$$

Similarly, ML in p.u. in TCT for LW, SN, and LN shading condition, as shown in Table 5.6, 5.8, and 5.10, is calculated as follows:

$$ML\,(TCT, LW) = 9(1 - K_G) = 9SF \tag{5.23}$$

$$ML\,(TCT, SN) = 6(1 - K_G) = 6SF \tag{5.24}$$

$$ML\,(TCT, LN) = 2(1 - K_G) = 2SF \tag{5.25}$$

The ML in p.u. in Futoshiki for LW, SN, and LN shading condition is calculated as follows:

$$ML\,(Futoshiki, LW) = 4(1 - K_G) = 4SF \tag{5.26}$$

$$ML\,(Futoshiki, SN) = (1 - K_G) = SF \tag{5.27}$$

$$ML\,(Futoshiki, LN) = 2(1 - K_G) = 2SF \tag{5.28}$$

Figure 5.12 shows the variation of ML calculated theoretically in per unit (pu) using (5.19) and (5.22)-(5.28) and simulated by using MATLAB simulation in watt with SF for four different shading conditions. It is observed that the ML in TCT increases sharply with the increase of SF for all different shading conditions. In Futoshiki configuration, the ML in SW shading condition is zero, and the increase of ML with SF for rest three different shading conditions is much less compared with TCT. It is demonstrated that the ML in Futoshiki configuration is less than the TCT configuration under four different shading conditions, and hence, the performance of Futoshiki configuration is superior to TCT.

To verify theoretical and simulation results, an experiment has been performed, which is reported in Figure 5.12. The solar irradiation calculated at the time of performing an experiment (11:00 A.M., July 27, 2014) was 823 W/m^2, and different levels of solar irradiation, such as 706, 588, 470, 416, 353, and 294 W/m^2, are obtained by putting the different thickness of transparent sheets on the modules. The ML of a 5×5 PV array for TCT and Futoshiki configuration is calculated theoretically, simulated by using MATLAB, and measured experimentally for these different levels of solar irradiation. Since it is impractical to obtain the standard solar irradiation of 1000 W/m^2, therefore, the solar irradiation of 823 W/m^2 obtained experimentally under unshading condition is assumed as the standard solar irradiation for SF calculation. It is observed from the experimental result that the ML measured in Futoshiki configuration is always much lesser than TCT configuration.

5.4 Summary of the chapter

A Futoshiki configuration technique for shade dispersion to increase the power generation of a PV array under PSC has been proposed in the present work. In this approach, only physical location of the PV modules are changed without changing the electrical connection of modules. The proposed

configuration is a onetime arrangement for the PV modules in an array. In this work, the GMPP of a 5×5 PV array calculated theoretically, simulated by MATLAB, and estimated experimentally is presented. It shows the GMPP in all the three cases matches closely, and there is a minor deviation because of the fluctuation in solar irradiation at the time of conducting the experiment. It is demonstrated that for a 5×5 PV array, the power enhancement in Futoshiki configuration with respect to TCT configuration has increased under four different shading patterns. However, for any random shading condition and any square size of a PV array, the proposed configuration will generate maximum power with respect to TCT configuration. The ML in Futoshiki configuration with respect to TCT configuration for any shading condition is always less. The power generation of a PV array by using the proposed configuration is same as EAR scheme for different shading conditions. Since the proposed configuration does not require switches and sensors, it is economical and simpler for the installation. Hence, considering all above facts, the proposed technique will help the PV installer to extract more power from the PV source under PSC.

Since the Futoshiki puzzle pattern is applicable only for an $m \times n$ ($m = n$) PV array, in the next chapter, for the improvement in the power generation of an array under PSC, a generalized algorithm for the PRM-FEC in the TCT configuration of an $m \times n$ ($m = n$ & $m \neq n$) array is presented.

Note: This work, Maximizing the Power Generation of a Partially Shaded PV Array has been published in IEEE Journal of Emerging and Selected Topics in Power Electronics.

6

Extraction of Maximum Power from a PV Array Under Nonuniform Irradiation Conditions

Contents

6.1 Introduction

Partial shading of a PV array occurs due to shadows of nearby trees or houses, moving clouds, and deposition of sand or dust on the modules.The ML occurs between the PV module parameters under PSC, because different intensities of solar irradiation are received by the modules. Hence, the power generated by an array decreases under PSC. The P-V characteristics of an array under PSC contain multiple peaks [59]. Different MPPT methods for tracking LMPP [48] and GMPP [60, 62–64] of a PV array have been proposed.

PV array topology is classified into four different types, such as SP, HC, BL, and TCT [66]. The TCT configuration of an array generates more output power than the other three configurations under PSC [1]. The PEE has been proposed for the elimination of multiple peaks in the P-V characteristics of an array under PSC and hence, there is an improvement in the generated power of an array [3]. However, for the implementation of PEE in a large scale PV farm needs lots of switches and sensors and a control algorithm. EAR technique is used to enhance the generated power output of a PV array in PSC [76–78, 110]. In the EAR technique, electrical connection of the PV modules is altered in accordance with the PSC. Thus, implementing a large scale PV farm under PSC needs lots of switches and sensors to alter the electrical connection of the modules.

To overcome the aforementioned limitations, a Futoshiki configuration of a PV array is proposed to improve the power generation under PSC and the rearrangement of the TCT configuration of an $m \times n$ (where m and n are the number of rows and columns) PV array is carried out for $m = n$ only as mentioned in Chapter 5. But, the Futoshiki configuration of a PV array is not applicable for m≠n. However, in the present analysis, a new approach for the PRM-FEC of the TCT configuration of an $m \times n$ ($m = n$ and m≠n) array is proposed for digit m that is either odd or even number. This provides a generalized algorithm of the proposed method for the rearrangement of row position of an $m \times n$ PV array. A comparison of the PRM-FEC configuration with different existing configurations, such as TCT and EAR of an $m \times n$ ($m = 7$ and $n = 5$) array in different shading patterns is carried out. In the PRM-FEC configuration, the physical position of the modules in an array is altered only once at the time of the installation without altering the electrical connection of the modules, and hence, lot of switches, sensors, and a control algorithm are not required for the real time implementation of the

present method in a large scale PV farm. This configuration distributes the shadows over the PV array and which ensure that there is a remarkable power improvement of a PV array under PSC.

6.2 Different configuration of solar PV array

The detail explanation of an electrical equivalent model of an SDM PV module is provided in Section 2.2 of Chapter 2.

6.2.1 TCT configuration of an array

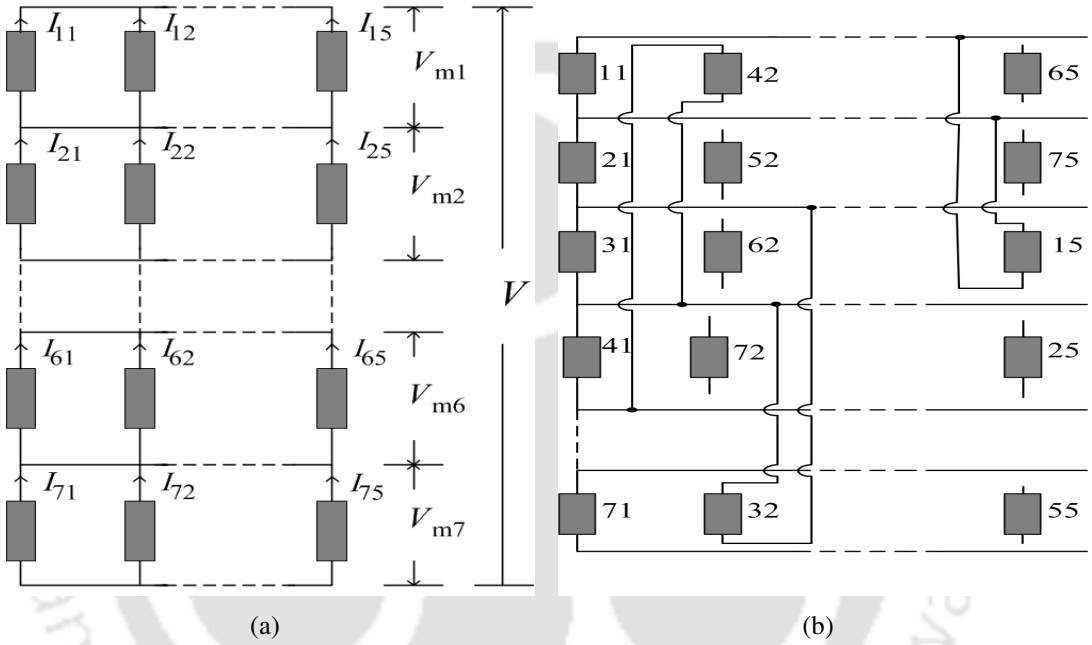

Figure 6.1: (a) TCT and (b) PRM-FEC configuration of a PV array.

A 7×5 PV array with TCT configuration (35 numbers of SDM module as shown in Figure 1.3(a)) as shown in Figure 6.1(a), is considered in the present study. The generated current from a PV module varies linearly with solar irradiation G and is given in (5.1).

The voltage of the array is given as follows:

$$V = \sum_{x=1}^{7} V_{mx} \tag{6.1}$$

where V_{mx} is the x^{th} row voltage of an array.

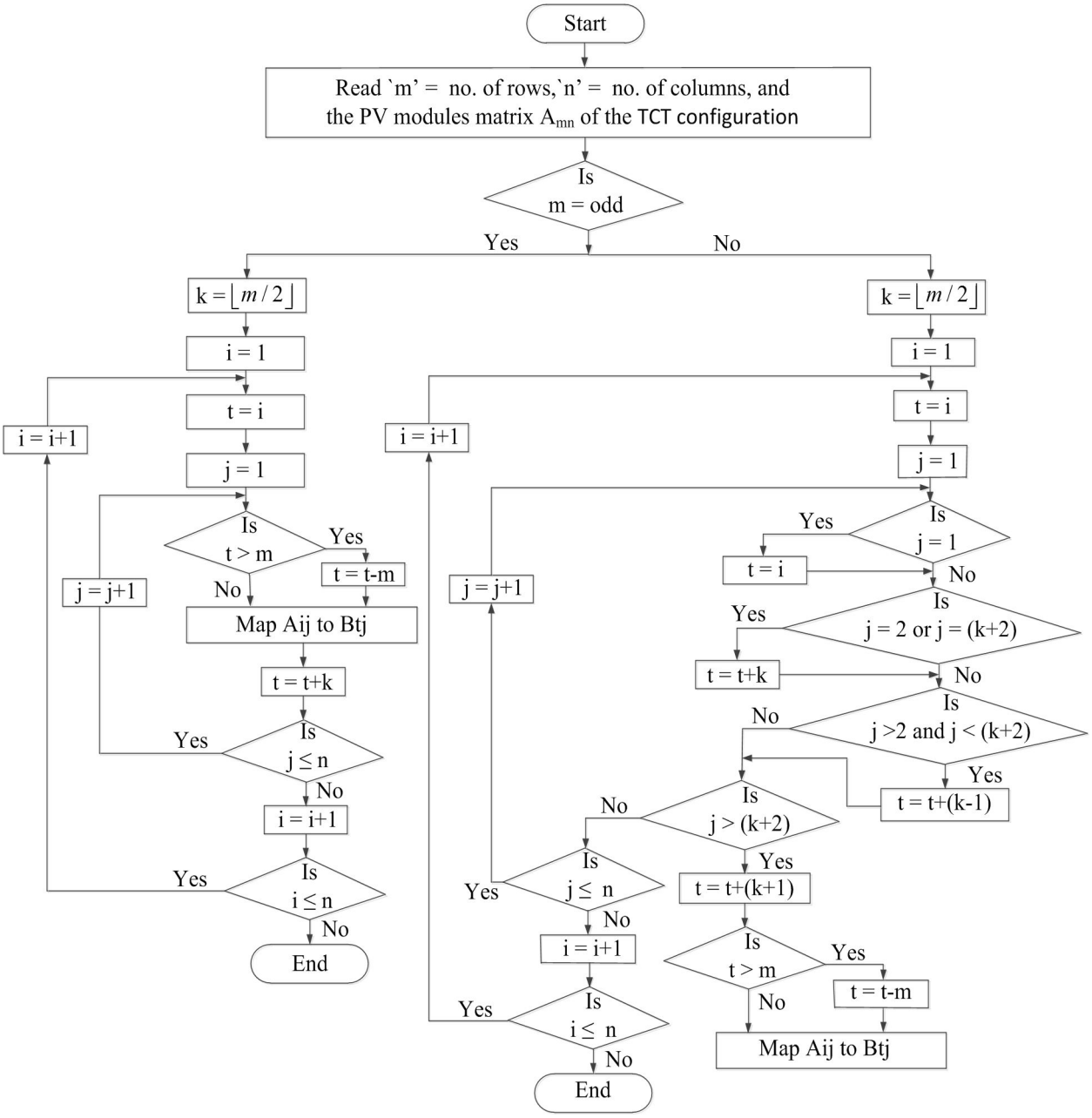

Figure 6.2: Flowchart of the proposed algorithm for the rearrangement of row position of an $m \times n$ PV array.

6.2.2 PRM-FEC configuration of an array

The prime objective of the PRM-FEC configuration is to distribute shadows over the array under PSC by arranging the row position of an $m \times n$ array using the digits 1 to m followed by the algorithm, as shown in Figure 6.2. The proposed algorithm is designed for m = odd and even for the arrangement of row position of an $m \times n$ PV array. In order to obtain the unique solution, the repetition of the digits in a particular row as well as a particular column (cln) of a PV array is avoided.

Let us consider

$$A(i,j) = \begin{bmatrix} 11 & 12 & .. & 1n \\ 21 & 22 & .. & 2n \\ .. & .. & .. & .. \\ .. & .. & .. & .. \\ m1 & .. & .. & mn \end{bmatrix} \tag{6.2}$$

is $m \times n$ PV array in the TCT configuration where $m \times n$ number of PV modules are placed. Without changing the cln position, the row position of an array is rearranged to get the PRM-FEC configuration. So

$$A(i,) = \begin{bmatrix} 1 & 1 & .. & 1 \\ 2 & 2 & .. & 2 \\ .. & .. & .. & .. \\ .. & .. & .. & .. \\ m & m.. & .. & m \end{bmatrix} \tag{6.3}$$

The rearrangement of the PV modules in an array under PSC depends on the row length of an array, such as m is odd or even number. For m = odd number, the PRM-FEC configuration of a PV array is achieved by using the following steps:

1. If m is an odd number, the positions of the PV modules in j=2 are arranged by adding k with the row position for j=1 as follows:

$$A(i,2) = \begin{bmatrix} k+1 & 2 \\ k+2 & 2 \\ .. & \\ .. & \\ k+m & 2 \end{bmatrix} \tag{6.4}$$

   where k = $\lfloor m/2 \rfloor$.

   If k+i ($i = 1, 2, ..., m$) > m, k+i will be replaced by k+i-m.

2. The positions of the PV modules in j=3 will be obtained by adding k with the row position of

an array for j=2.

3. Similarly, the row positions of an array for j=3, 4, ... ,n are obtained.

Table 6.1: Arrangement of the PRM-FEC configuration of a 7 × 5 array

Cln 1	Cln 2 (Cln 1+ 3)	Cln 3 (Cln 2+ 3)	Cln 4 (Cln 3+ 3)	Cln 5 (Cln 4+ 3)
1	4	7	10-7=3	6
2	5	8-7=1	4	7
3	6	9-7=2	5	8-7=1
4	7	10-7=3	6	9-7=2
5	8 – 7 = 1	4	7	10-7=3
6	9 – 7 = 2	5	8-7=1	4
7	10 – 7 = 3	6	9-7=2	5

For m = even number, the PRM-FEC configuration of a PV array is obtained by using the following steps:

1. The positions of the modules in an array for j = 2 are obtained in the similar way, as explained in step 1 for m = odd number.

2. The positions of the modules in an array for j = 3 are obtained by adding k-1 with modified row position for j =2 to avoid the repetition of the modules position with j=1.

3. For obtaining the next cln of an array, step 2 will be continued until there is no repetition of the module position with the earlier modified cln. If there is a repetition, then repeat the procedure of step 1 to obtain the module position in the next cln and so on.

In the present analysis, a TCT configuration of a 7 × 5 array, as shown in Figure 6.1(a), is considered. The PRM-FEC configuration of an array, as shown in Figure 6.1(b), is obtained from the TCT configuration by arranging the digits 1-7 in the row position by using aforementioned algorithm, as explained in Table 6.1. In the PRM-FEC configuration, keeping the cln position fix, the modules of the same row in the TCT configuration are shifted to a different row position. Hence, the effect of

shadows in the same row is reduced and the row current is enhanced. Therefore, the power generated by a PV array is enhanced under the PSC.

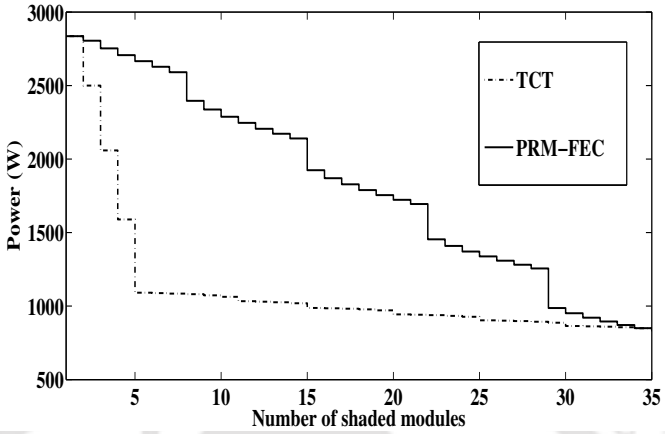

Figure 6.3: Power-number of shaded modules in row-wise curve for a 7×5 PV array.

To study the effect of PRM-FEC on the power generation of the array with respect to the TCT configuration, the modules of the array, as shown in Figure 6.1(a) and (b), are shaded one by one in the row sequence followed by 75, 74,....., 12, 11 and 55, 24,....., 42, 11 in the TCT and the PRM-FEC configuration respectively. Assuming that the unshaded and shaded modules receive solar irradiation of 1000 and 300 W/m^2, respectively. The datasheet values of the 85 W modules used for the PV array are as follows: I_{sc} = 5.17 A, V_{oc} = 21.90 V, I_{mp} = 4.84 A, V_{mp} = 17.9 V and N_s = 36. Figure 6.3 shows the power verses number of shaded modules of a 7×5 PV array. It is observed that there is an improvement in the output power in the PRM-FEC with respect to the TCT configuration in each shading condition during the modules are shaded in the aforementioned row sequence.

The output power of a PV array increases under PSC by using different configurations, such as EAR, Futoshiki, and the PRM-FEC. But, the real-time implementation of Futoshiki configuration of a 7×5 PV array is not applicable. The implementation of EAR technique and PRM-FEC configuration of a 7×5 PV array is applicable, but EAR technique requires lots of switches and sensors for altering the electrical connection of the modules in accordance with PSC. However, the PRM-FEC configuration does not require lots of sensors, and switches due to the electrical connection of the modules remains fixed. The rearrangement of PV modules in the TCT configuration of an array is performed once at the time of installation for the real-time implementation of the PRM-FEC configuration, and

this configuration is useful for any types of PSC.

To illustrate PRM-FEC method, a 35 × 200 large PV array of 1.75 MW and 1050 V, which can be integrated with the microgrid, is designed by assembling 200 numbers of 8.75 kW, 210 V, 7 × 5 small array arranged using the proposed method. Therefore, this large PV array is appeared as a 5 × 40 array, as shown in Figure 6.4. At the time of installation, the modules of all small arrays are rearranged using the proposed method so that when partial shading occurs on a 35 × 200 large array, the shade is dispersed in a 7 × 5 small arrays, which make sure the improvement in the power generation. Hence, the PRM-FEC method can be used for the power improvement of a large array under PSC.

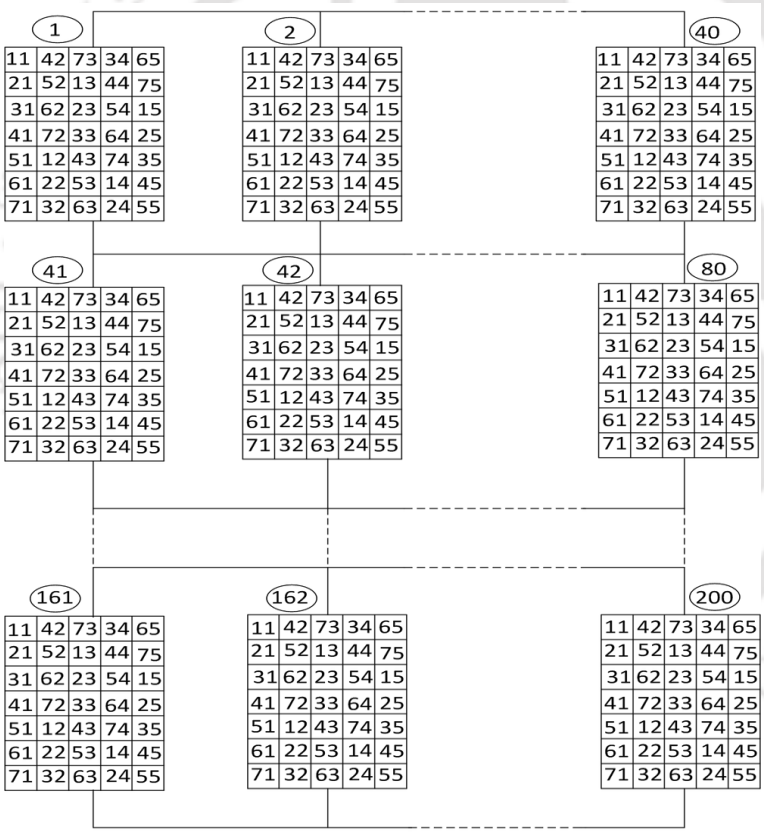

Figure 6.4: A 1.75 MW, 1050 V, 35 × 200 large PV array assembled by a 8.75 kW, 210 V, 7 × 5 small array arranged by the proposed method.

6.3 Simulation and experimental results

Two different shading patterns, such as pattern 1 and 2 of a 7 × 5 PV array as given in Table 6.2 and 6.3, are considered for the present study. The rearrangement of the PRM-FEC configuration

Table 6.2: Shading pattern 1 of a 7×5 PV array

891 W/m^2 621 W/m^2 513 W/m^2 270 W/m^2

(a) TCT configuration

11	12	13	14	15
21	22	23	24	25
31	32	33	34	35
41	42	43	44	45
51	52	53	54	55
61	62	63	64	65
71	72	73	74	75

(b) PRM-FEC

11	42	73	34	65
21	52	13	44	75
31	62	23	54	15
41	72	33	64	25
51	12	43	74	35
61	22	53	14	45
71	32	63	24	55

(c) Shade dispersion with PRM-FEC

11	12	13	14	15
21	22	23	24	25
31	32	33	34	35
41	42	43	44	45
51	52	53	54	55
61	62	63	64	65
71	72	73	74	75

Table 6.3: Shading pattern 2 of a 7×5 PV array

702 W/m^2 432 W/m^2 324 W/m^2

(a) TCT configuration

11	12	13	14	15
21	22	23	24	25
31	32	33	34	35
41	42	43	44	45
51	52	53	54	55
61	62	63	64	65
71	72	73	74	75

(b) PRM-FEC

11	42	73	34	65
21	52	13	44	75
31	62	23	54	15
41	72	33	64	25
51	12	43	74	35
61	22	53	14	45
71	32	63	24	55

(c) Shade dispersion with PRM-FEC

11	12	13	14	15
21	22	23	24	25
31	32	33	34	35
41	42	43	44	45
51	52	53	54	55
61	62	63	64	65
71	72	73	74	75

is named as shade dispersion with PRM-FEC configuration. Usually, bypassing of shaded modules takes place when the power generation of unshaded modules of an array is higher than the total power generation in the array with reduced current under different shading conditions (the generated current of the shaded modules limiting the string current). Since the above mentioned condition is rare in real-time scenario, the power generation without bypassing the rows is considered for the comparison of the proposed method with other existing methods.

It is observed from Figure 6.5 that the maximum power obtained from simulation in the TCT and the PRM-FEC configuration for shading pattern 1 is 50.83 and 73.55 W, respectively, and for shading pattern 2, the maximum power generation is 60.07 and 63.99 W, respectively. Hence, the power improvement in the PRM-FEC configuration with respect to the TCT configuration for shading pattern 1 and 2 is 30.89% and 6.12%, respectively.

To verify the simulation results experimentally for the TCT and the PRM-FEC configuration under PSC, a controlled experiment is performed in the Department of Electronics and Electrical Engineering, IIT Guwahati, by taking the PV modules of same rating (i.e., 3 W), two current and voltage

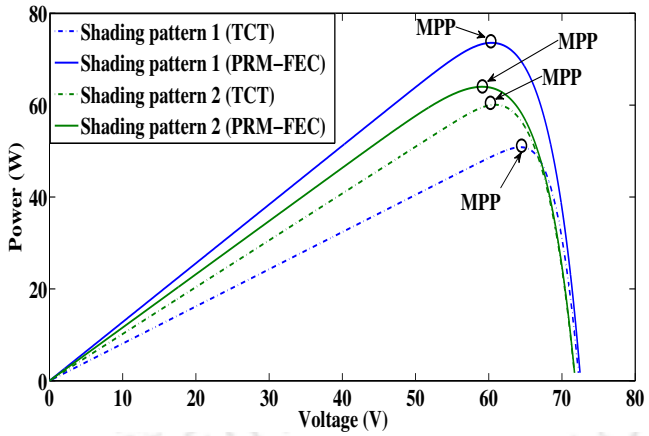

Figure 6.5: MPP results are obtained by simulation of a PV array for shading pattern 1 and 2.

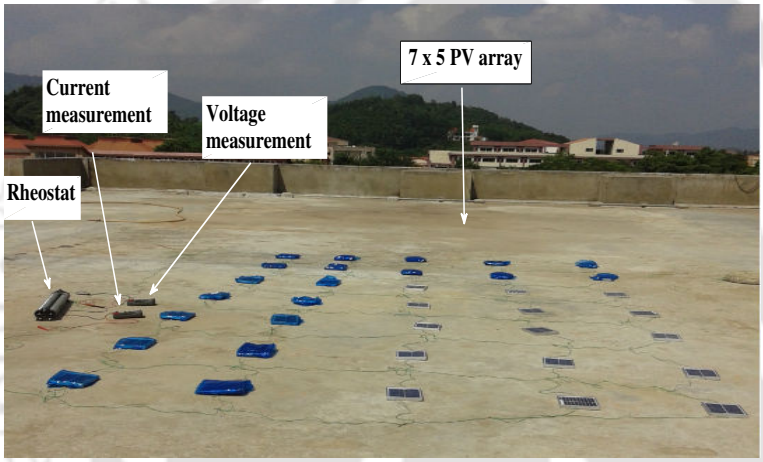

Figure 6.6: Laboratory scale experimental setup.

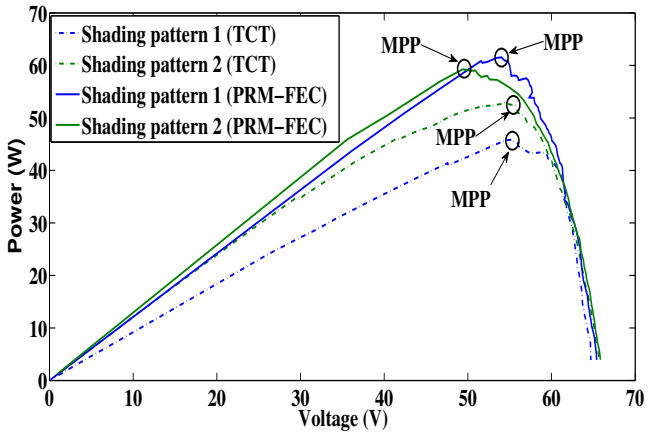

Figure 6.7: MPP results are obtained by experimentally of a PV array for shading pattern 1 and 2.

sensors, one rheostat (1000 Ω, 2 A), and the transparent papers of different thickness to set the different intensity of solar irradiance, as shown in Figure 6.6. The datasheet values of a 3 W PV module

provided by the manufacturer are I_{sc} = 0.37 A, V_{oc} = 10.60 V, V_{mp} = 8.70 V, I_{mp} = 0.34 A, and N_s = 18. The power generated from a 7×5 PV array is measured by considering the current and voltage sensor data. The level of solar irradiance while performing the experiment is calculated by using measured SCC and the data sheet values of the module provided by the manufacturer [12]. The power obtained experimentally for two different configurations, such as TCT and the PRM-FEC of a 7 × 5 PV array in two different PSC is shown in Figure 6.7. In Figure 6.7, it is observed that the power improvement in the PRM-FEC configuration with respect to the TCT configuration for shading patterns 1 and 2 is 25.43% and 10.98%, respectively.

Table 6.4: Shading pattern 3 of a 7 × 5 PV array

940 W/m^2 340 W/m^2 313 W/m^2 195 W/m^2

(a) TCT configuration

11	12	13	14	15
21	22	23	24	25
31	32	33	34	35
41	42	43	44	45
51	52	53	54	55
61	62	63	64	65
71	72	73	74	75

(b) PRM-FEC

11	42	73	34	65
21	52	13	44	75
31	62	23	54	15
41	72	33	64	25
51	12	43	74	35
61	22	53	14	45
71	32	63	24	55

(c) Shade dispersion with PRM-FEC

11	12	13	14	15
21	22	23	24	25
31	32	33	34	35
41	42	43	44	45
51	52	53	54	55
61	62	63	64	65
71	72	73	74	75

A real-time shading condition, i.e., shading pattern 3 as given in Table 6.4 occurs in a 7 × 5 PV array when the array is kept near the wall of the roof top of Electronics and Electrical Engineering Department, IIT Guwahati, as shown in Figure 6.8(a). The modules of the seventh row of an array, which are close to the wall, receive the solar irradiation of 195 W/m^2 and the modules of the sixth and fifth rows receive the solar irradiation of 313 and 340 W/m^2, respectively, whereas the rest of the modules of an array receive the solar irradiation of 940 W/m^2. The power obtained experimentally in two different configurations, such as TCT and the PRM-FEC of a 7 × 5 PV array for shading pattern 3 is 36.68 and 59.35 W, respectively, as shown in Figure 6.8(b). So the power improvement in the PRM-FEC configuration with respect to the TCT configuration is 38.19%.

It is observed from Figure 6.8(c) that the maximum power obtained from simulation in the TCT and the PRM-FEC configuration for shading pattern 3 is 41.06 and 70.26 W, respectively. Hence, the power improvement in the PRM-FEC configuration with respect to the TCT configuration is 41.55%.

It is observed from Table 6.5 that the amount of power improvement in the PRM-FEC with respect to TCT configuration of an array under PSC is significant.

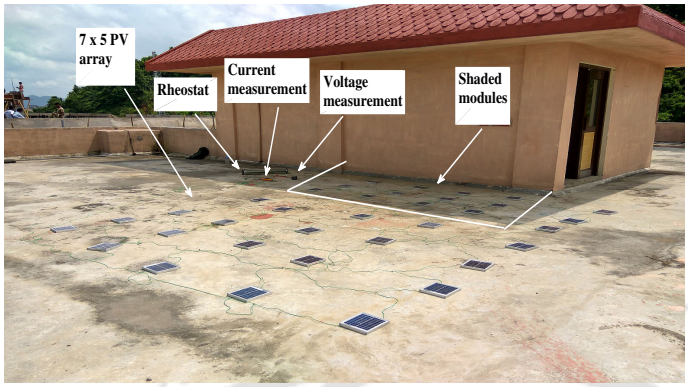

(a)

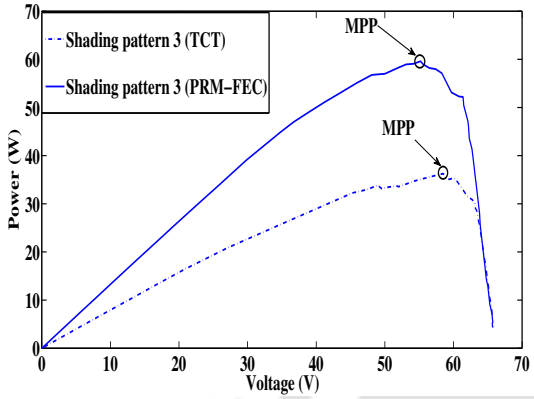

(b)

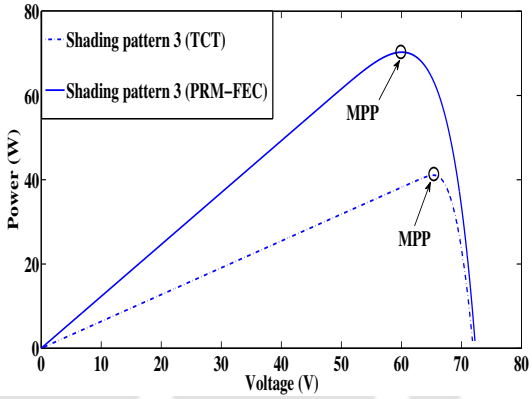

(c)

Figure 6.8: (a) Laboratory scale experimental setup for realistic shadow, (b) MPP results are obtained by experimentally of a PV array for shading pattern 3, and (c) MPP results are obtained by simulation of a PV array for shading pattern 3.

Table 6.5: A comparative results of power generation in different configurations such as TCT and PRM-FEC for different shading patterns

	TCT (Max Power)		PRM-FEC (Max Power)		Power Improvement (%)	
Shading pattern	Simulated (W)	Experimental (W)	Simulated (W)	Experimental (W)	Simulated	Experimental
1	50.83	45.90	73.55	61.56	30.89	25.43
2	60.07	52.77	63.99	59.28	6.12	10.98
3	41.06	36.68	70.26	59.35	41.55	38.19

Table 6.6: Different shading patterns of a 7×5 PV array

900 W/m^2 700 W/m^2 500 W/m^2 200 W/m^2

(a) Shading pattern 4

11	12	13	14	15
21	22	23	24	25
31	32	33	34	35
41	42	43	44	45
51	52	53	54	55
61	62	63	64	65
71	72	73	74	75

(b) Shading pattern 5

11	12	13	14	15
21	22	23	24	25
31	32	33	34	35
41	42	43	44	45
51	52	53	54	55
61	62	63	64	65
71	72	73	74	75

(c) Shading pattern 6

11	12	13	14	15
21	22	23	24	25
31	32	33	34	35
41	42	43	44	45
51	52	53	54	55
61	62	63	64	65
71	72	73	74	75

A comparison between the PRM-FEC and EAR techniques performed by using MATLAB simulink for aforementioned 85 W PV module, considering different shading patterns 1-6 of a 7×5 PV array as given in Table 6.2-6.4 and 6.6, is presented in Figure 6.9. It is observed from Figure 6.9 that the power generation in the PRM-FEC configuration is always higher than the TCT configuration and is the same as EAR technique in different shading patterns. However, for a few peculiar non-continuous shading patterns, the power generation for an EAR scheme may be slightly higher than PRM-FEC configuration. Since the real-time implementation of EAR technique in a large scale PV farm needs a large number of switches, sensors, and a complex control algorithm for changing the electrical connection of the PV modules dynamically, the implementation of EAR scheme is more complex and expensive. On the other hand, the implementation of the PRM-FEC configuration for the estimation of power generation of an array is simpler and economical.

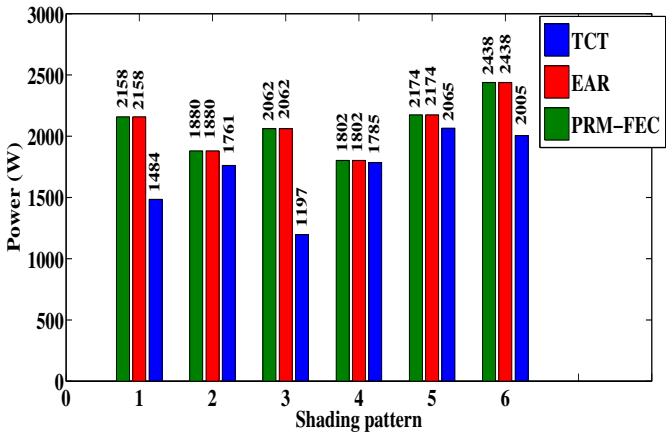

Figure 6.9: Maximum power generation of a 7×5 PV array in different technique under different shading patterns.

For a realistic assumption of PSC on a PV array, a home, which is constructed near the PV array,

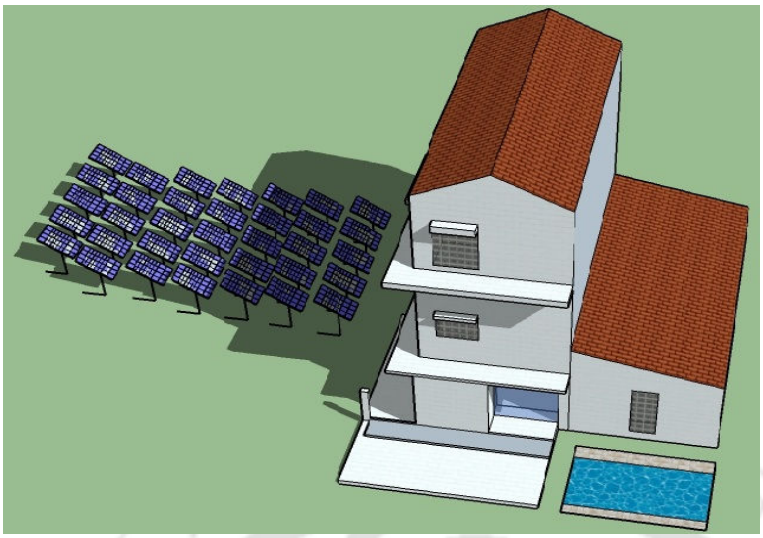

Figure 6.10: Realistic assumption of PSC on a 7 × 5 PV array at 9 h.

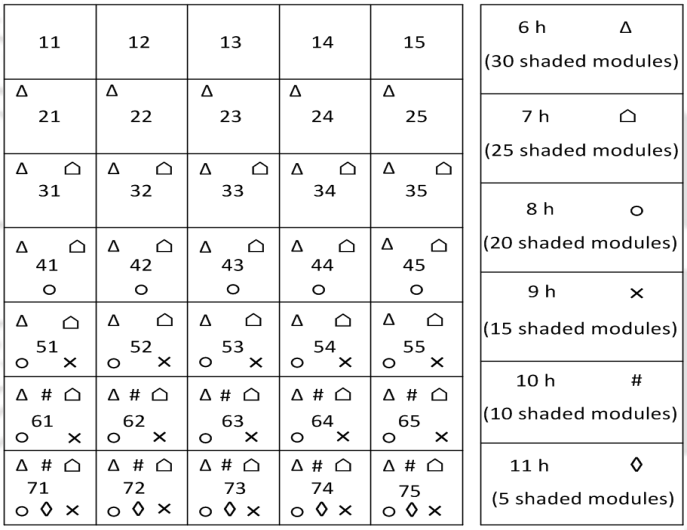

Figure 6.11: PSC on a 7 × 5 PV array on an hourly basis.

Table 6.7: Solar irradiation on hourly basis during sunshine hours

Sunshine hours	5	6	7	8	9	10	11	12	13	14	15	16	17
USI (W/m^2)	35	68	145	289	551	769	887	908	845	692	486	249	53
k	20	25	30	35	40	45	50	100	100	100	100	100	100

Note: SSI (W/m^2) = k% × USI.

is designed by using a 3D modeling tool as shown in Figure 6.10. For designing the array, 85 W PV modules are considered. In order to study the power enhancement in the proposed method in

real-time when the sun changes its position from east to west during the course of a day, a shading with different patterns and different intensities occurs in a 7×5 PV array on an hourly basis during sunshine hours of a day as mentioned in Figure 6.11 are considered. In Figure 6.11, it is assumed that all the modules are completely shaded at 5 h, the modules of the first row are unshaded at 6 h, the modules of the first and second row are unshaded at 7 h, and similarly the rest of the rows are unshaded at different instant of time. Finally the modules of an array are completely unshaded during 12-17 h. The shaded modules of an array represented by different symbols at each hour during PSC from 6-11 h.

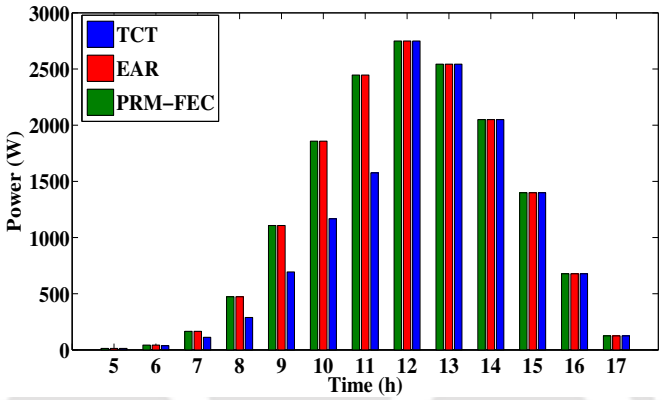

Figure 6.12: A comparison of power generation from an array during sunshine hours for different shading patterns.

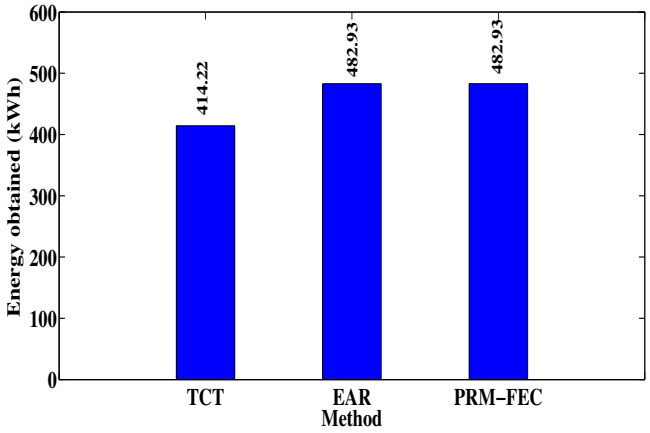

Figure 6.13: Energy obtained from an array in a month of March-2012.

An average solar irradiation on hourly basis during sunshine hours from 5 to 17 h in the month of March-2012 of Guwahati city (longitude = 91.73^o, Latitude = 26.18^o) as given in Table 6.7 is con-

sidered. In Table 6.7, it is assumed that the unshaded and shaded modules of an array receive USI and SSI, respectively, on an hourly basis during sunshine hours. Considering the solar irradiation mentioned in Table 6.7, the power generated from an array in the TCT, EAR, and PRM-FEC configuration for a day is estimated and the results are presented in Figure 6.12. It is observed from Figure 6.12 that the power generated in the PRM-FEC configuration is always higher than the TCT configuration and same as the EAR configuration during PSC on an array from 6 to 11 h. In addition, the energy obtained from an array in the TCT, EAR, and PRM-FEC configuration method in the month of March-2012 is presented in Figure 6.13. It is observed from Figure 6.13 that the energy obtained in PRM-FEC configuration is always higher than the TCT configuration and the same as the EAR configuration. Therefore, onetime arrangement of PRM-FEC configuration holds effective for any types of static and dynamic PSC.

6.4 Summary of the chapter

This work presents a generalized algorithm for the distribution of shading effect over the $m \times n$ ($m = n$ and $m \neq n$) array to improve the output power under PSC. In the present approach, the physical position of the modules is altered only once at the time of installation for any types of shading condition, without changing the electrical connection of modules. The power generated in the PRM-FEC configuration of a partially shaded PV array is same as the EAR scheme. The PRM-FEC configuration is economical and simpler for the real-time implementation of a large-scale PV farm, because it does not need lots of switches and sensors. It is observed that the generated power from a PV array under PSC in the PRM-FEC scheme is always more than the TCT configuration.

In the next chapter, conclusions and possible future works are presented.

Note: This work, Extraction of Maximum Power From a PV Array Under Nonuniform Irradiation Conditions has been published in IEEE Transaction on Electron Devices.

7

Conclusion and Future Works

Contents

7.1 Summary of the present work

This thesis presents novel MPP estimation schemes of an SDM and DDM PV module under DEC and maximizing the power generation of a PV array under PSC. PV array modeling, MPP estimation, and the enhancement of power generation of a partially shaded PV array are essential for the integration of solar power into the microgrid.

In Chapter 2, a new approach for the estimation of MPP of an SDM PV module on an hourly basis using meteorological data is presented. The estimation of MPP of a PV array based on its characteristic equation is performed using LM algorithm. The proper estimation of weather dependent GSI is essential for the estimation of MPP of an array. Therefore, the monthly averaged daily and hourly GSI is estimated for a certain location on the surface of the earth using empirical relations by taking RH and AT data. The estimated and an actual maximum power of a PV array of monthly average daily and hourly basis are presented against sunshine time. It is observed that the deviation of the estimated maximum power and the actual maximum power of an array on hourly basis is minimal. The MPP results estimated using the LM algorithm of a 15 W PV module under DEC are validated with the actual and experimental results. It is observed that the MPP of a PV array under PSC estimated numerically using the LM algorithm is more or less same as the actual MPP of an array. From the simulation results, it is observed that the accuracy of the proposed method is high and the time taken to achieve the MPP of an array is less as compared to the other methods such as PO based on PI, GA, and GS. Therefore, the proposed method for the estimation of MPP of a PV array is robust, accurate and computationally efficient.

In Chapter 3, a simple explicit function derived from the implicit function of an I-V relationship of a PV module is used to estimate the MPP of a module accurately. The MPP of a single diode PV module estimated using the proposed method is compared with the MPP obtained from different existing methods such as V_{frac} and PO method using Matlab program under DEC. It is observed that the estimated MPP of a PV module is more or less same as the actual MPP value under DEC and also, the absolute relative error of the proposed method is minimal as compare to other MPPT methods. The steady state performance of 250 W PV module under DEC are also performed experimentally, and it is observed from the experimental results that there is a minimal deviation between the P_{max}

obtained experimentally and by simulation using an explicit expression of current. Hence, the estimation of MPP of a PV module using the proposed method is simple, accurate and computationally efficient. Since the hardware setup to implement the proposed algorithm is cost effective, simple and the proposed algorithm is accurate and robust, it would be useful for the domestic and commercial applications.

In Chapter 4, the MPP of a DDM PV module based on its characteristic equation is estimated using robust LM algorithm under DEC. For the accurate estimation of MPP under DEC, the parameters of a DDM PV module are estimated using NR method considering the data sheet values at STC provided by the manufacturer. The MPP of a DDM PV module estimated using LM method under DEC is compared with six different existing methods, such as GA, PS, MVT, Saloux, NLS, and GS. It is observed from the simulation results that the proposed method is more accurate as compared to the other methods. The execution time to obtain the MPP of a DDM PV module in the LM method is low and slightly higher than the two explicit methods such as MVT and Saloux. However, the accuracy of the estimation of MPP of a DDM PV module in MVT and Saloux methods is less as compared to other methods. For further validation of the accuracy of the proposed method, the estimated MPP are compared with the MPP obtained experimentally for a 75 W PV array under DEC, and it is observed that the difference between the estimated, measured, and an actual MPP of a PV array is minimal. Therefore, the proposed method for the estimation of MPP of a DDM PV module is simple, robust, accurate and computationally efficient.

In Chapter 5, Futoshiki configuration technique for shade dispersion is proposed to enhance the power generation of a PV array under PSC. In this approach, only the physical location of the modules of an array is changed at the time of installation (one time arrangement) without changing the electrical connection of modules. In this chapter, the GMPP of an $m \times n$ ($m = n$, m = number of rows and n = number of columns) PV array calculated theoretically, simulated by MATLAB, and estimated experimentally in TCT and Futoshiki configurations for different shading conditions is presented. It shows the maximum power generated in all the three cases either in TCT or Futoshiki configuration matches closely, and there is a minor deviation because of fluctuation in solar irradiation at the time of conducting the experiment. However, for any shading condition of an array, the Futoshiki con-

figuration generates more power as compared to the TCT configuration and is the same as the EAR scheme. Since the proposed configuration does not require switches and sensors, it is economical and simpler for the installation. Therefore, considering aforementioned facts, the proposed approach will help the PV installer to extract more power from the PV source under PSC.

Since the Futoshiki configuration is applicable only for an $m \times n$ ($m = n$) PV array, a generalized algorithm for the distribution of shading effect over the $m \times n$ (m = n and $m \neq n$) array to improve the output power under PSC is proposed in Chapter 6. In this approach, the physical position of the modules is changed only once at the time of installation for any types of shading condition, without changing the electrical connection of modules. Since the PRM-FEC configuration does not need lots of switches and sensors, it is economical and simpler for the real-time implementation of a large-scale PV farm of any size. It is observed that the generated power from an array under PSC in the PRM-FEC scheme is always more than the TCT configuration and is same as EAR scheme.

7.2 Contribution of the thesis

The important contribution of the thesis for development of new MPP estimation schemes of a PV module and an improvement in the power generation of an array under PSC are given as follows:

- GSI during sunshine hours of Guwahati city by taking RH and AT data using empirical relations are presented for the accurate estimation of MPP of a PV array.
- The five parameters of an SDM and DDM PV module at STC using NR method by taking the data sheet values provided by the manufacturer are estimated.
- A robust LM algorithm is used for the estimation of MPP of an SDM and DDM PV module as well as an array based on its characteristic equation under DEC.
- The performance in terms of accuracy and computational efficiency of the proposed algorithm for the estimation of MPP of an SDM PV array under steady and rapid change of irradiation conditions are presented using MATLB/SIMULINK.
- A simple explicit expression of the current of a PV module derived from the implicit I-V characteristic is solved numerically using the BM to estimate the MPP accurately under DEC.

- The comparison of accuracy and computational time to obtain MPP of a DDM PV module under DEC by using the proposed algorithm with different existing methods is presented.
- Futoshiki puzzle pattern configuration for the enhancement of the power generation and the minimization of ML of an $m \times n$ ($m = n$) PV array under PSC is presented.
- A generalized algorithm for the physical relocation of the modules with a fixed electrical connection (PRM-FEC) in total cross tied (TCT) configuration of an $m \times n$ ($m = n$ & $m \neq n$) PV array under different shading patterns for the improvement of power generation is presented.

7.3 Suggestions for future research

The suggestions for further research are given as follows:

- Since the commercial PV modules are designed with different PV cell technology, such as mono-crystalline, poly-crystalline, and amorphous silicon, a generalized multidimensional diode model for the selection of optimal model for each cell technology is essential.
- For accurate MPP estimation, a simple and computationally efficient explicit expression of current for an SDM PV module under PSC is required.
- The explicit expression of a current in terms of voltage for a DDM PV module for accurate MPP estimation under DEC is required.
- An adaptive control algorithm for the optimized EAR configuration which requires less number of sensors and switches under PSC is essential.
- Since the power generation of a PV array decreases under PSC, a most optimized configuration of an array using the optimization technique is required to enhance the power generation of an array.

A

FPGA Program

A. FPGA Program

```
`timescale 1ns / 1ps
module sk(clk,l,m,n,o,p,q,r,clko,clkn);
input wire clk,l,m,n,o,p,q,r;
output wire clko,clkn;
reg [12:0] count;
reg [11:0] pulse_r;
reg clkr;
initial
begin
count<=0;
clkr<=0;
pulse_r<=0;
end
assign clko=clkr;
assign clkn=~clkr;
always@(posedge clk )
begin
 if(l==0 && m==0 &&n==0&&o==0&&p==0&&q==0&&r==0)
begin
pulse_r<=2340;
end
else if(l==0 && m==0 &&n==0&&o==0&&p==0&&q==0&&r==1)
begin
pulse_r<=2341;
end
else if(l==0 && m==0 &&n==0&&o==0&&p==0&&q==1&&r==0)
begin
pulse_r<=2342;
end
else if(l==0 && m==0 &&n==0&&o==0&&p==0&&q==1&&r==1)
begin
pulse_r<=2343;
end
else if(l==0 && m==0 &&n==0&&o==0&&p==1&&q==0&&r==0)
begin
pulse_r<=2344;
end
else if(l==0 && m==0 &&n==0&&o==0&&p==1&&q==0&&r==1)
begin
pulse_r<=2345;
end
else if(l==0 && m==0 &&n==0&&o==0&&p==1&&q==1&&r==0)
begin
pulse_r<=2346;
end
else if(l==0 && m==0 &&n==0&&o==0&&p==1&&q==1&&r==1)
begin
pulse_r<=2347;
end
else if(l==0 && m==0 &&n==0&&o==1&&p==0&&q==0&&r==0)
begin
pulse_r<=2348;
end
else if(l==0 && m==0 &&n==0&&o==1&&p==0&&q==0&&r==1)
begin
pulse_r<=2349;
end
else if(l==0 && m==0 &&n==0&&o==1&&p==0&&q==1&&r==0)
begin
pulse_r<=2350;
end
else if(l==0 && m==0 &&n==0&&o==1&&p==0&&q==1&&r==1)
begin
pulse_r<=2351;
end
else if(l==0 && m==0 &&n==0&&o==1&&p==1&&q==0&&r==0)
begin
pulse_r<=2352;
end
```

```
70  else if(l==0 && m==0 &&n==0&&o==1&&p==1&&q==0&&r==1)
71  begin
72  pulse_r<=2353;
73  end
74  else if(l==0 && m==0 &&n==0&&o==1&&p==1&&q==1&&r==0)
75  begin
76  pulse_r<=2354;
77  end
78  else if(l==0 && m==0 &&n==0&&o==1&&p==1&&q==1&&r==1)
79  begin
80  pulse_r<=2355;
81  end
82  else if(l==0 && m==0 &&n==1&&o==0&&p==0&&q==0&&r==0)
83  begin
84  pulse_r<=2356;
85  end
86  else if(l==0 && m==0 &&n==1&&o==0&&p==0&&q==0&&r==1)
87  begin
88  pulse_r<=2357;
89  end
90  else if(l==0 && m==0 &&n==1&&o==0&&p==0&&q==1&&r==0)
91  begin
92  pulse_r<=2358;
93  end
94  else if(l==0 && m==0 &&n==1&&o==0&&p==0&&q==1&&r==1)
95  begin
96  pulse_r<=2359;
97  end
98  else if(l==0 && m==0 &&n==1&&o==0&&p==1&&q==0&&r==0)
99  begin
100 pulse_r<=2360;
101 end
102 else if(l==0 && m==0 &&n==1&&o==0&&p==1&&q==0&&r==1)
103 begin
104 pulse_r<=2361;
105 end
106 else if(l==0 && m==0 &&n==1&&o==0&&p==1&&q==1&&r==0)
107 begin
108 pulse_r<=2362;
109 end
110 else if(l==0 && m==0 &&n==1&&o==0&&p==1&&q==1&&r==1)
111 begin
112 pulse_r<=2363;
113 end
114 else if(l==0 && m==0 &&n==1&&o==1&&p==0&&q==0&&r==0)
115 begin
116 pulse_r<=2364;
117 end
118 else if(l==0 && m==0 &&n==1&&o==1&&p==0&&q==0&&r==1)
119 begin
120 pulse_r<=2365;
121 end
122 else if(l==0 && m==0 &&n==1&&o==1&&p==0&&q==1&&r==0)
123 begin
124 pulse_r<=2366;
125 end
126 else if(l==0 && m==0 &&n==1&&o==1&&p==0&&q==1&&r==1)
127 begin
128 pulse_r<=2367;
129 end
130 else if(l==0 && m==0 &&n==1&&o==1&&p==1&&q==0&&r==0)
131 begin
132 pulse_r<=2368;
133 end
134 else if(l==0 && m==0 &&n==1&&o==1&&p==1&&q==0&&r==1)
135 begin
136 pulse_r<=2369;
137 end
138 else if(l==0 && m==0 &&n==1&&o==1&&p==1&&q==1&&r==0)
```

```
139  begin
140  pulse_r<=2370;
141  end
142  else if(l==0 && m==0 &&n==1&&o==1&&p==1&&q==1&&r==1)
143  begin
144  pulse_r<=2371;
145  end
146   else if(l==0 && m==1 &&n==0&&o==0&&p==0&&q==0&&r==0)
147  begin
148  pulse_r<=2372;
149  end
150  else if(l==0 && m==1 &&n==0&&o==0&&p==0&&q==0&&r==1)
151  begin
152  pulse_r<=2373;
153  end
154  else if(l==0 && m==1 &&n==0&&o==0&&p==0&&q==1&&r==0)
155  begin
156  pulse_r<=2374;
157  end
158  else if(l==0 && m==1 &&n==0&&o==0&&p==0&&q==1&&r==1)
159  begin
160  pulse_r<=2375;
161  end
162  else if(l==0 && m==1 &&n==0&&o==0&&p==1&&q==0&&r==0)
163  begin
164  pulse_r<=2376;
165  end
166  else if(l==0 && m==1 &&n==0&&o==0&&p==1&&q==0&&r==1)
167  begin
168  pulse_r<=2377;
169  end
170  else if(l==0 && m==1 &&n==0&&o==0&&p==1&&q==1&&r==0)
171  begin
172  pulse_r<=2378;
173  end
174  else if(l--0 && m--1 &&n--0&&o--0&&p--1&&q--1&&r--1)
175  begin
176  pulse_r<=2379;
177  end
178  else if(l==0 && m==1 &&n==0&&o==1&&p==0&&q==0&&r==0)
179  begin
180  pulse_r<=2380;
181  end
182
183  if(count<5000)
184  begin
185  if(count<pulse_r)
186  begin
187  clkr<=1;
188  end
189  else
190  begin
191  clkr<=0;
192  end
193  count<=count+1;
194  end
195  else
196  begin
197  count<=0;
198  end
199  end
200  endmodule
201
```

Bibliography

[1] L. Villa, D. Picault, B. Raison, S. Bacha, and A. Labonne, "Maximizing the power output of partially shaded photovoltaic plants through optimization of the interconnections among its modules," *IEEE J. of Photovol.*, vol. 2, no. 2, pp. 154–163, 2012.

[2] A. Chatterjee and A. Keyhani, "Neural network estimation of microgrid maximum solar power," *IEEE Trans. Smart Grid*, vol. 3, no. 4, pp. 1860–1866, Dec 2012.

[3] L. Villa, T. P. Ho, J. C. Crebier, and B. Raison, "A power electronics equalizer application for partially shaded photovoltaic modules," *IEEE Trans. Ind. Electron.*, vol. 60, no. 3, pp. 1179–1190, 2013.

[4] M. A. G. de Brito, L. Galotto, L. P. Sampaio, G. d. A. e Melo, and C. A. Canesin, "Evaluation of the main MPPT techniques for photovoltaic applications," *IEEE Trans. Ind. Electron.*, vol. 60, no. 3, pp. 1156–1167, March 2013.

[5] W. Li and X. He, "Review of nonisolated high-step-up dc/dc converters in photovoltaic grid-connected applications," *IEEE Trans. Ind. Electron.*, vol. 58, no. 4, pp. 1239–1250, April 2011.

[6] N. Mutoh, M. Ohno, and T. Inoue, "A method for mppt control while searching for parameters corresponding to weather conditions for pv generation systems," *IEEE Trans. Ind. Electron.*, vol. 53, no. 4, pp. 1055–1065, June 2006.

[7] C. Hua, J. Lin, and C. Shen, "Implementation of a dsp-controlled photovoltaic system with peak power tracking," *IEEE Trans. Ind. Electron.*, vol. 45, no. 1, pp. 99–107, Feb 1998.

[8] J. Prakash and H. P. Garg, *Solar Energy Fundamental and Application*. 1st Edition, Tata McGraw-Hill Education, 2006.

[9] J. A. Gow and C. D. Manning, "Development of a photovoltaic array model for use in power-electronics simulation studies," *IEE Proc. Electric Power Appl.*, vol. 146, no. 2, pp. 193–200, Mar 1999.

[10] A. Chatterjee, A. Keyhani, and D. Kapoor, "Identification of photovoltaic source models," *IEEE Trans. Energy Convers.*, vol. 26, no. 3, pp. 883–889, Sept 2011.

[11] D. S. H. Chan and J. C. H. Phang, "Analytical methods for the extraction of solar-cell single- and double-diode model parameters from I-V characteristics," *IEEE Trans. Electron Devices*, vol. 34, no. 2, pp. 286–293, Feb 1987.

[12] D. Sera, R. Teodorescu, and P. Rodriguez, "PV panel model based on datasheet values," in *2007 IEEE International Symposium on Industrial Electronics*, June 2007, pp. 2392–2396.

[13] N. Femia, G. Petrone, G. Spagnuolo, and M. Vitelli, "Optimization of perturb and observe maximum power point tracking method," *IEEE Trans. Power Electron.*, vol. 20, no. 4, pp. 963–973, July 2005.

[14] F. Blaabjerg, Z. Chen, and S. B. Kjaer, "Power electronics as efficient interface in dispersed power generation systems," *IEEE Trans. Power Electron.*, vol. 19, no. 5, pp. 1184–1194, Sept 2004.

[15] W. Xiao, W. Dunford, P. Palmer, and A. Capel, "Regulation of photovoltaic voltage," *IEEE Trans. Ind. Electron.*, vol. 54, no. 3, pp. 1365–1374, June 2007.

[16] E. Karatepe, M. Boztepe, and M. olak, "Development of a suitable model for characterizing photovoltaic arrays with shaded solar cells," *Solar Energy*, vol. 81, no. 8, pp. 977 – 992, 2007.

[17] H. Patel and V. Agarwal, "Matlab-based modeling to study the effects of partial shading on PV array characteristics," *IEEE Trans. Energy Convers.*, vol. 23, no. 1, pp. 302–310, March 2008.

[18] K. H. Hussein, I. Muta, T. Hoshino, and M. Osakada, "Maximum photovoltaic power tracking: an algorithm for rapidly changing atmospheric conditions," *IEE Proc. Gener. Transm. Distrib.*, vol. 142, no. 1, pp. 59–64, Jan 1995.

[19] E. Koutroulis, K. Kalaitzakis, and N. C. Voulgaris, "Development of a microcontroller-based, photovoltaic maximum power point tracking control system," *IEEE Trans. Power Electron.*, vol. 16, no. 1, pp. 46–54, Jan 2001.

[20] S. Jain and V. Agarwal, "A new algorithm for rapid tracking of approximate maximum power point in photovoltaic systems," *IEEE Power Electron. Lett.*, vol. 2, no. 1, pp. 16–19, March 2004.

[21] Q. Li and P. Wolfs, "A review of the single phase photovoltaic module integrated converter topologies with three different dc link configurations," *IEEE Trans. Power Electron.*, vol. 23, no. 3, pp. 1320–1333, May 2008.

[22] A. Goetzberger, C. Hebling, and H.-W. Schock, "Photovoltaic materials, history, status and outlook," *Materials Science and Engineering: R: Reports*, vol. 40, no. 1, pp. 1 – 46, 2003.

[23] M. G. Villalva, J. R. Gazoli, and E. R. Filho, "Comprehensive approach to modeling and simulation of photovoltaic arrays," *IEEE Trans. Power Electron.*, vol. 24, no. 5, pp. 1198–1208, May 2009.

[24] A. N. Celik and N. Acikgoz, "Modelling and experimental verification of the operating current of mono-crystalline photovoltaic modules using four- and five-parameter models," *Applied Energy*, vol. 84, no. 1, pp. 1 – 15, 2007.

[25] R. Kadri, J. P. Gaubert, and G. Champenois, "An improved maximum power point tracking for photovoltaic grid-connected inverter based on voltage-oriented control," *IEEE Trans. Ind. Electron.*, vol. 58, no. 1, pp. 66–75, Jan 2011.

[26] B. N. Alajmi, K. H. Ahmed, S. J. Finney, and B. W. Williams, "A maximum power point tracking technique for partially shaded photovoltaic systems in microgrids," *IEEE Trans. Ind. Electron.*, vol. 60, no. 4, pp. 1596–1606, April 2013.

[27] Y. Mahmoud and E. F. El-Saadany, "A photovoltaic model with reduced computational time," *IEEE Trans. Ind. Electron.*, vol. 62, no. 6, pp. 3534–3544, June 2015.

[28] K. Ishaque, Z. Salam, and A. Syafaruddin, "A comprehensive matlab simulink PV system simulator with partial shading capability based on two-diode model," *Solar Energy*, vol. 85, no. 9, pp. 2217 – 2227, 2011.

[29] L. H. I. Lim, Z. Ye, J. Ye, D. Yang, and H. Du, "A linear identification of diode models from single I - V characteristics of pv panels," *IEEE Trans. Ind. Electron.*, vol. 62, no. 7, pp. 4181–4193, July 2015.

[30] F. Bryant and R. Glew, "Analysis of the current-voltage characteristics of cadmium sulphide solar cells under varying light intensities," *Energy Convers.*, vol. 14, no. 34, pp. 129 – 133, 1975.

[31] J. P. Charles, I. M. Alaoui, G. Bordure, and P. Mialhe, "A critical study of the effectiveness of the single and double exponential models for I-V characterization of solar cells," *Solid-State Electron.*, vol. 28, no. 8, pp. 807 – 820, 1985.

[32] K. Ishaque, Z. Salam, and H. Taheri, "Simple, fast and accurate two-diode model for photovoltaic modules," *Sol. Energy Mater. Sol. Cells*, vol. 95, no. 2, pp. 586 – 594, 2011.

[33] N. M. A. A. Shannan, N. Z. Yahaya, and B. Singh, "Single-diode model and two-diode model of PV modules: A comparison," in *Control System, Computing and Engineering (ICCSCE), 2013 IEEE International Conference on*, Nov 2013, pp. 210–214.

[34] M. Hejri, H. Mokhtari, M. R. Azizian, M. Ghandhari, and L. Soder, "On the parameter extraction of a five-parameter double-diode model of photovoltaic cells and modules," *IEEE J. Photovolt.*, vol. 4, no. 3, pp. 915–923, May 2014.

[35] J. S. C. M. Raj and A. E. Jeyakumar, "A novel maximum power point tracking technique for photovoltaic module based on power plane analysis of I - V characteristics," *IEEE Trans. Ind. Electron.*, vol. 61, no. 9, pp. 4734–4745, Sept 2014.

[36] K. Spokas and F. Forcella, "Estimating hourly incomming solar radiation from limited metrological data," *Weed Sci.*, vol. 54, pp. 66–75, 2006.

[37] D. F. A. Riza, S. I. H. Gillani, and M. S. Aris, "Hourly solar radiation estimation using ambient temperature and relative humidity data," *Int. J. Environ. Sci. Dev.*, vol. 2, pp. 188–193, 2011.

[38] T. Esram and P. L. Chapman, "Comparison of photovoltaic array maximum power point tracking techniques," *IEEE Trans. Energy Convers.*, vol. 22, no. 2, pp. 439–449, June 2007.

[39] B. Subudhi and R. Pradhan, "A comparative study on maximum power point tracking techniques for photovoltaic power systems," *IEEE Trans. Sustain. Energy*, vol. 4, no. 1, pp. 89–98, Jan 2013.

[40] V. Salas, E. Olas, A. Barrado, and A. Lzaro, "Review of the maximum power point tracking algorithms for stand-alone photovoltaic systems," *Sol. Energy Mater. Sol. Cells*, vol. 90, no. 11, pp. 1555 – 1578, 2006.

[41] A. Safari and S. Mekhilef, "Simulation and hardware implementation of incremental conductance MPPT with direct control method using cuk converter," *IEEE Trans. Ind. Electron.*, vol. 58, no. 4, pp. 1154–1161, April 2011.

[42] Y.-C. Kuo, T.-J. Liang, and J.-F. Chen, "Novel maximum-power-point-tracking controller for photovoltaic energy conversion system," *IEEE Trans. Ind. Electron.*, vol. 48, no. 3, pp. 594–601, Jun 2001.

[43] O. Wasynezuk, "Dynamic behavior of a class of photovoltaic power systems," *IEEE Trans. Power Appl. Syst.*, vol. PAS-102, no. 9, pp. 3031–3037, Sept 1983.

[44] D. Sera, R. Teodorescu, J. Hantschel, and M. Knoll, "Optimized maximum power point tracker for fast-changing environmental conditions," *IEEE Trans. Ind. Electron.*, vol. 55, no. 7, pp. 2629–2637, July 2008.

[45] F. Liu, S. Duan, F. Liu, B. Liu, and Y. Kang, "A variable step size INC MPPT method for PV systems," *IEEE Trans. Ind. Electron.*, vol. 55, no. 7, pp. 2622–2628, July 2008.

[46] P. C. Sekhar and S. Mishra, "Takagi-sugeno fuzzy-based incremental conductance algorithm for maximum power point tracking of a photovoltaic generating system," *IET Renew. Power Gener.*, vol. 8, no. 8, pp. 900–914, 2014.

[47] W. Xiao, W. G. Dunford, P. R. Palmer, and A. Capel, "Application of centered differentiation and steepest descent to maximum power point tracking," *IEEE Trans. Ind. Electron.*, vol. 54, no. 5, pp. 2539–2549, Oct 2007.

[48] E. Koutroulis and F. Blaabjerg, "A new technique for tracking the global maximum power point of PV arrays operating under partial-shading conditions," *IEEE J. Photovol.*, vol. 2, no. 2, pp. 184–190, 2012.

[49] C. S. Krishnamoorthy and S. Rajeev, "Artificial intelligence and expert systems for engineers," *CRC Press, Boca Raton, FL, USA*, 1996.

[50] B. N. Alajmi, K. H. Ahmed, S. J. Finney, and B. W. Williams, "Fuzzy-logic-control approach of a modified hill-climbing method for maximum power point in microgrid standalone photovoltaic system," *IEEE Trans. Power Electron.*, vol. 26, no. 4, pp. 1022–1030, April 2011.

[51] W. M. Lin, C. M. Hong, and C. H. Chen, "Neural-network-based MPPT control of a stand-alone hybrid power generation system," *IEEE Trans. Power Electron.*, vol. 26, no. 12, pp. 3571–3581, Dec 2011.

[52] Syafaruddin, E. Karatepe, and T. Hiyama, "Artificial neural network-polar coordinated fuzzy controller based maximum power point tracking control under partially shaded conditions," *IET Renew. Power Gener.*, vol. 3, no. 2, pp. 239–253, June 2009.

[53] M. A. S. Masoum, H. Dehbonei, and E. F. Fuchs, "Theoretical and experimental analyses of photovoltaic systems with voltage and current-based maximum power-point tracking," *IEEE Trans. Energy Convers.*, vol. 17, no. 4, pp. 514–522, Dec 2002.

[54] C. Rodriguez and G. A. J. Amaratunga, "Analytic solution to the photovoltaic maximum power point problem," *IEEE Trans. Circuits Syst. I, Reg. Papers*, vol. 54, no. 9, pp. 2054–2060, Sept 2007.

[55] W. Xiao, M. G. J. Lind, W. G. Dunford, and A. Capel, "Real-time identification of optimal operating points in photovoltaic power systems," *IEEE Trans. Ind. Electron.*, vol. 53, no. 4, pp. 1017–1026, June 2006.

[56] V. V. R. Scarpa, S. Buso, and G. Spiazzi, "Low-complexity MPPT technique exploiting the PV module MPP locus characterization," *IEEE Trans. Ind. Electron.*, vol. 56, no. 5, pp. 1531–1538, May 2009.

[57] B. K. Nayak, A. Mohapatra, and K. B. Mohanty, "Parameters estimation of photovoltaic module using nonlinear least square algorithm: A comparative study," in *2013 Annual IEEE India Conference (INDICON)*, Dec 2013, pp. 1–6.

[58] M. Swaleh and M. Green, "Effect of shunt resistance and bypass diodes on the shadow tolerance of solar cell modules," *Solar Cells*, vol. 5, no. 2, pp. 183 – 198, 1982.

[59] H. Patel and V. Agarwal, "Maximum power point tracking scheme for PV systems operating under partially shaded conditions," *IEEE Trans. Ind. Electron.*, vol. 55, no. 4, pp. 1689–1698, 2008.

[60] Y. H. Ji, D. Y. Jung, J. G. Kim, J. H. Kim, T. W. Lee, and C. Y. Won, "A real maximum power point tracking method for mismatching compensation in PV array under partially shaded conditions," *IEEE Trans. Power Electron.*, vol. 26, no. 4, pp. 1001–1009, 2011.

[61] T. L. Nguyen and K. S. Low, "A global maximum power point tracking scheme employing direct search algorithm for photovoltaic systems," *IEEE Trans. Ind. Electron.*, vol. 57, no. 10, pp. 3456–3467, 2010.

[62] Syafaruddin, E. Karatepe, and T. Hiyama, "Performance enhancement of photovoltaic array through string and central based MPPT system under non-uniform irradiance conditions," *Energy Convers and Manag*, vol. 62, no. 0, pp. 131 – 140, 2012.

[63] E. Karatepe, T. Hiyama, M. Boztepe, and M. Colak, "Voltage based power compensation system for photovoltaic generation system under partially shaded insolation conditions," *Energy Convers and Manag*, vol. 49, no. 8, pp. 2307 – 2316, 2008.

[64] S. R. Chowdhury and H. Saha, "Maximum power point tracking of partially shaded solar photovoltaic arrays," *Sol Energy Mater Sol C*, vol. 94, no. 9, pp. 1441 – 1447, 2010.

[65] Z. Salam, J. Ahmed, and B. S. Merugu, "The application of soft computing methods for MPPT of PV system: A technological and status review," *Appl Energy*, vol. 107, no. 0, pp. 135 – 148, 2013.

[66] N. Kaushika and N. Gautam, "Energy yield simulations of interconnected solar PV arrays," *IEEE Trans. Energy Convers.*, vol. 18, no. 1, pp. 127–134, 2003.

[67] Y. J. Wang and P. C. Hsu, "Analysis of partially shaded PV modules using piecewise linear parallel branches model," *World Academy of Science, Engineering and Technology*, 2009.

[68] D. Picault, B. Raison, S. Bacha, J. de la Casa, and J. Aguilera, "Forecasting photovoltaic array power production subject to mismatch losses," *Solar Energy*, vol. 84, no. 7, pp. 1301 – 1309, 2010.

[69] Z. M. Salameh and F. Dagher, "The effect of electrical array reconfiguration on the performance of a PV-powered volumetric water pump," *IEEE Trans. Energy Convers.*, vol. 5, no. 4, pp. 653–658, Dec 1990.

[70] Z. M. Salameh and C. Liang, "Optimum switching points for array reconfiguration controller," in *Photovoltaic Specialists Conference, 1990., Conference Record of the Twenty First IEEE*, May 1990, pp. 971–976 vol.2.

[71] B. Patnaik, P. Sharma, E. Trimurthulu, S. P. Duttagupta, and V. Agarwal, "Reconfiguration strategy for optimization of solar photovoltaic array under non-uniform illumination conditions," in *Photovoltaic Specialists Conference (PVSC), 2011 37th IEEE*, June 2011, pp. 001 859–001 864.

[72] L. A. R. Tria, M. T. Escoto, and C. M. F. Odulio, "Photovoltaic array reconfiguration for maximum power transfer," in *TENCON 2009 - 2009 IEEE Region 10 Conference*, Jan 2009, pp. 1–6.

[73] P. D. Santos, E. M. Vicente, and E. R. Ribeiro, "Reconfiguration methodology of shaded photovoltaic panels to maximize the produced energy," in *Power Electronics Conference (COBEP), 2011 Brazilian*, Sept 2011, pp. 700–706.

[74] M. Z. S. El-Dein, M. Kazerani, and M. M. A. Salama, "Optimal photovoltaic array reconfiguration to reduce partial shading losses," *IEEE Trans. Sustain Energy*, vol. 4, no. 1, pp. 145–153, Jan 2013.

[75] ——, "An optimal total cross tied interconnection for reducing mismatch losses in photovoltaic arrays," *IEEE Trans. Sustain. Energy*, vol. 4, no. 1, pp. 99–107, Jan 2013.

[76] G. Velasco-Quesada, F. Guinjoan-Gispert, R. Pique-Lopez, M. Roman-Lumbreras, and A. Conesa-Roca, "Electrical PV array reconfiguration strategy for energy extraction improvement in grid-connected PV systems," *IEEE Trans. Ind. Electron.*, vol. 56, no. 11, pp. 4319–4331, 2009.

[77] D. Nguyen and B. Lehman, "An adaptive solar photovoltaic array using model-based reconfiguration algorithm," *IEEE Trans. Ind. Electron.*, vol. 55, no. 7, pp. 2644–2654, 2008.

[78] J. Storey, P. Wilson, and D. Bagnall, "Improved optimization strategy for irradiance equalization in dynamic photovoltaic arrays," *IEEE Trans. Power Electron.*, vol. 28, no. 6, pp. 2946–2956, June 2013.

[79] D. Marquardt, "An algorithm for least-squares estimation of nonlinear parameters," *SIAM J. Appl. Math.*, vol. 11, pp. 431–441, 1963.

[80] A. I. Chrysochos, T. A. Papadopoulos, and G. K. Papagiannis, "Robust calculation of frequency-dependent transmission-line transformation matrices using the Levenberg-Marquardt method," *IEEE Trans. Power Deliv.*, vol. 29, no. 4, pp. 1621–1629, Aug 2014.

[81] S. Moballegh and J. Jiang, "Modeling, prediction, and experimental validations of power peaks of PV arrays under partial shading conditions," *IEEE Trans. Sustain. Energy*, vol. 5, no. 1, pp. 293–300, Jan 2014.

[82] G. Walker, "Evaluating MPPT converter topologies using a matlab PV model," *Journal of Electrical and Electronics Engineering, Australia*, vol. 21, pp. 49–55, 2001.

[83] D. Goswami, F. Kreith, and Kreider, "Principles of solar engineering," *Taylor and Francis*, vol. 2nd edn., 1999.

[84] B. Liu and R. Jordan, "The interrelationship and characterstics distribution of direct, diffuse, and total solar irradiation," *Sol. Energy*, vol. 4, pp. 1–19, 1960.

[85] N. Campbell, S. Gaylon and M. John, "Introduction to environmental biophysics," *Springer*, vol. 2nd edn., 1998.

[86] B. M. Wilamowski and H. Yu, "Improved computation for Levenberg-Marquardt training," *IEEE Trans. Neural Netw.*, vol. 21, no. 6, pp. 930–937, June 2010.

[87] C. R. Sullivan, J. J. Awerbuch, and A. M. Latham, "Decrease in photovoltaic power output from ripple: Simple general calculation and the effect of partial shading," *IEEE Trans. Power Electron.*, vol. 28, no. 2, pp. 740–747, Feb 2013.

[88] W. Xiao, W. Dunford, P. Palmer, and A. Capel, "Regulation of photovoltaic voltage," *IEEE Trans. Ind. Electron.*, vol. 54, no. 3, pp. 1365–1374, June 2007.

[89] R. Faraji, A. Rouholamini, H. R. Naji, R. Fadaeinedjad, and M. R. Chavoshian, "FPGA-based real time incremental conductance maximum power point tracking controller for photovoltaic systems," *IET Power Electron.*, vol. 7, no. 5, pp. 1294–1304, May 2014.

[90] M. Rashid, *Power Electronics: Circuits, Devices, and Applications.* 3rd Edition, Pearson Education, 2009.

[91] B. Singh, D. T. Shahani, and A. K. Verma, "Neural network controlled grid interfaced solar photovoltaic power generation," *IET Power Electron.*, vol. 7, no. 3, pp. 614–626, March 2014.

[92] Y. Jiang and J. A. A. Qahouq, "Single-sensor multi-channel maximum power point tracking controller for photovoltaic solar systems," *IET Power Electron.*, vol. 5, no. 8, pp. 1581–1592, September 2012.

[93] B. R. Lin and C. L. Huang, "Analysis and implementation of an integrated sepic-forward converter for photovoltaicbased light emitting diode lighting," *IET Power Electron.*, vol. 2, no. 6, pp. 635–645, Nov 2009.

[94] G. Araujo, E. Snchez, and M. Mart, "Determination of the two-exponential solar cell equation parameters from empirical data," *Solar Cells*, vol. 5, no. 2, pp. 199 – 204, 1982.

[95] A. Hovinen, "Fitting of the solar cell IV-curve to the two diode model," *Physica Scripta*, vol. 54, no. T54, pp. 175–176, 1994.

[96] E. Saloux, A. Teyssedou, and M. Sorin, "Explicit model of photovoltaic panels to determine voltages and currents at the maximum power point," *Solar Energy*, vol. 85, no. 5, pp. 713 – 722, 2011.

[97] E. I. Batzelis, G. E. Kampitsis, S. A. Papathanassiou, and S. N. Manias, "Direct MPP calculation in terms of the single-diode PV model parameters," *IEEE Trans. Energy Convers.*, vol. 30, no. 1, pp. 226–236, March 2015.

[98] J. C. H. Phang, D. S. H. Chan, and J. R. Phillips, "Accurate analytical method for the extraction of solar cell model parameters," *Electronics Letters*, vol. 20, no. 10, pp. 406–408, May 1984.

[99] W. D. Soto, S. Klein, and W. Beckman, "Improvement and validation of a model for photovoltaic array performance," *Solar Energy*, vol. 80, no. 1, pp. 78 – 88, 2006.

[100] C.-S. Moo and G.-B. Wu, "Maximum power point tracking with ripple current orientation for photovoltaic applications," *IEEE J. Emerg. Sel. Topics Power Electron.*, vol. 2, no. 4, pp. 842–848, Dec 2014.

[101] A. Elrayyah, Y. Sozer, and M. Elbuluk, "Modeling and control design of microgrid-connected PV-based sources," *IEEE J. Emerg. Sel. Topics Power Electron.*, vol. 2, no. 4, pp. 907–919, Dec 2014.

[102] R. Surapaneni and A. Rathore, "A single-stage CCM zeta microinverter for solar photovoltaic AC module," *IEEE J. Emerg. Sel. Topics Power Electron.*, vol. 3, no. 4, pp. 892–900, Dec 2015.

[103] S. Mishra and P. Sekhar, "TS fuzzy based adaptive perturb algorithm for MPPT of a grid connected single stage three phase VSC interfaced PV generating system," in *IEEE Power and Energy Society General Meeting*, July 2012, pp. 1–7.

[104] R. Bell and R. Pilawa-Podgurski, "Decoupled and distributed maximum power point tracking of series-connected photovoltaic submodules using differential power processing," *IEEE J. Emerg. Sel. Topics Power Electron.*, vol. 3, no. 4, pp. 881–891, Dec 2015.

[105] S. De Leon-Aldaco, H. Calleja, and J. Aguayo Alquicira, "Reliability and mission profiles of photovoltaic systems: A fides approach," *IEEE Trans. Power Electron.*, vol. 30, no. 5, pp. 2578–2586, May 2015.

[106] P. Mazumdar, P. Enjeti, and R. Balog, "Analysis and design of smart PV modules," *IEEE J. Emerg. Sel. Topics Power Electron.*, vol. 2, no. 3, pp. 451–459, Sept 2014.

[107] Y. H. Ji, D. Y. Jung, J. G. Kim, J. H. Kim, T. W. Lee, and C. Y. Won, "A real maximum power point tracking method for mismatching compensation in PV array under partially shaded conditions," *IEEE Trans. Power Electron.*, vol. 26, no. 4, pp. 1001–1009, 2011.

[108] S. R. Chowdhury and H. Saha, "Maximum power point tracking of partially shaded solar photovoltaic arrays," *Sol Energy Mater Sol C*, vol. 94, no. 9, pp. 1441 – 1447, 2010.

[109] F. D. Croce, "LP, or not LP: that is the question," *6th Multidisciplinary International Conference on Scheduling : Theory and Applications (MISTA 2013)*, pp. 849–865, 2010.

[110] J. Storey, P. R. Wilson, and D. Bagnall, "The optimized-string dynamic photovoltaic array," *IEEE Trans. Power Electron.*, vol. 29, no. 4, pp. 1768–1776, April 2014.

List of Publications

Journal Publications

1. **H. S. Sahu** and S. K. Nayak, "**Estimation of maximum power point of a double diode model photovoltaic module**," *IET Power Electron.*, vol. 10, no. 6, pp. 667-675, May 2017.

2. **H. S. Sahu** and S. K. Nayak, "**Extraction of Maximum Power From a PV Array Under Nonuniform Irradiation Conditions**," *IEEE Trans. Electron Devices*, vol. 63, no. 12, pp. 4825-4831, Dec. 2016.

3. **H. S. Sahu** and S. K. Nayak, "**Numerical approach to estimate the maximum power point of a photovoltaic array**," *IET Gener. Transm. Distrib.*, vol. 10, no. 11, pp. 2670-2680, August 2016.

4. **H. S. Sahu**; S. K. Nayak and S. Mishra, "**Maximizing the Power Generation of a Partially Shaded PV Array**," *IEEE J. Emerg. Sel. Topics Power Electron.*, vol. 4, no. 2, pp. 626-637, June 2016.

Conference publications:

1. **H. S. Sahu** and S. K. Nayak, "**Extraction of Maximum Power from a PV Array Under Partial Shading Conditions**," Presented in Global Energy Technology Summit (GETS-2015), NTPC, Power Management Institute (PMI) Noida, PP. 1-11, Nov. 2015 (**Best paper award**).

2. **H. S. Sahu** and S. K. Nayak, "**A novel approach to extract maximum power from partially shaded PV array**," *IEEE Power, Communication and Information Technology Conference (PCITC), Bhubaneswar*, PP. 337-342, Oct. 2015.

3. P. Saha, S. Kumar, S. K. Nayak and **H. S. Sahu**, "**Parameter estimation of double diode photo-voltaic module**," Power, *1st Conference on Dielectric and Energy Management at NERIST (ICPDEN), Itanagar*, Jan. 2015, pp. 1-4.

4. **H. S. Sahu** and S. K. Nayak, "**Improvement in the power generation of a PV array under partial shading conditions**," *Eighteenth National Power Systems Conference (NPSC), IIT Guwahati*, PP. 1-6, Dec. 2014.

5. **H. S. Sahu** and S. K. Nayak, "**A novel approach to improve power output of PV array under different shading conditions**," *6th IEEE Power India International Conference (PIICON), Delhi*, PP. 1-6, Dec. 2014.

6. **H. S. Sahu** and S. K. Nayak, "**Power enhancement of partially shaded PV array by using a novel approach for shade dispersion**," *IEEE PES Innovative Smart Grid Technologies - Asia (ISGT ASIA), Kuala Lumpur*, pp. 498-503, May 2014.

7. **H. S. Sahu**, S. Roy and S. K. Nayak, "**Estimation of Maximum Power Point of PV array using datasheet values for microgrid integration**," *IEEE PES Innovative Smart Grid Technologies - Asia (ISGT ASIA), Kuala Lumpur*, pp. 754-759, May 2014.